Doctoral Dissertation

Preparation of organosilica membranes and the application to gas separation in the presence of water vapor

（オルガノシリカ膜の作製と水蒸気共存下でのガス分離への応用）

Xiuxiu Ren

Supervisors: Toshinori Tsuru

Department of Chemical Engineering,

Graduate school of Engineering, Hiroshima University

（広島大学大学院工学研究科 化学工学専攻）

September, 2015

論文の要旨

題目　Preparation of organosilica membranes and the application to gas separation in the presence of water

（オルガノシリカ膜の作製と水蒸気共存下でのガス分離への応用）

氏名：任秀秀

Organosilica membranes based gas separations have been considered to clean and low energy system, such as in natural gas purification, or CO_2 capture from coal-fired power plant. Most of membranes were prepared with great hydrophilicity from top to bottom to enhance membrane performance. However, water vapor has a great effect on these hydrophilic membranes. The development of hydrophobic top and intermediate layers for organosilica membranes, and improvement of separation performance become very important. The key objective of this thesis is to study the effect of water vapor on organosilica membranes, and prepare hydrophobic organosilica membranes which are expected to keep separation performance under wet conditions as well as under dry conditions. The main work of this research is as follow.

Chapter 1 is "**General introduction**". The research background of membranes for gas separation under dry and wet conditions was overviewed and the purpose of this study was proposed.

Chapter 2 is "**CO_2 permeation through hybrid organosilica membranes in the presence of water vapor**". Two types of organoalkoxysilanes, bis(triethoxysilyl)ethane (BTESE) and bis(triethoxysilyl)octane (BTESO) were used as precursors to prepare membranes via sol-gel method. The two membranes showed distinct properties on porous structures and water affinity because of differences in the bridging methylene numbers between the two Si atoms. Under dry conditions, the BTESE and BTESO membranes showed CO_2 permeances as high as 7.66×10^{-7} and 6.63×10^{-7} mol m^{-2} s^{-1} Pa^{-1} with CO_2/N_2 selectivities of 36.1 and 12.6 at 40 ℃, respectively. In the presence of water vapor, the CO_2 permeances were decreased for both membranes, but the effect of water vapor on CO_2 permeation is slighter for BTESO membranes than that for BTESE membranes due to more hydrophobicity and denser structures with a longer linking-bridge group. Both of hybrid organosilica membranes showed good reproducibility and stability in water vapor.

Chapter 3 is "**Preparation of organosilica membranes on hydrophobic intermediate layers and evaluation of gas permeation in the presence of water vapor**". Hydrophobic Me-SiO_2 sols were prepared by using tetraethoxysilane (TEOS) and methyltrimethoxysilane

(MTMS) as co-precursors, coated on macroporous α-Al_2O_3 supports through multi-layered coatings. By characterization of nanopermporometry using hexane and water as condensable vapors, Me-SiO_2 layers showed pore diameter of approximately 2 nm and exhibited hydrophobic properties and that SiO_2-ZrO_2 layers were hydrophilic. Under dry conditions, BTESO/Me-SiO_2 showed a gas permeation trend that was similar to that of BTESO/SiO_2-ZrO_2. The selectivity of H_2/SF_6 for BTESE/Me-SiO_2 (334) was much lower than that of BTESE/SiO_2-ZrO_2 (>20,000) due to the inhomogeneous coatings of BTESE on the Me-SiO_2 layers. Under humidified conditions, BTESE/Me-SiO_2 and BTESO/Me-SiO_2 with hydrophobic intermediate layers, exhibited less decrease in CO_2 permeance compared with either BTESE/SiO_2-ZrO_2 or BTESO/SiO_2-ZrO_2, both of which were prepared with hydrophilic intermediate layers. The water vapor resulted in a negligible effect on gas permeance for totally hydrophobic BTESO/Me-SiO_2, while a little larger decrease was observed for hydrophilic top layers of BTESE/Me-SiO_2, showing that membranes with hydrophobic surface chemistry can effectively resist water vapor condensation or adsorption during gas permeation.

Chapter 4 is "**Plasma-assisted multi-layered coating towards improved gas permeation properties for organosilica membranes**". H_2O vapor plasma was used for the modification of hydrophobic Me-SiO_2 intermediate layer by generating hydrophilic groups on the surface without changing either the bulk hydrophobicity or the pore size. After plasma treatment of the Me-SiO_2 layers, BTESE or BTESO-derived sols were coated as separation layers. The gas selectivity for BTESE membrane was improved after water plasma treatment, which allowed better adhesion between each layer via the enhanced hydrophilic modification by water plasma. Under wet conditions, the CO_2 permeance for both membranes were decreased, slightly larger decrease than for membranes without plasma treatment, but much less than the BTESE and BTESO membranes prepared on hydrophilic SiO_2-ZrO_2 intermediate layers. High gas permeation properties were obtained in the presence of water for organosilica membranes prepared from hydrophobic top layers to hydrophobic intermediate layers via plasma-assisted multi-layered coatings.

Chapter 5 is "**Conclusions**". Several important conclusions of this study are given in detail and suggestions are provided for further study.

CONTENTS

Chapter 1

General Introduction

1.1 Membrane for separation applications

Membranes have gained great attention for industrial applications on solving resource shortage, energetic and environmental problems. The key property of membranes on separation applications is the ability to control the permeation rate of species. There are large varieties of membrane processes in the separation technology, including reverse osmosis, ultrafiltration, microfiltration, electrodialysis, gas separation, pervaporation, contactors, facilitated transport [1-5], etc. The first four processes have been well-developed industrial application since in 1980 mainly for water treatment. Gas separation and pervaporation are developing industrial applications and a large number of plants have been installed [2]. The different processes are used according to the objectives of separations based on concentration, purification, fractionation or reaction [5]. The membranes also can be used in sensors and fuel cell. In medical applications, the great achievement have obtained in artificial kidneys, blood oxygenators and controlled release pharmaceuticals, saving many people's lives [7-9].

Recently, the capture of CO_2 becomes very important because it is considered to be the primary cause of global warming [6,10]. The world's reliance on fossil fuels for energy generation is responsible for increased concentrations of CO_2 emissions in atmosphere. The emission sources could come from electric power plants, natural gas field or other industrials [11]. The currently available technology is absorption, by using alkanolamines (or variants) to selectively absorb CO_2 [12]. Despite the significant improvements in terms of liquid stability and the regeneration of the amine solution, this process is still highly energy intensive [13,14].

Membrane-based gas separation provides attractive alternative technology to conventional gas treating options due to the lower energy requirements (no phase changes), lower cost

(easier operations, less land used and continuous process), and more friendly to the environment (no corrosion issues). There are at least 20 companies' worldwide membrane-based gas separation systems. Major applications are the separation of H_2/N_2, N_2/air and CO_2/CH_4 in natural gas operations [2]. However, membranes are still confronted with challenges that have limited membrane separation technology to turn into the industrial applications for CO_2 capture, such as the selectivity challenge, the productivity challenge [15]. A great many of researches have focused on solving these problems, including optimization of existing membrane and development of new materials. The progress made it possible to promote extensive membrane applications in industrial fields.

1.2 Overview membranes for gas separation

Membrane gas separation process is a field of considerable current interest, and the number of applications is expanding rapidly. In gas separation, membranes as a selective barrier allow the separation of one or more species from a mixture [5], and permeation of the membrane is enriched with favorable species, as shown in Figure 1.1.

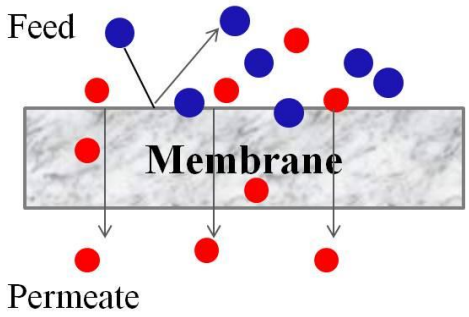

Figure 1.1 Schematic diagram of gas separation of membranes.

1.2.1 Gas separation mechanism

Membranes can be simply divided into two types based on the structures: dense (or nonporous) membranes and porous membranes. Dense membranes consist of polymer and

polymer-related materials such as some electrically charged membranes. Porous membranes include isotropic and anisotropic membranes. The anisotropic membranes refer to an extremely thin layers act as separation layer coated on thicker and larger porous substrates which provide mechanical strength. The transport rate of species through membranes is inversely proportional to the thickness of separation layers. Therefore, thinner layers of the membranes are major breakthroughs for elevating gas flux.

The mechanism of gas permeation through dense and porous membranes is very different. The schematic mechanism of gas transport is illustrated in Figure 1.2. If the pore size of membranes is larger than 0.1 μm, gases transport through the membrane is by convective flow and no effective separations occur. When the pore diameter is in the range of 1-50 nm, comparable to or smaller than the mean free path of the gas molecules, the diffusion is governed by Knudsen diffusion. The selectivity is proportional to the inverse square root of its molecular weight.

$$\alpha_{A/B,Knud} = \sqrt{M_B / M_A} \qquad (1.1)$$

When the pores of porous membranes are on the order of sub-nanometers, then gases are separated by molecular sieving. Gas molecules with a diameter that is smaller than the pores of a membrane can be transported through the membranes while gas molecules with a larger diameter would be prohibited. In the case of surface diffusion, gas molecules adsorb on the pore walls, and diffuse along the adsorption gradient. For capillary condensation, as an extension of surface diffusion, the low pressure of vapor in the micropores causes vapor condensation, which prohibits the permeation of other gases through membranes [16]. The solution-diffusion mechanism is used to describe the molecules permeation through polymer membranes.

There are two main characteristics that dictate gas separation membrane performances: permeability and selectivity. Permeability is the gas flux permeation through the membranes. The ideal selectivity is defined by the ratio of the permeability of the individual component:

$$\alpha_{i/j} = P_i / P_j \qquad (1.2)$$

In practical measurement of binary gases, separation factor is to describe the selectivity as follows:

$$SF = \frac{(\chi_i / \chi_j)_p}{(\chi_i / \chi_j)_F} \qquad (1.3)$$

Where x represent the mole fractions in the permeate stream (P) and in the feed stream (F).

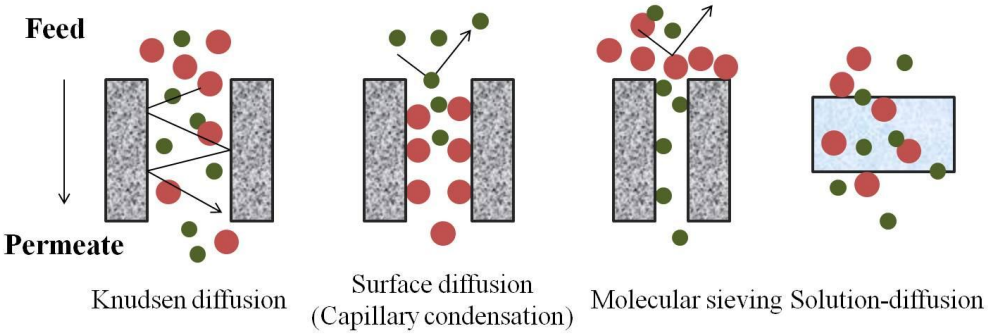

Figure 1.2 Schematic diagram of mechanism of gas transport through membranes.

1.2.2 Gas separation properties

A large number of comprehensive reviews were to investigate the types of membranes for gas separation. Membranes most commonly used are made from polymeric materials. Today, information on gas permeation properties is available for more than 1000 polymers including glassy and rubbery ones [17,18]. The gas separation performance of polymers have been summarized by Robeson in 1991 and revisited in 2008 [19,20], as shown in Figure 1.3. The permeability of CO_2 are most around 1-100 barrers (10^{10}cm^3(STP) cm/(cm^2·s·cmHg)). The selectivity of CO_2/CH_4 is mostly in the range of 10-100 and CO_2/N_2 in the range of 10-50. In these polymers, TR (thermally rearranged), 6FDA-based polyimide (the polyimides 2, 2'-bis(3,4'-dicarboxyphenyl) exafluoropropane dianhydrid), PIM (polymers of intrinsic microporosity) showed relatively high permeability and selectivity [21-23].

However, the significant improvement of membranes is not observed in years from 1991 to 2008. A general trade-off exists between permeability and selectivity, limiting the polymer performance. In addition, polymeric membranes suffered from chemical degradation, thermal instability and fouling with last of time. This has resulted in extensive shift of research trend

toward inorganic membranes with well-known superior thermal and chemical stability. Inorganic membranes include zeolite membranes, carbon molecular sieve membranes, silica membranes, metallic membranes, etc. M. Pera-Titus summarized some inorganic membranes for CO_2/N_2 and CO_2/CH_4 separation, as illustrated in Figure 1.4 [24]. Among the zeolite membranes, NaY and MFI-zeolite membranes offer the best trade-off between CO_2 permeability and CO_2/N_2 separation ability, exceeding the Robeson's upper bound. The other membranes such as silica and MOF membranes for CO_2/N_2 separation are below of Robeson's line. For CO_2/CH_4 separation, performances of almost membranes were higher than those of polymers. R.M. de Vos and H. Verweij reported silica membranes with 30 nm thin layers that the CO_2 permeance was above 10^{-7} $mol \cdot m^{-2} \cdot s^{-1} \cdot Pa^{-1}$ (10 barrer) and CO_2/CH_4 selectivity was larger than 100 [25]. In addition, carbon molecular sieve membranes also showed high permeability and selectivity. A PEI-derived carbon molecular sieve membrane showed CO_2 permeability of 222.5 barrer and CO_2/CH_4 selectivity of 75, respectively [25].

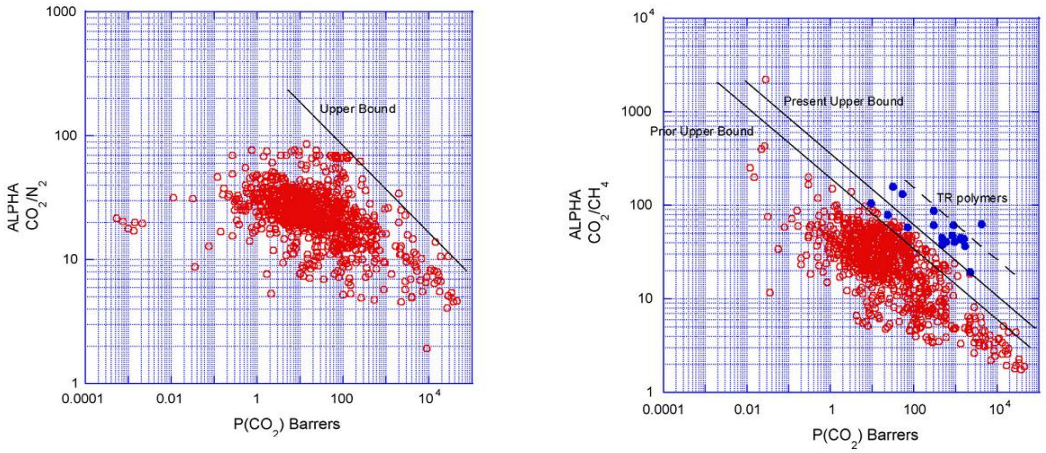

Figure 1.3 Robeson's upper bound correlations for CO_2 /N_2 and CO_2/CH_4 separation [20].

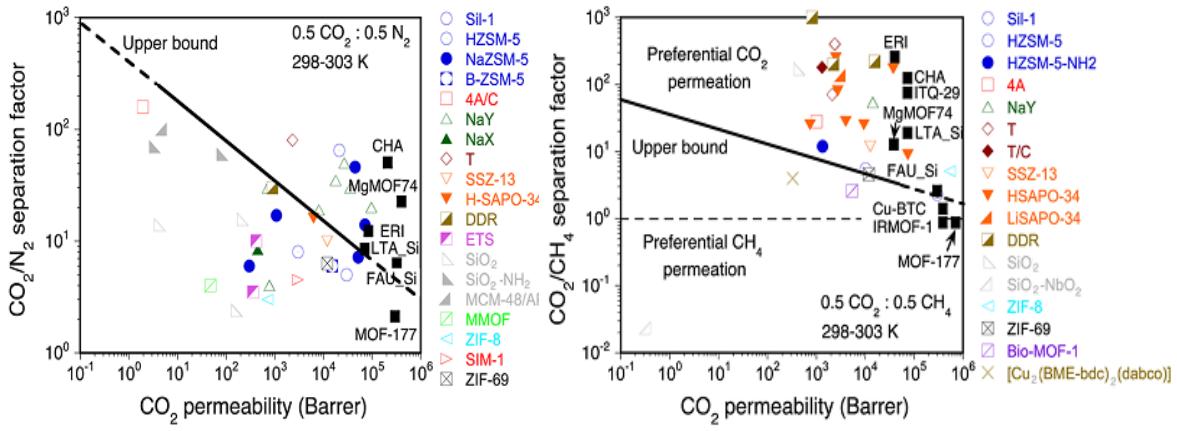

Figure 1.4 Taxonomy of silica, zeolite, and MOF/ZIF materials for CO_2/N_2 and CO_2/CH_4 separation at near room temperature and comparison with Robeson's upper bounds (black line) for polymeric membranes [23].

1.3 The effect of water vapor on membranes for CO_2 separation.

Currently, most of membranes were reported under dry conditions. In industrial process, water is commonly present in the removal of CO_2 gas separation applications. In the raw natural gas without impurity, the presence of H_2O and acid gases CO_2 (>50%) may cause corrosion in pipelines for gas transport [27-29]. It is required that water vapor is lower than 120 ppm for delivery to the US national pipeline [3]. In the capture of CO_2 from the flue gas, the water also exists in the process [13, 30]. Water molecular shows very different behavior and mechanisms compared to other gases even at minor contents [16]. This is due to a small kinetic diameter which can result in high diffusivity. On the other hand, high critical temperature of water results in large amount of adsorption in the membranes, even possibility of condensation. This will create an additional transfer resistance for the gases to permeate, reducing gas performance. The kinetic diameter and critical temperature of some molecules are shown in Table 1.1

Table 1.1 Kinetic diameter and critical temperature of some molecules.

Gas	Kinetic diameter [Å]	Critical temperature [K]
H_2O	2.65	647.3
H_2	2.89	33.2
CO_2	3.3	304.2
O_2	3.46	154.6
N_2	3.64	126.2
CF_4	4.8	227.5
SF_6	5.5	318.7

1.3.1 The effect of water vapor on polymers

Membranes based gas- and vapor separation has emerged into an important unit operation in the chemical industry during the past thirty years. The efficiency of this technology strongly depends on the selection of membrane materials, their physical-chemical properties, and the mechanism through which permeation occurs. The transport of water vapor through polymeric films is often complex due to non-ideal solubilization of the water molecules in the polymer and anomalous diffusivity inside the polymer network. Depending on the polymer, the diffusivity of water vapor may increase or decrease with the amount of water in the polymer [16]. The complex mechanism of water vapor sorption or diffusion in the polymer can affect the transport behavior of CO_2 or other gas through the polymer. For example, CARDO/ODA (9,9-Bis(4-aminophenyl)fluorine/Oxydianiline) polymer showed a converse trend at different water activity in the feed. The gas permeability was decreased for RH lower than 70% and then increased at higher RH than 70% [31]. The permeability of gases were changed in the presence of water vapor, as shown in Table 1.2.

Table 1.2 Gas permeability of polymers at under dry and wet conditions

Membrane	Gas	Permeability (Barrer)		Feed	%loss	Temperature [ºC]	Reference
		Dry	Wet	RH%			
CARDO	CO_2	164	51	100	69	20	31
ODA	CO_2	5.2	12	100	-130	20	31
CARDO/ODA	CO_2	70	42	100	40	20	31
Cardo-type PI	CH_4	0.027	0.019	60	28	30	32
PPO	CO_2	-	-	60	11	30	32
	CH_4	0.156	0.147	60	6	30	32
PDMS	CO_2	1950	1850	40	5	35	33
6FDA-TMPDA	CO_2	5.4	-	90	70	35	34
	CH_4	0.224	-	90	70	35	34
Matrimid®5218	CO_2	1311	-	95	45	35	34
	CH_4	30.5	-	95	25	35	34
Matrimid®5218	CO_2	9.7	5.1	75	47	35	35
	CH_4	0.24	0.12	75	50	35	35
PEBAX®1074	N_2	~6	~4.5	100	25	50	36
PEO-PBT	N_2	2	2	20-60	0	30	37
PEO-PPO	CO_2	~500	~350	90	30	50	38
	N_2	~13	~10	90	23	50	38
SPEEK	N_2	0.003	0.14	93	-400	30	39
PEBAX®1074	N_2	2.45	1.92	93	22	30	39

CARDA: 9,9-Bis(4-aminophenyl)fluorine; ODA: Oxydianiline; PPO: poly(2,6-dimethyl-1,4-phenylene oxide); PI: polyimide; PDMS: polydimethyl siloxane; SPEEK: sulfonated poly(ether ether ketone); 6FDA-TMPDA: the polyimides 2, 2'-bis(3,4'-dicarboxyphenyl) exafluoropropane dianhydrid-2, 3, 5, 6-tetramethyl-1,4-phenylenediamine; PEO-PBT: poly(ethylene oxide) multi-block poly(butylenes terephthalate) copolymers

M. Wessling and co-works reported the water vapor and gas transport through a series of poly-(ethylene oxide) (PEO)-based block polymers [29, 30, 36-39]. The materials based on a soft hydrophilic PEO segmented block copolymers are well-known for a reasonably high CO_2 permeability with good CO_2/light gas selectivity in dry streams, which provide an interesting candidate for CO_2 capture [40]. PEO-PBT block copolymer consisted of the hard hydrophobic PBT (poly(butylenes terephthalate)) segment which provides mechanical strength and a soft hydrophilic PEO segment which provides flexibility to the polymer. It was reported that the N_2 permeability in the presence of water vapor is equal to the permeability without water vapor and remains constant with increasing water vapor activity [29,37]. The rubbery PEBAX®1074 polymer with hydrophilic properties showed Flory-Huggins type of sorption in water vapor sorption isotherms. The water vapor permeability increases exponentially with increasing water vapor activity, which was due to the swelling of the polymer caused by high amounts of water absorption [36, 39]. However, the N_2 permeability slightly decreases even at high water vapor activity, 75-78% of the dry nitrogen permeability, as shown in Table 1.2. They explained nitrogen molecules that dissolved in and diffused through the film experience a more water-like environment, rather than the polymer environment. The lower decrease of gas permeability in the water vapor also can be found in the PEO-ran-PPO (poly(2,6-dimethyl-1,4-phenylene oxide)) polymer [38]. The permeability of CO_2 and N_2 at a high relative humidity of 90% were decreased to 23 and 30% of the dry permeability. They mainly discussed the water vapor permeations, whereas the mechanism for the gas transport under the wet conditions was not so clearly explained.

Till now, only a few of studies have been extended to the effects of water on the permeation properties of other gases. S.E. Kentish and her co-workers paid much attention to the effect of water vapor in the feed stream on gas separation for the practical application, such as CO_2 capture in natural gas or flue gas. 6FDA-TMPDA (the polyimides 2, 2'-bis(3,4'-dicarboxyphenyl) exafluoropropane dianhydrid-2, 3, 5, 6-tetramethyl-1,4- phenylenediamine) and Matrimid®5218 were exposed to humidified mixtures of CO_2 and CH_4 at 35 ºC [34]. Water vapor permeabilities were increased from 3200 to 3900 barrer and from 20000 to 27000 barrer as the water activity increased for 6FDA-TMPDA and Matrimid, respectively. The increase trend in water permeability was due to the increase in water vapor solubility and possibly plasticization of polymer matrix by water vapor. On the other hand, water clusters may restrict the diffusivity of water vapor in the polyimide. This explanation was confirmed

by a model studied on the sorption and transport properties [41]. Conversely, for Matrimid, the permeability of CH_4 reduced to 75% of its original value at saturation at either total feed pressure, while CO_2 permeability had a decrease of 45% and 35% of the initial value at 2 and 7.5 bar total feed pressure, respectively. The permeability decline was due to the competitive sorption of water and CO_2 plasticization, which was confirmed by the following study in the thickness effect on the polymer [42]. Similarly, the CH_4 permeability for 6FDA-TMPDA declined to around 30% of its original value at saturation, and the decline in CO_2 permeability with increasing water content is slightly less than that of CH_4. They also reported other polymers such as TR (Thermal rearrangement) PBO and PI (α-hydroxyl-polyimides) membranes showed similar conclusion that the presence of water reduced the permeability in CO_2 and CH_4 for membranes due to competitive sorption [43].

For many polymers, the permeability of gases were decreased in the presence of water vapor. It should be noted that the presence of water does not always reduce the performance of membranes, such as SPEEK [39]. The increased trend of gas in the presence of water vapor was due to the hydrophilic nature of the sulfonated polymer and the accompanying high swelling degree in polymer. Especially for facilitated transport systems, the presence of water is essential to enhance the transport of CO_2 [44,45].

1.3.2 The effect of water vapor on inorganic membranes

Under wet conditions for CO_2 capture, polymer membranes suffered from the problems of physical aging, plasticization or swelling induced by water as well as CO_2 [42], which restrict the long-term applications. It has been well-known that the inorganic membranes offer a higher physical, chemical and thermal stability with the comparison of polymeric materials. Most ceramic or zeolite membranes do not suffer from swelling or fouling problems as polymers. The gas separation performances for inorganic membranes were summarized in Table 1.3.

Table 1.3 Gas permeability through inorganic membranes under dry and wet conditions.

Family	Membrane	Gas	Permeance (10^{-8} mol·m^{-2}·s^{-1}·Pa^{-1})		Feed	%loss	Temperature [ºC]	Reference
			Dry	Wet	water			
Silica	amorphous	CO_2	~90	~0.9	35%RH	99	35	46
		H_2	~200	~22	50%RH	89	35	46
Zeolite	NaY	CO_2	~6.1	~1	14mol%	83	200	47
		N_2	~3.2	~0.2	14mol%	93.7	200	47
	MCM-48	CO_2	2.4	0.3	2.6%	87.5	20	48
		N_2	2.9	0.9	2.6%	69	20	48
	SAPO-34	CO_2	10	0.08	0.6%	99.2	-	49
	DDR	CO_2	25	11	3%	56	25	50
		CH_4	0.11	0.11	3%	0	25	50
	ZSM-5	H_2	~56	34.9	61%	38	550	51
		CO_2	~15	9.4	61%	37	550	51
	Silicate	H_2	~59	51.6	61%	12.5	550	51
		CO_2	~16	12.5	61%	22	550	51
Carbon	molecular sieve	O_2	0.74	0.518	85%RH	30	-	52
		N_2	0.074	0.065	85%RH	12.5	-	52
		CO_2	0.296	0.148	32.5%RH	50	32	53
Others	ZIF-7	H_2	-	-	3mol%	2	220	54
		CO_2	-	-	3mol%	0	220	54
	Graphene oxide (GO)	CO_2	33	38	85%RH	-8%	25	55

Inorganic membranes for gas separation included silica, zeolite, carbon, and metal-organic frameworks, and so on. Silica membranes with amorphous structures were commonly derived from TEOS, which showed small pore size with high permeance of H_2. Zeolites are the aluminosilicate members of the family with regular pore structures of molecular dimensions. Zeolite membranes were commonly prepared by crystallization of a silica-alumina gel in the presence of alkalis and organic templates to hydrothermal growth on porous supports. The variety of zeolite membranes based on the size of the cages and the affinity of species can be prepared to achieve high performance on separation. Carbon molecular sieving membranes were pyrolyzed by some organic material, which separated the gas in molecular level, resulted in high selectivity. The metal-organic framework membranes, such as ZIF-7 and GO are the recently developing membrane materials.

In Table 1.3, for most of inorganic membranes, the gas permeance was decreased largely in the presence of water vapor. The porous silica membranes fabricated by the sol-gel procedures were quite stable, and had high CO_2 permeance of 9×10^{-7} mol·m^{-2}·s^{-1}·Pa^{-1} and CO_2/CH_4 selectivity of 112 under dry conditions [46]. In humid conditions, however, the gas permeances of CO_2 decreased drastically, 1% of the dry value. The permeance of H_2 was also largely decreased, and the selectivity of H_2/CH_4 was reduced from 105 to about 40. Similar observations of CO_2 permeances of the moist mixture were far below those for the dry mixtures in the zeolite membranes, such as DDR, SAPO-34 and NaY membranes [47,49,50].

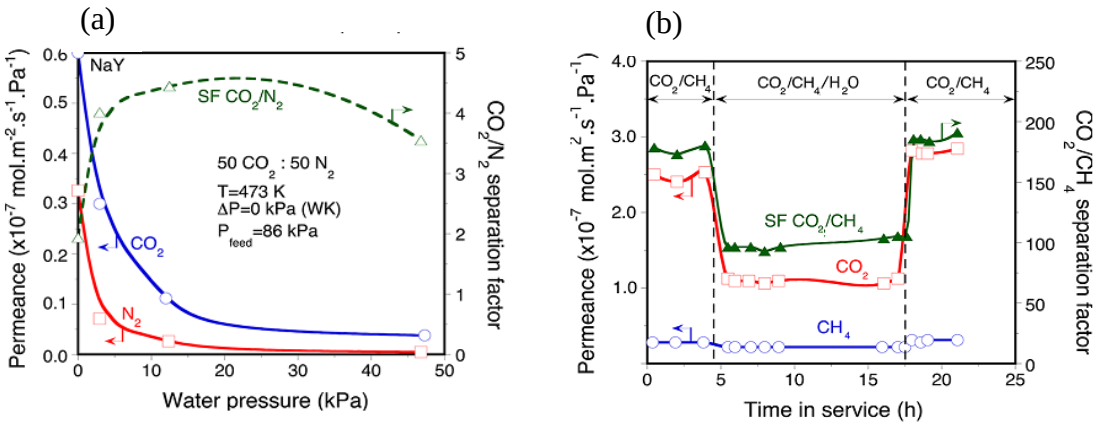

Figure 1.5 Gas Permeance and selectivity of equimolar mixture (a) CO_2/N_2 as a function of the water partial pressure for NaY membranes and (b) CO_2/CH_4 for a DDR membrane at 298 K with 3% water. Images are adapted from Gu et al. [47] and S. Hemeno et al. [50].

A typical permeation pattern observed for NaY and DDR membranes were shown in Figure 1.5. Both of CO_2 and N_2 permeances for NaY membranes were decreased largely even at low water pressure, and gradually decreased as the water pressure increased. The separation factors of CO_2/N_2 were increased and then decreased as the water pressure increase. The introduction of water vapor to the feed stream for both CO_2 and N_2 permeances were below those for the dry mixture which confirmed in a temperature range of 23-200 ℃. The decreased permeance was due to the fact that adsorbed H_2O molecules reduced the zeolite pore volume [47]. In the case of DDR membranes, the introduction of water resulted in a significant decrease in CO_2 permeance with no change in CH_4 permeance, so that the separation factor was decreased to 100. However, the influence of water on the loss of CO_2 permeance for DDR membranes was less than those of SAPO-34 and NaY membranes, which may be due to the all-silica DDR membranes with hydrophobic nature that reduced the ability of water block in the pores [50]. The similar results are confirmed in ZSM-5 and silicate both of which belong to MFI groups [51]. The suppression effect of water vapor on H_2 and CO_2 permeation was larger for the hydrophilic ZSM-5 zeolite membrane than for the hydrophobic Silicate membrane, even having the same pore structures.

For carbon molecular sieve membranes with microporous structures, the loss of gas permeance occurred at relative humidity from 23-85%, and most of performance lost was in the initial period of exposure to water vapor [52]. The influence of water on gas performance was related to the polarity of the carbon surface, the size and shape of the micropores. Including these inorganic membranes, few papers on ZIF-7 and GO membranes were reported for gas separation under wet conditions. In ZIF-7 membranes, H_2 permeance was slightly decreased and CO_2 permeance was not lost due to the ultra-hydrophobic properties of ZIF-7 membranes. In the GO (graphene oxide) membranes, the CO_2 permeance was even slightly higher in the presence of water vapor than that of in the dry graphene oxide (GO) membrane. However, other gas permeances such as H_2, N_2, CH_4, were significantly reduced at high RH. This behavior is primarily due to the hydrophilic nature of GO sheets that the water was strongly adsorbed between GO layers. Due to the strong affinity between CO_2 molecules and water molecules, higher CO_2 sorption in water overwhelms the reduced CO_2 diffusivity in water, so that high CO_2 separation performance was obtained under wet conditions.

The mechanism of water and gas through membranes are complex. The effect of water vapor on gas separation performance is expected to depend on many factors in the membranes, such as pore size, pore shape and chemical properties.

1.4 New membrane materials-hybrid silica

Hybrid organic-inorganic materials have advantages of not only to combine the properties of both organic and inorganic parts but also to create entirely new compositions with distinguishing properties [56,57]. Hybrid organosilica are a family of hybrid materials, which can be prepared as gels, nanoparticles, films, or membranes and applied in optical device fabrication [58], protection [59] or separation [60,61]. Recently, functional bridged polysilsesquioxanes have been prepared for use as high-capacity adsorbents [62].

The typical monomers contain one or more functional silyl groups with a variable pendent or bridged organic group, as shown in Figure 1.6. The organic R1 parts as pendant groups, and the organic R2 as bridged groups can be alkane, alkene, alkyne, aromatic, and so on [56-66]. On the other hand, the groups $-OC_2H_5$ can be further replaced by other organic functionality [67]. A typical route for the synthesis of this hybrid silica material is sol-gel process, which involves the hydrolysis and condensation of the monomers of organosilane under the catalyzed reactions [63,64]. The reactions are displayed as follows.

$$\equiv Si\text{-}OR + H_2O \leftrightarrow \equiv Si\text{-}OH + ROH \quad \text{(hydrolysis)} \quad (1.4)$$

$$\equiv Si\text{-}OR + HO\text{-}Si\equiv \leftrightarrow \equiv Si\text{-}O\text{-}Si\equiv + ROH \quad \text{(condensation)} \quad (1.5)$$

$$\equiv Si\text{-}OH + HO\text{-}Si\equiv \leftrightarrow \equiv Si\text{-}O\text{-}Si\equiv + H_2O \quad \text{(condensation)} \quad (1.6)$$

The networks can be formed through the reactions and varied in length, rigidity, functionality and porosity by using a variety of monomers. The bridged groups are covalently attached to the silicon atoms through Si-C bonds can be tuned to control the size of silica networks. The schematic of networks were shown in Figure 1.7. The variability of organic group as an integral component of the materials, provides an opportunity to modulate bulk properties such as refractive index, chemical resistance, and thermal stability [68-70].

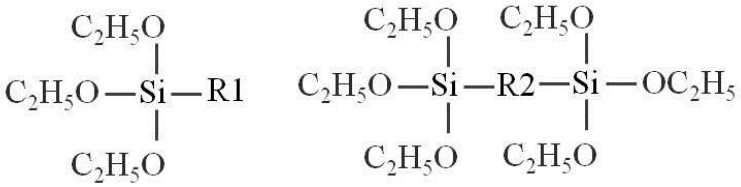

Figure 1.6 Representative monomers used to prepare organosilica materials.

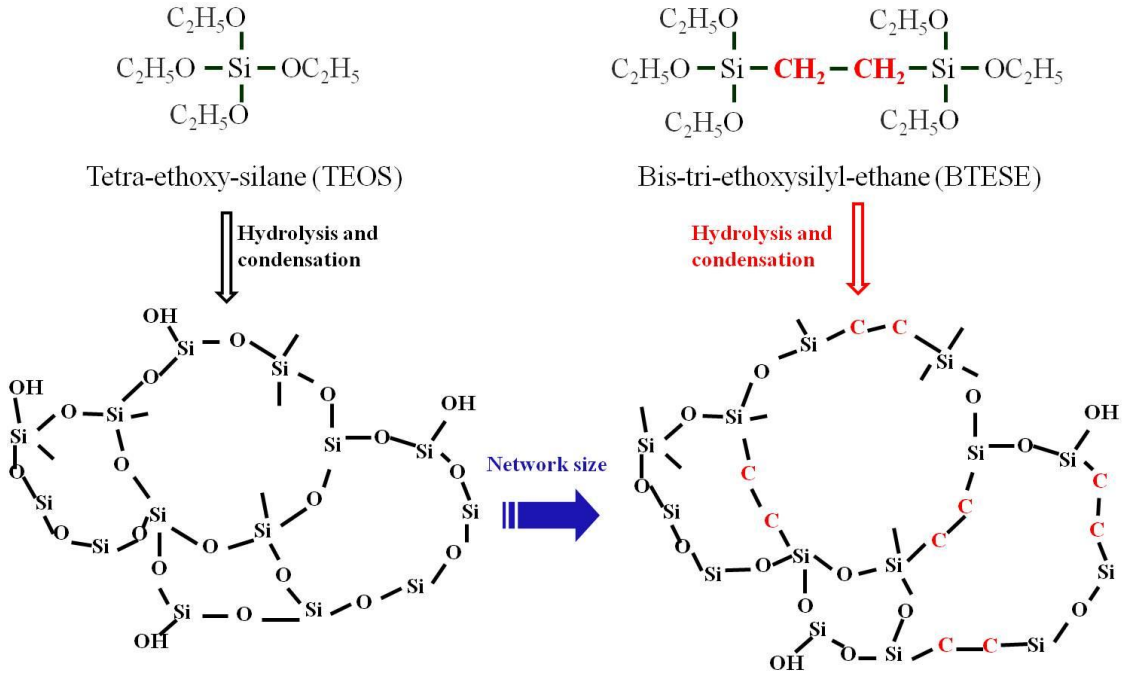

Figure 1.7 Schematic images of amorphous silica networks derived by TEOS and BTESE.

1.4.1 Organosilica films

The thin films are commonly prepared on plate substrates, such as glass, silicon, or polymer, and the thickness is ranging from a nanometer to several micrometers. They have great application in semiconductor, optical, or protective coating. In addition, certain properties of thin films coating on nonporous silicon or glass substrates were applied in the evaluation of the properties of membranes. The thin films can be prepared by sol-gel [71-75] or chemical vapor deposition (plasma) [76,77] method. At present, the sol-gel process in

combination with a dip- or spin-coating step is the most facile and versatile method for preparing organosilica thin films.

G. Dubois et al. prepared significantly tougher hybrid thin-films by introducing carbon bridging units between silicon atoms in the silica networks [71]. The inorganic materials are hard but are prone to be brittle and fractured, while the organics introduced tend to be soft that crack resistant films can be obtained at high levels of porosity. The hybrid thin films have opened potential applications in the fields of microelectronics industries. G. Gong et al. also reported a hybrid organosilica thin films prepared onto polysulfone substrates via a sol-gel process using spin coating [72]. The precursor was used by 1,2-bis(triethoxysilyl)ethane (BTESE, $\equiv$Si–C–C–Si$\equiv$ unit), which contains bridged organic functional groups between 2 silicon atoms. This BTESE-PSF double-layer composite film had a uniform and high-quality layer with a thickness of approximately 200 nm.

Y. Mizuta et al. using pendant-type alkoxides consisted of phenyl-triethoxysilane (PhTES) and tetraethoxysilane (TEOS) prepared organosilica film on polycarbonate (PC) substrate via a sol-gel process combined dip-coating [74]. It was found that phenyl groups in the coating migrated to the PC substrate side and a high adhesion was obtained. Other alkoxide precursors such as 3-glicidoxipropyl-trimetoxisilano (GPTMS) and TEOS were under hydrolysis and condensation to prepare sols. The hybrid organosilica films were formed by sol-gel dip-coatings on carbon steel substrates for corrosion protection [78].

Alternatively, hybrid network materials also can be formed by using a UV curable binder system which can avoid damaging thermo-sensitive substrates. Han et al. reported the hybrid coating materials were all optically transparent by UV-curing [79]. It was found the transparent coatings were robust in scratch and abrasion tests on the substrates. Wouters groups also prepared UV curable antistatic transparent hybrid coatings on polycarbonate [80]. Moreover, large-mesoporous silica thin films were prepared to assess their applicability to selective-controlling dosing and chemical species transport in solution [81].

1.4.2 Organosilica membranes

Amorphous silica membranes can be used in various types of separation applications with high chemical, thermal stability and low energy consumption. Porous silica membranes are commonly fabricated with three layers: α-alumina support layer (pore size: 100-50 nm),

intermediate layer (5-1 nm), and ultrathin silica top-layer (0.1-0.6 nm). The schematic of structures of membranes is shown in Figure 1.8. The intermediate layers are coated on the support in order to prevent the penetration of silica sols into the support and form the ultrathin top layers. The top layer mainly determines the permeability and selectivity. The thin top layer can provide a high flux of gas because the transport rate of a gas is in inverse proportion to the thickness of the membrane.

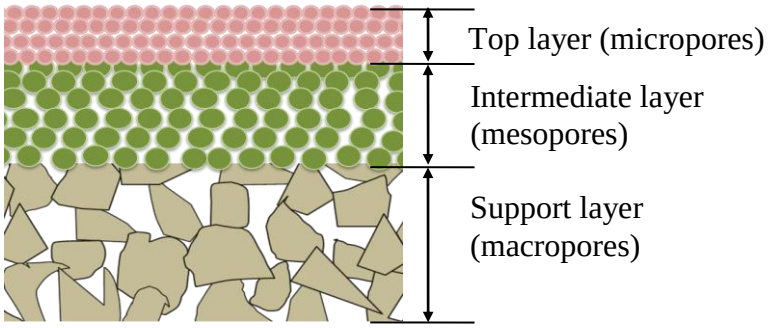

Figure 1.8 Schematic structures of the porous organosilica supported-membranes.

TEOS-derived microporous silica membranes have been studied most extensively for gas separation by chemical vapor deposition (CVD) or sol-gel method [13, 82, 83]. However, TEOS-derived membranes lack of hydrothermal stability in the presence of steam, resulting in a reduction of microporosity [13]. This was because the condensed silanol groups in the silica layer re-hydrolyzed, and migrated to narrow pores. M.C. Duke et al. improved the hydrothermal stability of silica membranes by incorporation of methyl moieties to replace of surface silanol groups, acting as molecular barriers, which can block silanol migration and condensation [84].

Organosilica membranes showed a significant breakthrough in hydrothermal stability of silica membranes since the functional organic groups are homogeneously incorporated in the three-dimensional silica networks. A preventive organosilica membrane prepared by the hydrolysis and condensation of 1,2-bis(triethoxysilyl)ethane (BTESE) with an ethane between the two silicon atoms, has shown stable performance in 1,000 days for the pervaporation of n-butanol/water at 150 ℃ [85]. Our research group prepared BTESE membranes also showed an excellent degree of chlorine resistance on water desalination via reverse osmosis [86]. The

pore size of amorphous membranes can be tuned using alkoxides to the kinetic diameter of gas molecules to achieve high performance of gas separation [87-90]. In our previous report, BTESE- or TEDMDS (1,1,3,3-tetraethoxy-1,3-dimethyldisiloxane)-derived silica membrane showed high permeance of hydrogen separation via a "spacer" technique [91,92]. Well-designed membranes will show high flux of CO_2 and considerable selectivity for CO_2 to large gas molecules such as CH_4 which offer perspective applications on flue gas or natural gas.

1.4.3 Preparation of organosilica membranes

Membranes prepared by sol-gel process have been extensively studied due to the excellent processability, precise pore size control, and thin top layers which are responsible for high gas permeation rates [93]. Moreover, it also allows for synthesis of mixed mixing metal ions into the silica matrix [94]. There are two main types of sol-gel route: polymeric route and colloidal route. In the polymeric route, usually a silicon alkoxide through hydrolysis and condensation reactions can be either acid or base catalyzed. Acid catalyzed reactions will result in microporous materials, and base catalyzed synthesis result in a large and highly cross-linked particles. Tsuru et al. prepared methylated SiO_2 membranes with base NH_3 as a catalyst. The membrane formed mesoporous structures which showed good performance for the nanofiltration of polyolefin oligomers in hexane solution [95]. The effects of amount of water or pH of the solution was found to affect the microstructure of the sols for membrane fabrication due to the rates of hydrolysis and condensation [93,96]. Niimi et al. reported the effect of water amount for BTESE-derived organosilica membranes. The high amount of water resulted in the BTESE better hydrolyzed with higher density of the silanol groups, followed by an increased densification of the silica-networks [97]. The structure could change from linear to weakly branched polymers with more amount of water. For the formation of microporous silica membranes, short branched linear polymers are the most preferred in this case [98]. Qureshi and co-workers found that the acid and the amount of water affected BTESE particle size and size distribution [99].The concentration of sols coating on substrates also affected the membrane performance on gas separation. In the colloidal route, a solid nanoparticles dispersed stably in a liquid, which is achieved by adjusting the reaction of reactants solvent, catalyst, water, temperature, etc., resulting in a highly branched polymer.

This rapid condensation process causes particulate growth and/or the formation of precipitates [100-102]. Preparation of mesoporous silica layers can be considered by using colloidal dispersion.

Chemical vapor deposition (CVD) is an alternative way to prepare organosilica membranes. It consisted of thermal decomposition of a silicon-based precursor with an oxidant gas reaction either on the surface or in the pores of a hot substrate in one step, minimizing the drying and calcination steps as in sol-gel process. Low-temperature CVD can be realized by using strong oxidizing agents, plasma (plasma-enhanced CVD), or by incorporating a catalyst [13]. Ngamou et al. via prepared BTESE-derived silica membrane by an expanding thermal plasma chemical vapor deposition (ETP-CVD) technique [103]. The defect free films showed pervaporation performances of butanol/water comparable with sol-gel process. Nagasawa et al. also reported the fabrication of hexamethyldisiloxane (HMDSO)-derived amorphous silica membranes. This Ar-PECVD membrane showed CO_2/N_2 selectivity reached 130 due to the surface diffusion. The 2-step PECVD membrane showed high He and H_2 permeances with He/N_2 and H_2/N_2 permeance ratios of 4200 and 1900 at 400 ^oC, respectively [104]. New method by using photo-induced sol–gel processing was reported to fabricate silica membranes at low temperature. Radical and cationic polymerization of silica membranes showed high pervaporation performance for water/isopropanol separation [105].

1.4.4 Gas separation under dry and wet conditions

Castricum and his co-workers prepared hybrid organosilica membranes by flexible and rigid bridged silsesquioxane precursors, and adjusted the size, flexibility, shape, and electronic structure to tailor the separation performance [90]. The highest CO_2/H_2 permeance ratios, are obtained for longer ($Si\text{-}C_8H_{16}\text{-}Si$) alkene and aryl bridges due to the affinity of adsorption in the material. The membranes with a thin thickness of 160 nm showed a CO_2 permeance was as high as above10^{-7} mol $m^{-2}s^{-1}Pa^{-1}$, and the selectivity of CO_2/H_2 and CO_2/N_2 was 1.5-1.7 and 11-13 at 523k, respectively. Xu et al. studied Bis(triethoxysilyl) ethylene-derived organosilica membranes prepared with ethylene bridges (Si-CH=CH-Si). The membranes showed high permeance of CO_2 with a high selectivity CO_2/N_2 of 32 at 50^oC, which was explained to the strong CO_2 adsorption on the network with π -bond electrons [106]. Li et al. reported the effect of pendant groups on the organosilica membranes by using methyltriethoxysilane (MTES) and phenyltriethoxysilane (PhTES) precursors [89]. The

Si-MTES membrane had a high H_2/C_3H_8 selectivity of 1300, while Si-PhTES membrane had a selectivity of only 13.1, suggesting that Si-PhTES membrane had a much looser structure. Both of Si-MTES and Si-PhTES membranes showed hydrophobic properties compared with BTESE or BTESM membranes. Octyltriethoxysilane-derived silica membranes with pedant $-C_8H_{17}$ showed the H_2/N_2 and CO_2/N_2 selectivities of approximately 100 and 8, respectively [107].

Most of the membranes for gas separation performance were evaluated under dry conditions. Although the organosilica showed stability in water, the effect of water vapor on separation is not so clear. Xomeritakis et al. prepared a new aminosilicate membrane, and the CO_2 permeance was decreased as the relative humidity increased [108]. The CO_2 permeance decreased by a factor of six when the RH increased from 2-20%, and the selectivity of CO_2/N_2 from ~40 to~95 for the same increase in RH for membranes with ratio of NH_2 : Si = 0.2. At higher load of amine (NH_2 : Si = 0.5), the membranes showed less effect of water vapor on the CO_2 permeance and selectivity CO_2/N_2. Moreover, highly permeable and selective organosilica membranes were prepared on hydrophilic intermediate layers such as γ-Al_2O_3, SiO_2-ZrO_2 or TiO_2. Although the intermediate layers make no contribution to the separation performance, water capillary condensation in the pores and/or adsorption on the pore walls could occur. de Vos et al. prepared hydrophobic membranes by coating hydrophobic MeSi (400) top layers on hydrophilic γ-Al_2O_3 intermediate layers [109]. It was found some stabilization time was still needed for drying the hydrophobic membrane prior to conducting the gas permeance experiment. They concluded water adsorbed in the supported MeSi(400) membranes that was only likely to be present in the hydrophilic γ-Al_2O_3 intermediate layers. Few of research were done for gas separation through organosilica membranes under wet conditions.

1.5 Scope of this thesis

Organosilica membranes based gas separation have been considered to clean and low energy system, such as in natural gas purification, or CO_2 capture from coal-fired power plant. Most of membranes were prepared with great hydrophilicity from top to bottom to enhance

membrane performance. However, water vapor has a great effect on these hydrophilic membranes. The key objective of this thesis is to study the effect of water vapor on organosilica membranes, and prepare hydrophobic organosilica membranes which are expected to keep separation performance under wet conditions as well as under dry conditions. The main work of this research is as follows:

(1) The fabrication of organosilica membranes with a new type of hydrophobic bridged alkoxide with long organic chains.
(2) The development of hydrophobic intermediate layers with co-precursors under base catalyst.
(3) Improvement of separation performance of hydrophobic/hydrophobic organosilica membranes by plasma modification.

This thesis consists of 5 chapters, as follows:

Chapter 1 is "**General introduction**". The research background of gas separation of membranes were introduced under dry and wet conditions, and the purpose of this study was proposed.

Chapter 2 is "**CO_2 Permeation through Hybrid Organosilica Membranes in the Presence of Water Vapor**". Two types of organoalkoxysilanes, bis(triethoxysilyl)ethane (BTESE) and bis(triethoxysilyl)octane (BTESO) were used as precursors to prepare membranes via sol-gel method. The two membranes showed distinct properties on porous structures and water affinity because of differences in the bridging methylene numbers between the two Si atoms. Under dry conditions, the BTESE and BTESO membranes showed CO_2 permeances as high as 7.66×10^{-7} and 6.63×10^{-7} mol m^{-2} s^{-1} Pa^{-1} with CO_2/N_2 selectivities of 36.1 and 12.6 at 40 ℃, respectively. In the presence of water vapor, the CO_2 permeances were decreased for both membranes, but the effect of water vapor on CO_2 permeation is slighter for BTESO membranes than that for BTESE membranes due to more hydrophobicity and denser structures with a longer linking-bridge group. Both of hybrid organosilica membranes showed good reproducibility and stability in water vapor.

Chapter 3 is "**Preparation of organosilica membranes on hydrophobic intermediate layers and evaluation of gas permeation in the presence of water vapor**". Hydrophobic Me-SiO_2 sols were prepared by using tetraethoxysilane (TEOS) and methyltrimethoxysilane (MTMS) as co-precursors, coated on macroporous α-Al_2O_3 supports through multi-layered coatings. By characterization of nanopermporometry using hexane and water as condensable vapors, Me-SiO_2 layers showed pore diameter of approximately 2 nm and exhibited hydrophobic properties and that SiO_2-ZrO_2 layers were hydrophilic. Under dry conditions, BTESO/Me-SiO_2 showed a gas permeation trend that was similar to that of BTESO/SiO_2-ZrO_2. The selectivity of H_2/SF_6 for BTESE/Me-SiO_2 (334) was much lower than that of BTESE/SiO_2-ZrO_2 (>20,000) due to the inhomogeneous coatings of BTESE on the Me-SiO_2 layers. Under humidified conditions, BTESE/Me-SiO_2 and BTESO/Me-SiO_2 with hydrophobic intermediate layers, exhibited less decrease in CO_2 permeance compared with either BTESE/SiO_2-ZrO_2 or BTESO/SiO_2-ZrO_2, both of which were prepared with hydrophilic intermediate layers. The water vapor resulted in a negligible effect on gas permeance for totally hydrophobic BTESO/Me-SiO_2, while a little larger decrease was observed for hydrophilic top layers of BTESE/Me-SiO_2, showing that membranes with hydrophobic surface chemistry can effectively resist water vapor condensation or adsorption during gas permeation.

Chapter 4 is "**Plasma-assisted multi-layered coating towards improved gas permeation properties for organosilica membranes**". H_2O vapor plasma was used for the modification of hydrophobic Me-SiO_2 intermediate layer by generating hydrophilic groups on the surface without changing either the bulk hydrophobicity or the pore size. After plasma treatment of the Me-SiO_2 layers, BTESE or BTESO-derived sols were coated as separation layers. The gas selectivity for BTESE membrane was improved after water plasma treatment, which allowed better adhesion between each layer via the enhanced hydrophilic modification by water plasma. Under wet conditions, the CO_2 permeance for both membranes were decreased, slightly larger decrease than for membranes without plasma treatment, but much less than the BTESE and BTESO membranes prepared on hydrophilic SiO_2-ZrO_2 intermediate layers. High gas permeation properties were obtained in the presence of water for organosilica membranes

prepared from hydrophobic top layers to hydrophobic intermediate layers via plasma-assisted multi-layered coatings.

Chapter 5 is "**Conclusions**". Several important conclusions of this study are given in detail and suggestions are provided for further study.

References

[1] K.P. Lee, T.C. Arnot, D. Mattia. A review of reverse osmosis membrane materials for desalination-Development to date and future potential. J. Membr. Sci. 370 (2011) 1-22.

[2] B.D. Freeman, I. Pinnau. Gas and Liquid Separations Using Membranes: An Overview. ACS Symposium Series, Washington, DC, 2004.

[3] R.W. Baker. Membrane technology and applications. Membrane Technology and Research, Inc. Menlo Park, California, Second edition, 2004.

[4] Y. Yampolskii, B.D. Freeman. Membrane Gas Separation. John Wiley & Sons Ltd., Singapore, First edition, 2010.

[5] M. Mulder. Basic Principles of Membrane Technology. Kluwer Academic publishers, Netherland, 1996.

[6] C.A. Scholes, K.H. Smith, S.E. Kentish, G.W. Stevens. CO_2 capture from pre-combustion processes-Strategies for membrane gas separation. Int. J. Greenh. Gas Con. 4 (2010) 739-755.

[7] M.L. Keen, F.A. Gotch. Dialyzers and Delivery Systems in Introduction to Dialysis. New York, (1991) 1-7.

[8] G. MacLaren, A. Combes, R.H. Bartlett. Contemporary extracorporeal membrane oxygenation for adult respiratory failure: life support in the new era. Intensive Care Med. 38 (2012) 210-220.

[9] J. Shaw. Development of Transdermal Therapeutic Systems. Drug. Dev. Ind. Pharm. 9 (1983) 579.

[10] J. Wilcox. Carbon Capture. Springer Science+Business Media, 2012.

[11] J. Kim, M. Abouelnasr, L.C. Lin, B. Smit. Large-Scale Screening of Zeolite Structures for CO_2 Membrane Separations. J. Am. Chem. Soc. 135 (2013) 7545-7552.

[12] G.T. Rochelle. Amine Scrubbing for CO_2 Capture. Science. 325 (2009) 1652-1654.

[13] M. Pera-Titus. Porous Inorganic Membranes for CO_2 Capture: Present and Prospects. Chem. Rev. 114 (2014) 1413-1492.

[14] M. Aresta. A. Dibenedetto. Carbon Dioxide Fixation into Organic Compounds. In Carbon Dioxide Recovery and Utilization; Kluwer Academic Publishers, The Netherlands, 2003.

[15] E. Favre. Carbon dioxide recovery from post-combustion processes: Can gas permeation membranes compete with absorption? J. Membr. Sci. 294 (2007) 50-59.

[16] C.A. Scholes, S.E. Kentish, G.W. Stevens. Effects of Minor Components in Carbon Dioxide Capture Using Polymeric Gas Separation Membranes. Sep. Purif. Rev. 38 (2009) 1-44.

[17] I.C. Omole, R.T. Adams, S.J. Miller, W.J. Koros. Effects of CO_2 on a High Performance Hollow-Fiber Membrane for Natural Gas Purification. Ind. Eng. Chem. Res. 49 (2010) 4887-4896.

[18] Y. Yampolskii, I. Pinnau, B.D. Freeman. Materials Science of Membranes for Gas and Vapor Separation. John Wiley & Sons, Ltd. England, 2006.

[19] L.M. Robeson. Correlation of separation factor versus permeability for polymeric membranes. J. Membr. Sci. 62 (1991) 165-185.

[20] L.M. Robeson. The upper bound revisited. J. Membr. Sci. 320 (2008) 390-400.

[21] H.B. Park, C.H. Jung, Y.M. Lee, A.J. Hill, S.J. Pas, S.T. Mudie, E. Van Wagner, B.D. Freeman, D.J. Cookson. Polymers with cavities tuned for fast selective transport of small molecules and ions. Science 318 (2007) 254-258.

[22] P.M. Budd, K.J. Msayib, C.E. Tattershall, B.S. Ghanem, K.J. Reynolds, N.B. McK-eown, D. Fritsch. Gas separation membranes from polymers with intrinsic microporosity. J. Membr. Sci. 251 (2005) 263-269.

[23] C. Nagel, K. Günther-Schade, D. Fritsch, T. Strunskus, F. Faupel. Free volume and transport properties in highly selective polymer membranes. Macromolecules. 35 (2002) 2071-2077.

[24] M. Pera-Titus. Porous Inorganic Membranes for CO_2 Capture: Present and Prospects. Chem. Rev. 114 (2014) 1413-1492.

[25] R.M. de Vos, H. Verweij. High-Selectivity, High-Flux Silica Membranes for Gas Separation. Science. 279 (1998) 1710-1711.

[26] H.H. Tseng, P.T. Shiu, Y.S. Lin, J. Int. Effect of mesoporous silica modification on the structure of hybrid carbon membrane for hydrogen separation. Int. J. Hydrogen Energy. 36 (2011) 15352-15363.

[27] R.W. Baker, K. Lokhandwala. Natural gas processing with membranes: An overview. Ind. Eng. Chem. Res. 47 (2008) 2109 - 2121.

[28] R.W. Baker. Future directions of membrane gas separation technology. Ind. Eng. Chem. Res. 41 (2002) 1393-1411.

[29] S.J. Metz, W.J.C. van de Ven, M.H.V. Mulder, M. Wessling. Transport of water vapor and inert gas mixtures through highly selective and highly permeable polymer membranes. J. Membr. Sci. 251 (2005) 29-41.

[30] H. Sijbesma, K. Nymeijer, R. van Marwij, R. Heijboer, J. Potreck, M. Wessling. Flue gas dehydration using polymer membranes. J. Membr. Sci. 313 (2008) 263-276.

[31] F. Piroux, E. Espuche, R. Mercier. The effects of humidity on gas transport properties of sulfonated copolyimides. J. Membr. Sci. 232 (2004) 115-122.

[32] M. P. Chenar, M. Soltanieh, T. Matruura, A. Tabe-mohammadi, K.C. Khulbe. The effect of water vapor on the performance of commercial polyphenylene oxide and Cardo-type polyimide hollow fiber membranes in CO_2/CH_4 separation applications. J. Membr. Sci. 285 (2006) 265-271.

[33] C. A. Scholes, G. W. Stevens, S. E. Kentish. The effect of hydrogen sulfide, carbon monoxide and water on the performance of a PDMS membrane in carbon dioxide/nitrogen separation. J. Membr. Sci. 350 (2010) 189-199.

[34] G.Q. Chen, C.A. Scholes, G.G. Qiao, S. E. Kentish. Water vapor permeation in polyimide membranes. J. Membr. Sci. 379 (2011) 479- 487.

[35] L. Ansaloni, M. Minelli, M. Giacinti Baschetti, G.C. Sarti. Effect of relative humidity and temperature on gas transport in Matrimids : Experimental study and modeling. J. Membr. Sci. 471 (2014) 392 -401.

[36] J. Potreck, K. Nijmeijer, T. Kosinski, M. Wessling. Mixed water vapor/gas transport through the rubbery polymer PEBAX®1074. J. Membr. Sci. 338 (2009) 11-16.

[37] S.J. Metz, W.J.C. Ven, M.H.V. Mulder, M. Wessling. Mixed gas water vapor/N_2 transport in poly(ethylene oxide) poly(butylene terephthalate) block copolymers. J. Membr. Sci. 266 (2005) 51-61.

[38] S.R. Reijerkerk, R. Jordana, K. Nijmeijer, M. Wessline. Highly hydrophilic, rubbery membranes for CO_2 capture and dehydration of flue gas. Int. J. Greenh. Gas. Con. 5 (2011) 26-36.

[39] H. Sijbesma, K. Nymeijer, R. V. Marwijk, R. Heijboer, J. Potreck, M. Wessling. Flue gas dehydration using polymer membranes. J. Membr. Sci. 313 (2008) 263-276.

[40] S.R. Reijerkerk, A.C. IJzer, K. Nymeijer, A. Arun, R.J. Gaymans, M. Wessling.

Subambient Temperature CO_2 and Light Gas Permeation through Segmented Block Copolymers with Tailored Soft Phase. Appl. Mater. Interf. 2 (2010) 551-560.

[41] G.Q. Chen, C.A. Scholes, C.M. Doherty, A.J. Hill, G.G. Qiao, S. E. Kentish. Modeling of the sorption and transport properties of water vapor in polyimide. J. Membr. Sci. 4090-410 (2012) 96-104.

[42] G.Q. Chen, C.A. Scholes, C.M. Doherty, A.J. Hill, G.G. Qiao, S. E. Kentish. The thickness dependence of Matrimid films in water vapor permeation. Chem. Eng. J. 209 (2012) 301-312.

[43] C.A. Scholes, B.D. Freeman, S. E. Kentish. Water vapor permeability and competitive sorption in thermally rearranged (TR) membranes. J. Membr. Sci. 470 (2014) 132-137.

[44] J. Zou, W.S.W. Ho. CO_2-selective membranes containing dimethylglycine mobile carriers and polyehtylenimine fixed carrier. J. Membr. Sci. 286 (2006) 310-321.

[45] A. Ito, M.Sato, T. Anma. Permeability of CO_2 Through chitosan membrane swollen by water vapor in feed gas. Angew. Makromol. Chem. 248 (1997) 85-94.

[46] M. Asaeda, S. Yamasaki. Separation of inorganic/organic gas mixtures by porous silica membranes. Sep. Purif. Technol. 25 (2001) 151-159.

[47] X. Gu, J. Dong, T. M. Neoff. Synthesis of Defect-Free FAU-Type Zeolite Membranes and Separation for Dry and Moist CO_2/N_2 Mixtures. Ind. Eng. Chem. Res. 44 (2005) 937-944.

[48] P. Kumar, S. Kim, J. Ida, V.V. Guliants. Polyethyleneimine-Modified MCM-48 Membranes: Effect of Water Vapor and Feed Concentration on N_2/CO_2 Selectivity. Ind. Eng. Chem. Res. 47 (2008) 201-208.

[49] J.C. Poshusta, R.D. Noble, J.L. Falconer. Characterization of SAPO-34 membranes by water adsorption. J. Membr. Sci. 186 (2008) 25-41.

[50] T. Tomita, K. Suzuki, K. Nakayama, K. Yajima. S. Yoshida. Synthesis and Permeation Properties of a DDR-Type Zeolite Membrane for Separation of CO_2/CH_4 Gaseous Mixtures. Ind. Eng. Chem. Res. 46 (2007) 6989-6997.

[51] H. Wang, Y.S. Lin. Effects of Water Vapor on Gas Permeation and Separation Properties of MFI Zeolite Membranes at High Temperatures. AlChE J. 58 (2012) 153-162.

[52] C.W. Jones, W. J. Koros. Characterization of Ultramicroporous Carbon Membranes with Humidified Feeds. Ind. Eng. Chem. Res. 34 (1995) 158-163.

[53] S. Lagorsse, F.D. Magalhães, A. Mendes. Aging study of carbon molecular sieve membranes. J. Membr. Sci. 310 (2008) 494-502.

[54] Y. Li, F. Liang, H. Bux, W. Yang, J. Caro. Zeolitic imidazolate framework ZIF-7 based molecular sieve membrane for hydrogen separation. J. Membr. Sci. 354 (2010) 48-54.

[55] H.W. Kim, H.W. Yoon, B.M. Yoo, J.S. Park, K.L. Gleason, B.D. Freeman, H.B. Park. High-performance CO_2-philic graphene oxide membranes under wet-conditions. Chem. Commun. 50 (2014)13563-13566.

[56] R. Ciriminna, A. Fidalgo, V. Pandarus, F. Béland, L.M. Ilharco, M. Pagliaro, The Sol-Gel Route to Advanced Silica-Based Materials and Recent Applications. Chem. Rev. 113 (2013) 6592-6620.

[57] K.J. Shea, D.A. Loy. Bridged Polysilsesquioxanes. Molecular-Engineered Hybrid Organic-Inorganic Materials. Chem. Mater. 13 (2001) 3306-3319.

[58] G. Cerveau, R.J.P. Corriu, E. Framery. Influence of the nature of the catalyst on the textural properties of organosilsesquioxane materials. Polyhedron. 19 (2000) 307-313.

[59] M.F. Montemor. Functional and smart coatings for corrosion protection: A review of recent advances. Surf. Coat. Technol. 258 (2014) 17-37.

[60] T. Ribeiro, C. Baleizão, J.P.S. Farinha. Functional Films from Silica/Polymer Nanoparticles. Mater. 7 (2014) 3881-3900.

[61] M. Kanezashi, K. Yada, H. T.Yoshioka, T. Tsuru. Design of Silica Networks for Development of Highly Permeable Hydrogen Separation Membranes with Hydrothermal Stability. J. Am. Chem. Soc. 131(2009) 414-415.

[62] G. Qi, L. Fu, X. Duan, B.H. Choi, M. Abraham. E.P. Giannelis. Mesoporous amine-bridged polysilsesquioxane for CO_2 capture. Greenh. Gases. 1 (2011) 278-294.

[63] N. N. Khimich. Synthesis of Silica Gels and Organic-Inorganic Hybrids on Their Base. Glass. Phys. Chem. 30 (2004) 430-442.

[64] D.A. Loy, K.J. Shea. Bridged polysilsesquioxanes. Highly porous hybrid organic -inorganic materials. Chem. Rev. 95 (1995) 1431-1442.

[65] H.L. Castricum, G.G. Paradis, M.C. Mittelmeijer-Hazeleger, R. Kreiter, J.F. Vente, J.E. Ten Elshof. Tailoring the separation behavior of hybrid organosilica membranes by adjusting the structure of the organic bridging group. Adv. Funct. Mater. 21 (2011) 2319-29.

[66] I. Agirre, P.L. Arias, H.L. Castricum, M. Creatoree, J.E. ten Elshof, G.G. Paradis, P.H.T.

Ngamou, H.M. van Veen, J.F. Vente. Hybrid organosilica membranes and processes: Status and outlook. Sep. Sci. Technol. 121 (2014) 2-12.

[67] H.R. Lee. Fabrication and Evaluation of Pore-size-tuned silica membranes with Disiloxane Alkoxides for gas separation. Thesis, 2011.

[68] S. Dash, S. Mishra, S. Patel. B.K. Mishra. Organically modified silica: Synthesis and applications due to its surface interaction with organic molecules. Adv. Colloid. Interf. Sci. 140 (2008) 77- 94.

[69] R.A. Fleming, M. Zou. Silica nanoparticle-based films on titanium substrates with long-term superhydrophilic and superhydrophobic stability. Appl. Sur. Sci. 280 (2013) 820-827.

[70] H.L. Castricum, G.G. Paradis, M.C. Mittelmeijer-Hazeleger, R. Kreiter, J.F. Vente, J.E. ten Elshof. Tailoring the Separation Behavior of Hybrid Organosilica Membranes by Adjusting the Structure of the Organic Bridging Group. Adv. Funct. Mater. 21(2011) 2319-2329.

[71] G. Dubois, W. Volksen, T. Magbitang, M.H. Sherwood, R.D. Miller, D.M. Gage, R.H. Dauskardt. Superior mechanical properties of dense and porous organic/inorganic hybrid thin films. J Sol-Gel. Sci. Technol. 48 (2008)187-193.

[72] G. Gong, J. Wang, H. Nagasawa, M. Kanezashi, T. Yoshioka, T. Tsuru. Sol-gel spin coating process to fabricate a new type of uniform and thin organosilica coating on polysulfone film. Mater. Lett. 109 (2013) 130-133.

[73] Y.H. Han, A. Taylor, K.M. Knowles. Characterisation of organic–inorganic hybrid coatings deposited on aluminium substrates. Surf. Coat. Technol. 202 (2008) 1859-1868.

[74] M. Yutaka, D. Yusuke, M. Atsushi, K. Masafumi, Y. Tetsuo. Phase-separation and distribution of phenyl groups for PhTES-TEOS coatings prepared on polycarbonate substrate. J. Sol-Gel. Sci. Technol. 58 (2011) 80-84.

[75] A.V. Rao, S. S. Latthe, D/Y. Nadargi, H. Hirashima, V. Ganesan. Preparation of MTMS based transparent superhydrophobic silica films by sol-gel method. J. Colloid. Interf. Sci. 332 (2009) 484-490.

[76] O Görbig, S Nehlsen, J Müller. Hydrophobic properties of plasma polymerized thin film gas selective membranes. J. Membr. Sci. 138 (1998) 115-121.

[77] A. Kuzminova, A. Shelemin, O. Kylián, M. Petr, J. Kratochvíl, P. Solař, H. Biederman. From super-hydrophilic to super-hydrophobic surfaces using plasma polymerization

combined with gas aggregation source of nanoparticles. Vac. 110 (2014) 58-61.

[78] I. Santana, A. Pepe, E. Jimenez-Pique, S. Pellice, S. Ceré. Silica-based hybrid coatings for corrosion protection of carbon steel. Part I: Effect of pretreatment with phosphoric acid. Surf. Coat. Technol. 236 (2013) 476-484.

[79] Y.-H. Han, A. Taylor, M.D. Mantle, K.M. Knowles. UV curing of organic-inorganic hybrid coating materials. J. Sol-Gel. Sci. Technol. 43 (2007) 111-123.

[80] M.E.L. Wouters. D. Wolfs, M.V.D. Linde, J. Hovens, A. Tinnemans. Transparent UV curable antistatic hybrid coatings on polycarbonate prepared by the sol-gel method. Progress. Organic. Coatings. 51 (2004) 312-320.

[81] R. Nisticò, D. Scalarone, G. Magnacca. Preparation and physico-chemical characterization of large-mesopore silica thin films templated by block copolymers for membrane technology. Microporous and Mesoporous Materials. 190 (2014) 208-214.

[82] G. Gopalakrishnan, J.C. D. da Costa. Hydrogen gas mixture separation by CVD silica membrane. J Membr Sci. 323 **(**2008) 144-147.

[83] T. Tsuru, S. Shigemoto, M. Kanezashi, T. Yoshioka. 2-Step plasma-enhanced CVD for low-temperature fabrication of silica membranes with high gas-separation performance. Chem. Commun. 47 (2011) 8070-8072.

[84] M.C. Duke, J.C.D. Da Costa, D.D. Do, P. G. Gray, G.Q. Lu. Hydrothermally robust molecular sieve silica for wet gas separation. Adv. Funct. Mater. 16 (2006) 1215-1220.

[85] H.M. Van Veen, M.D. Rietkerk, D.P. Shanahan, M. van Tuel, R. Kreiter, H.L. Castricum, J.F. Vente. Pushing membrane stability boundaries with HybSi@ pervaporation membranes, J. Membr. Sci. 380 (2011) 124-131.

[86] R. Xu, J. Wang, M. Kanezashi, T. Yoshioka, T. Tsuru. Development of robust organosilica membranes for reverse osmosis. Langmuir. 27 (2011) 13996-13999.

[87] R. Kreiter, M.D.A. Rietkerk, H.L. Castricum, H.M. Van Veen, J.E. Ten Elshof, J.F. Vente. Evaluation of hybrid silica sols for stable microporous membranes using high-throughput screening. J. Sol-Gel Sci. Technol. 57 (2011) 245-252.

[88] M. Kanezashi, M. Kawano, T. Yoshioka, T. Tsuru. Organic-Inorganic Hybrid Silica Membranes with Controlled Silica Network Size for Propylene/Propane Separation. Ind. Eng. Chem. Res. 51 (2012) 944-953.

[89] G. Li, M. Kanezashi, T. Tsuru. Preparation of organic-Inorganic hybrid silica

membranes usin organoalkoxysilanes: The effect of pendant groups. J. Membr. Sci. 379 (2011) 287-295.

[90] H.L. Castricum, G.G. Paradis, M.C. Mittelmeijer-Hazeleger, R. Kreiter, J.F. Vente, J.E. ten Elshof. Tailoring the Separation Behavior of Hybrid Organosilica Membranes by Adjusting the Structure of the Organic Bridging Group. Adv. Funct. Mater. 21 (2011) 2319-2329.

[91] M. Kanezashi, K. Yada, T. Yoshioka, T. Tsuru. Design of Silica Networks for Development of Highly Permeable Hydrogen Separation Membranes with Hydrothermal Stability. J. Am. Chem. Soc. 131 (2009) 414-415.

[92] H.R. Lee, M. Kanezashi, Y. Shimomura, T. Yoshioka, T. Tsuru. Evaluation and fabrication of pore-size-tuned silica membranes with tetraethoxydimethyl disiloxane for gas separation. AlChE J. 57 (2011) 2755-2765.

[93] M. Naito, K. Nakahira, Y. Fukuda, H. Mori, J. Tsubaki. Process conditions on the preparation of supported microporous SiO_2 membranes by sol-gel modification techniques. J. Membr. Sci.129 (1997) 263-269.

[94] M. Kanezashi, S. Miyauchi, H. Nagasawa, T. Yoshioka, T. Tsuru. Gas permeation properties through Al-doped organosilica membranes with controlled network size. J. Membr. Sci. 466 (2014) 246 -252.

[95] T. Tsuru, T Nakasuji, M Oka, M Kanezashi, T. Yoshioka. Preparation of hydrophobic nanoporous methylated SiO_2 membranes and application to nanofiltration of hexane solutions. J. Membr. Sci. 384 (2011) 149-156.

[96] R.J.R. Uhlhorn, K. Keizer, A.J. Burggraaf. Gas transport and separation with ceramic membranes. Part II. Synthesis and separation properties of microporous membranes. J. Membr. Sci. 66 (1992) 271-287.

[97] T. Niimi, H. Nagasawa, M. Kanezashi, T. Yoshioka, K. Ito, T. Tsuru. Preparation of BTESE-derived organosilica membranes for catalytic membrane reactors of methylcyclohexane dehydrogenation. J. Membr. Sci. 455 (2014) 375-383.

[98] K. Kuraoka, N. Kubo, T. Yazawa. Microporous Silica Xerogel Membrane with High Selectivity and High Permeance for Carbon Dioxide Separation. J. Sol-Gel. Sci. Technol. 19 (2000) 515-518.

[99] H.F. Qureshi, A. Nijmeijer, L. Winnubst. Influence of sol-gel process parameters on the micro-structure and performance of hybrid silica membranes. J. Membr. Sci. 446 (2013)

19-25.

[100] T. Tsuru. Porous Ceramics for Filtration, Handbook of Advanced Ceramics. Academic Press, Oxford, 2003, 291-312.

[101] T. Tsuru. Nano/subnano-tuning of porous ceramic membranes for molecular separation. J. Sol-Gel. Sci. Technol. 46(2008)349-361.

[102] Z.Y. Yeo, T.L. Chew, P.W. Zhu, A.R. Mohamed, S.P. Chai. Synthesis and performance of microporous inorganic membranes for CO_2 separation: a review. J. Porous. Mater. 20(2013) 1457-1475.

[103] P.H.T. Ngamou, J.P. Overbeek, R. Kreiter, H.M. van Veen, J.F. Vente, I.M. Wienk, P.F. Cuperusc, M. Creatore. Plasma-deposited hybrid silica membranes with a controlled retention of organic bridges. J. Mater. Chem. A. 1 (2013) 5567-5576.

[104] M. Nishibayashi, H. Yoshida, M. Uenishi, M. Kanezashi, H. Nagasawa, T. Yoshioka, T. Tsuru. Photo-induced sol-gel processing for low-temperature fabrication of high-performance silsesquioxane membranes for use in molecular separation. Chem. Commun. 51 (2015) 9932-9935.

[105] H. Nagasawa, H. Shigemoto, M. Kanezashi, T. Yoshioka, T. Tsuru. Characterization and gas permeation properties of amorphous silica membranes prepared *via* plasma enhanced chemical vapor deposition. J. Membr. Sci. 441 (2013): 45-53

[106] R. Xu, M. Kanezashi, T. Yoshioka, T. Okuda, J. Ohshita, T. Tsuru. Tailoring the Affinity of Organosilica Membranes by Introducing Polarizable Ethenylene Bridges and Aqueous Ozone Modification. ACS Appl. Mater. Interf. 5 (2013) 6147-6154.

[107] K. Kusakabe, S. Sakamoto, T. Saie, S. Morooka. Pore structure of silica membranes formed by a sol–gel technique using tetraethoxysilane and alkyltriethoxysilanes. Sep. Purif. Technol. 16 (1999) 139-146.

[108] G. Xomeritakis, C.Y. Tsai, C.J. Brinker. Microporous sol-gel derived aminosilicate membrane for enhanced carbon dioxide separation. Sep. Purif. Technol. 42 (2005) 249-257.

[109] R.M. de Vos, W.F. Maier, H.Verweij. Hydrophobic silica membranes for gas separation. J. Membr. Sci. 158 (1999) 277-288.

Chapter 2

CO_2 permeation through hybrid organosilica membranes in the presence of water vapor

2.1 Introduction

Currently, the capture and separation of CO_2 from gas mixtures have become very important commercial activities in many applications. Several techniques are available including commercialized amine-solvent absorption, but the use of membrane-based CO_2 separation is a potential technology due to the advantages of simplicity and high-energy efficiency. Large varieties of membranes have been developed to achieve high CO_2 permeation performance [1-3]. Polymeric membranes for CO_2 separation have been summarized by Robeson [4]. In Robeson's correlation, most polymers showed CO_2 permeability of 1-100 barrer with CO_2/N_2 selectivity lower than 40 and that of CO_2/CH_4 lower than 100. Lin and Hirayama et al. reported that blend membranes with ethylene oxide as the unit showed a relatively high CO_2 permeability in a range of 510-62 barrer and selectivity 36-69 [5-6]. The main problems that limit the use of polymeric membranes are their poor thermal, mechanical and chemical stability at high pressure and temperature. Since the 1990s, membranes or films coated with zeolite and zeolite-like materials have been prepared and applied because of the molecular sieving properties, and high thermal and chemical stability. Some types of zeolite membranes showed high permeance and relatively high selectivity for CO_2 separation. It is reported that FAU, DDR, SAPO-34 and MFI-zeolite membrane showed CO_2 permeances on the order of 10^{-8}-10^{-7} mol m^{-2} s^{-1} Pa^{-1} and a higher CO_2/N_2 selectivity that ranged from 20 to 100 [7-10].

Most of the membranes for gas permeation were evaluated under dry conditions. In industrial applications, however, most of the operations, such as removing CO_2 from flue gases, capturing CO_2 from natural gas, are processed in the presence of water vapor [11-14]. The transport of gas mixed with water vapor through membranes has become very important.

It should be noted that the water molecule shows very different behaviors owing to a small kinetic diameter and high critical temperature, and even a minor amount of water vapor may affect the permeation properties of other gases [13]. Reijerkerk et al. [12] and Chen et al. [15] reported that CO_2 permeability for polymers in the presence of water vapor were decreased by about 30% of that under dry conditions. For zeolite membranes, the hydrophilic FAU membranes with micropores showed a drastic decrease in CO_2 and N_2 permeances of nearly 99.6% and 88% at 50 ℃ [16]. Funke et al. reported that for a hydrophobic silicalite zeolite membrane, the N_2 permeance was decreased to 50% of its dry values [17]. However, sufficient information currently is not available to draw conclusions and tendencies on gas permeation in the presence of water vapor.

Organosilica membranes are a type of organic-inorganic hybrid membranes, which can be easily prepared via sol-gel method with thin films, controlled permeation properties with various organic functional groups, and maintaining the thermally stable structures at a temperature as high as 300 ℃ even in an oxidative atmosphere due to the inorganic silica in the structure [18]. Recently, new organoalkoxides, instead of tetraethoxysilane (TEOS), have been proposed as precursor materials to prepare organosilica membranes by several groups [19-28]. In particular, bridge alkoxides consisting of two Si atoms and organic linking groups, such as bis(triethoxysilyl)ethane (BTESE) and bis(triethoxysilyl)methane (BTESM), were used to prepare organosilica membranes with controllable pore sizes, which were confirmed by NKP (Normalized Knudsen-based permeance) method analysis [22-24]. These kinds of hybrid organosilica membranes showed good performance in dry gas separation and water system applications with thermally and chemically stable structures. Kanezashi et al. reported a high H_2 permeance of 6×10^{-6} mol m^{-2} s^{-1} Pa^{-1} with high separation selectivity for H_2/SF_6 of 25500, and moderate values for H_2/N_2 of 23 and CO_2/N_2 of 5 at 200 ℃ by using BTESE [23]. Kreiter et al. reported CO_2 permeance for BTESM and BTESE membranes almost on the order of 10^{-7} mol m^{-2} s^{-1} Pa^{-1} but with different H_2/N_2 and H_2/CO_2 selectivities [27]. The traits of excellent long stability were shown in water on the applications of reverse osmosis (RO) even at 90 ℃ and pervaporation at 150 ℃ [18, 19]. It also should be noted that surface properties including hydrophilicity-hydrophobicity can be controlled by the linking group [21,22]. Therefore, a better understanding of the hybrid silica membranes prepared with different bridged alkoxides, and the performance of gas permeation under the dry or wet conditions, is very important to develop high-performance membranes and realize efficient

applications in practical industries in the future. To the best of our knowledge, the effects of water vapor on organosilica membranes with different linking groups have not reported.

In this work, bridged organoalkoxysilanes, bis(triethoxysilyl)ethane (BTESE) and bis(triethoxysilyl)octane (BTESO), as shown in Figure 2.1, were investigated to prepare organosilica membranes via a sol-gel method. The two materials were characterized by FT-IR, adsorption isotherms and water contact angle. The membranes with different numbers of methylene linking groups into silica networks were systematically studied by single gas permeation properties under dry conditions. The effects of the presence of water vapor on CO_2 gas permeation for BTESE and BTESO membranes were examined at 40 ℃.

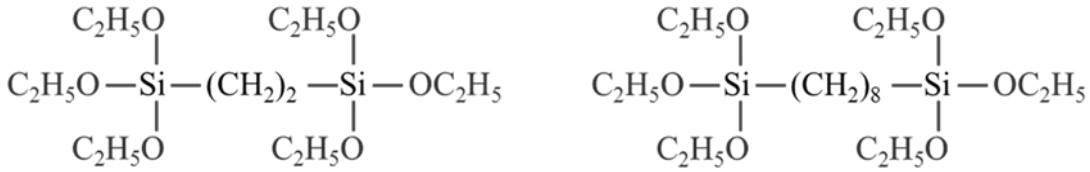

(a) BTESE (b) BTESO

Figure 2.1 Structures of bridged organoalkoxysilanes used in this work (a) Bis(triethoxysily)ethane (BTESE) and (b) Bis(triethoxysily)octane (BTESO).

2.2 Experimental section

2.2.1 Preparation of hybrid organosilica sols and membranes

Hybrid organosilica sols were prepared by hydrolysis and polymerization of bridged alkoxide BTESE and BTESO purchased from Gelest, Inc. The monomer alkoxides were homogeneously dissolved in ethanol, water and HCl as catalyst with molar ratios of BTESE/H_2O/HCl = 1: 60: 0.1 and BTESO/H_2O/HCl = 1: 120: 0.1. Then the solutions were under continuous stirring in a closed system at 25 ℃ to prepare stable and clear silica sols. The weight concentrations of BTESE and BTESO were kept at 5.0 wt.%, respectively. The BTMSH monomer alkoxide with molar ratios of BTMSH/H_2O/HCl = 1: 120: 0.1 was used for comparision. The preparation steps for BTMSH membrane were the same as that of BTESE and BTESO membranes.

Porous α-alumina tubes (average pore size: 1-2 μm) were used for supports as previously reported [23]. First, two types of α-Al_2O_3 particles (2 and 0.2 μm) were coated on the outer surface of the support and then fired at 550 ℃. These procedures were repeated several times in order to cover larger pores. Then the SiO_2-ZrO_2 sols (Si/Zr=1/1) were deposited onto the pre-heated support at 200 ℃, followed by firing at 550 ℃. These procedures also were repeated several times to form an intermediate layer with a pore size of about 1-2 nm. Finally, the top layer was fabricated by coating BTESE or BTESO-derived silica sols, followed by drying and calcination at 300 ℃ for 30 min. Hereafter, the membranes will be referred to as BTESE and BTESO membrane. A homogeneous silicone rubber (SR) membrane (outside diameter: 9 mm, inside diameter: 7 mm) was kindly supplied by Nagayanagi CO., LTD. (Japan) and used for comparison.

2.2.2 Characterization of hybrid organosilica sols and membranes

The hybrid organosilica films were formed on KBr plates via dip-coating method and were characterized at room temperature by Fourier transform infrared (FT-IR) spectroscopy (FT-IR-4100, JASCO). The silica gel powders were characterized by N_2 and H_2O adsorption/desorption isotherms measurements (Belsorp MAX, BEL Japan, Inc.) at 77 K and 298 K, respectively. The hydrophilicity of the silica films was measured using a microscopic contact angle meter with FAMAS software (DropMaster DM-300, KYOWA INTERFACE SCIENCE, Co., Ltd). Membrane morphology and thickness was examined by scanning electron microscopy (JCM-5700, JEOL).

2.2.3 Gas permeation measurement

Two types of measurements were carried out to evaluate the gas permeance. A schematic diagram of the apparatus for the dry gas permeation tests was found in a previous paper [22]. The membrane was dehydrated first by helium at 200 ℃ for 10 h. Then a single gas was tested at 40 ℃. The pressure drop through the membranes was maintained at 1bar, while the permeate stream was kept at atmospheric pressure.

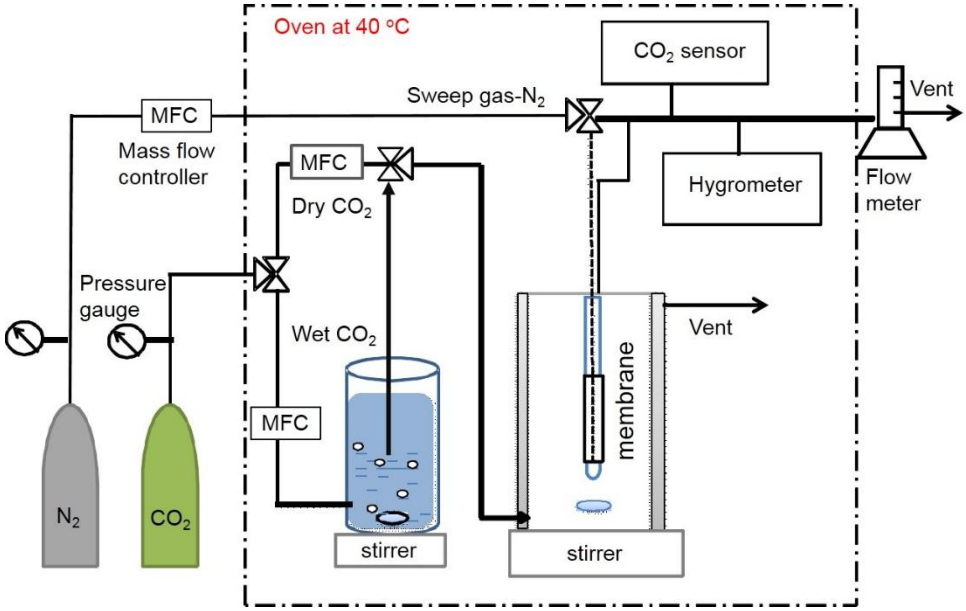

Figure 2.2 Schematic diagram of gas/water vapor mixtures permeation testing apparatus.

The schematic permeation equipment of gas/water vapor mixtures is shown in 2.2. The feed and permeate streams were kept at atmospheric pressure. Here, the water activity in feed was controlled by mixing two streams. One stream was CO_2 being bubbled through water to obtain wet CO_2 gas. The other stream was the dry CO_2 gas. By controlling the flow rate of the two streams (total feed flow rate was a constant), the different water activities were obtained and measured using a hygrometer (HygroFlex, error range: ±2% RH, Rotonic, Switzerland). The temperature was maintained at 40 °C. In the permeate stream, N_2 was fed as sweep gas to carry permeated CO_2 and water vapor continuously to CO_2 sensor (GMT221 and GMT222, error range: ± 0.02% and 20 ppm, Vaisala, Finland) and the hygrometer. The total flow rate was measured with a bubble film meter.

The CO_2 and H_2O permeances were calculated by the following equations:

$$P_i = \frac{F_i}{A} \bullet \frac{1}{\Delta p_i} \qquad (2.1)$$

F_i is the permeated molar flow rate of the component *i* and can be calculated by using total flow rate F_t as follows

CO_2 flow rate: $$F_{CO_2} = F_t \bullet C_{CO_2} \qquad (2.2)$$

H_2O flow rate:

$$F_{H_2O} = F_t \bullet \frac{p_{H_2O,S}}{p_{atm}} \bullet RH\% \qquad (2.3)$$

Where C_{CO2} is the CO_2 concentration and *RH%* is the water relative humidity in the permeate stream. Δp_i is an average driving force of CO_2 gas or H_2O vapor for permeation, which can be calculated by using the following logarithmic average:

$$\Delta p_i = \frac{\Delta p_1 - \Delta p_2}{\ln \frac{\Delta p_1}{\Delta p_2}} = \frac{(p_f - p_{p,in}) - (p_r - p_{p,out})}{\ln \frac{(p_f - p_{p,in})}{(p_r - p_{p,out})}} \qquad (2.4)$$

where Δp_1, Δp_2 are the partial pressure differences of the component *i* between the feed and permeate stream at the entrance and the exit of the module, respectively. The partial pressure of CO_2 and H_2O was zero in the permeate stream ($p_{p,\,in} = 0$) at the entrance of the module. At the exit of the permeate stream, the partial pressure $p_{p,\,out}$ was obtained by CO_2 concentration and relative humidity. In the retentate stream, the partial pressures (p_r) of CO_2 and H_2O were calculated by mass balances over the module.

Thus, the permeance can be calculated by using the following equations:

CO_2 permeance:

$$Perm_{CO_2} = \frac{F_{CO_2}}{A\,\Delta P} = \frac{F_t \times \frac{P_{CO2,\,P}}{P_{atm}}}{A \cdot \frac{P_{CO2,\,P}}{\ln \frac{P_{CO2,\,f} - P_{CO2,\,P}}{P_{CO2,\,f}}}} = \frac{F_t}{\frac{A\,P_{atm}}{\ln\left[\frac{P_{atm} - P_{H2O,\,f}}{(P_{atm} - P_{H2O,\,f}) - P_{atm} \times C_{CO2,\,P}}\right]}} \qquad (2.5)$$

H_2O permeance:

$$Perm_{H_2O} = \frac{F_{H2O}}{A\,\Delta P} = \frac{F_t \times \frac{P_{H2O,\,P}}{P_{atm}}}{A \cdot \frac{P_{H2O,\,P}}{\ln \frac{P_{H2O,\,f} - P_{H2O,\,P}}{P_{H2O,\,f}}}} = \frac{F_t}{\frac{A\,P_{atm}}{\ln\left[\frac{P_{H2O,\,f}}{P_{H2O,\,f} - RH\% \times P_{H2O,\,S}}\right]}} \qquad (2.6)$$

where C_{CO2} is the CO_2 concentration, *RH%* is the water relative humidity in the permeate stream, and F_t is the total flow rate in permeate steam.

2.3 Results and disccussion

2.3.1 Characterization of BTESE and BTESO

Figure 2.3 shows the FT-IR spectra of BTESE and BTESO films coated on KBr plates and fired at 300 ℃. The vibrations appearing at 3000-2800 cm^{-1} and 1487-1270 cm^{-1} were assigned to the C-H stretching and blend vibration [29, 30]. The BTESO films showed apparent characteristic peaks of $-CH_2$ due to a large number of $-CH_2-$ in the silicon network compared with that in BTESE. Both films showed strong peaks at 1000-1100 cm^{-1} that can be assigned to the Si-O-Si groups, indicating successful hydrolysis and condensation of the monomers. The broad adsorption band observed at 3200-3800 cm^{-1} was attributed to OH stretching mode of silanols [31]. BTESE films showed a higher absorbance ratio of $Abs_{(Si\text{-}O\text{-}H)}/Abs_{(Si\text{-}O\text{-}Si)}$ than that of BTESO, indicating more number of silanol groups probably were in the silica structures, with the propensity to absorb a higher amount of water.

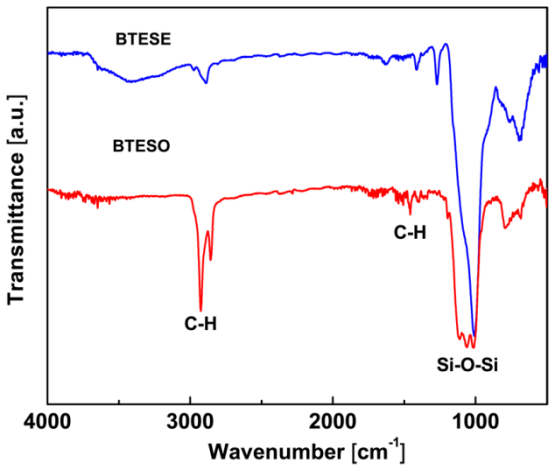

Figure 2.3 FT-IR spectra of BTESE and BTESO films fired at 300 ℃.

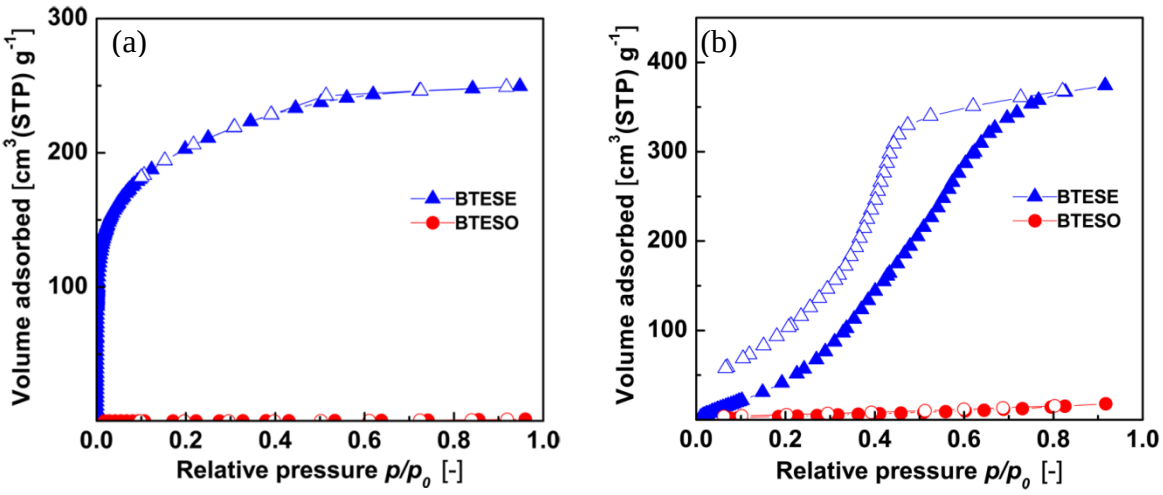

Figure 2.4 Adsorption/desorption isotherms of (a) N_2 at 77 K and (b) H_2O at 298 K for BTESE and BTESO gel powders, respectively. (closed: adsorption, open: desorption)

The contact angles of water droplets on surfaces of the silica films were measured. The film samples were prepared by coating silica sols on slide glasses and firing at 300 ℃. The contact angles for BTESE and BTESO were 58 ° and 86 °, respectively. This obviously indicates that the BTESO film was more hydrophobic than the BTESE film. Li et al. [22] reported the use of methyltriethoxysilane (MTES) and phenyltriethoxysilane (PhTES) as Si precursors, which showed higher contact angles than TEOS due to the presence of hydrophobic methyl and phenyl groups. Using a silica precursor with long carbon chains like BTESO is another way to obtain more hydrophobic surface chemistry.

Figure 2.4 shows the adsorption/desorption isotherms of N_2 and H_2O on BTESE and BTESO silica gel powders. BTESE gel showed type I isotherm curve that indicated its microporous properties. According to BET and MP methods, the surface area and micropores were 722 m^2 g^{-1} and 0.6 nm, respectively. However, BTESO gel showed a very low N_2 adsorption volume, indicating that a limited number of pores were available in the silica gels. In Figure 2.4 (b), the water sorption volume of BTESO gel was also much smaller than that of BTESE gel, which showed approximately the same order as the adsorption amount of N_2. The types of linking units clearly affected the structures. Octane, a long bridge-linking unit between two silicon atoms (BTESO), is more flexible than ethane (BTESE). Shea and Los [32] reported that the formation of network is a function of the degree of condensation at the silicon and flexibility of the bridging group, which determined the porosity of the materials. A

long flexible alkylene in BTESO is such an example that can lead to collapse of the porosity, and formed a dense structure.

Based on the characterizations of FT-IR, contact angles and adsorption/desorption isotherms, the organosilica gels of BTESE showed properties of hydrophilicity and a microporous structure compared with BTESO gels that have hydrophobic property and a limited number of pores.

2.3.2 Permeation properties of dry gas through BTESE and BTESO membranes

The single gas permeances of He, H_2, CO_2, O_2, N_2, C_3H_8, CF_4 and SF_6 at 40 ℃ are shown for BTESE and BTESO membranes in Figure 2.5. BTESE and BTESO membranes showed a high CO_2 permeance of 7.66×10^{-7} and 6.63×10^{-7} mol m^{-2} s^{-1} Pa^{-1}, respectively. The permeance of CO_2 was higher than that of He and H_2, despite a larger kinetic diameter. This is because a strong affinity for CO_2 can occur at a lower temperature, resulting in a large sorption or solubility by hybrid organosilica membranes. The tendency also can be found in other types of SiO_2 membranes [33-35]. Moreover, both membranes showed high selectivity toward CO_2 over N_2; the highest selectivity was 36.1 for BTESE and 12.6 for BTESO. Compared with polymer and zeolite membranes, as presented in Figure 2.6, the hybrid organosilica membranes of BTESE and BTESO showed higher CO_2 permeance and relatively high CO_2/N_2 selectivity. However, the selectivities of He/N_2 (15.5) and CO_2/N_2 for BTESE membrane were more than twice that of BTESO membrane at 40 ℃. Kreiter et al. [27] also showed a similar trend that the short bridging group resulted in high selectivity. This is probably because BTESE with 2 methylene groups between two Si atoms formed microporous structure that was suitable for gas separation, while BTESO structure was less microporous with 8 methylene groups. In addition, the apparent activation energy of N_2 for BTESO membrane was higher than that of BTESE (as discussed later in Figure 2.7b), which also indicated a flexible structure. The permeances of other gasses such as He and H_2 for BTESO membranes were similar to that of BTESE, indicating that the octane bridge is more randomly flexible than staggered, which would leave ample space between the Si-O-Si groups for molecular transport [33].

Various bridged alkoxides of Si-(CH_2)x-Si were used as organosilica membrane materials to detailedly investigate the effect of the linking units on membrane permeation properties. A

polyethylene membrane with an infinite methylene number was shown for comparison. Figure 2.7(a) shows the selectivity of He/N_2 for BTESM, BTESE, BTMSH (bis-trimethoxysily-hexane), BTESO and PE membranes. The scattered values of selectivities were due to the different preparation conditions; in particular, the water ratio to bridged alkoxides in hydrolysis greatly affected the permeation properties. Here, curves were drawn based on the average selectivities. As the methylene number increased, the selectivities were found to decrease. The permeation selectivities for the long chains of -CH_2- membranes (octyl) seemed to approach those of PE. This suggests that the network from a looser structure gradually changed into non-porous structures with an increase of carbon number in the linking groups. The apparent activation energy is summarized in Figure 2.7 (b), calculated by the following equation [34] with temperature dependence of gas permeance.

$$P = P_0 \exp(-\frac{E_A}{RT}) \qquad (2.7)$$

where P is the gas permeance and E_A is the apparent activation energy. As shown in the figure, the E_A value of N_2 permeation increased as the methylene number increased. The polyethylene membrane [37] with -CH_2-CH_2 backbones showed an apparent activation energy of 33.6 kJ mol^{-1}, which was much higher than other hybrid organosilica membranes. It should be noted that the silicone rubber membrane consisting of Si-O-Si backbones and organic pendant groups showed an E_A value of just 6.58 kJ mol^{-1} for the permeance of N_2 [38], which was nearly the same as the 8Me (BTESO) membrane.

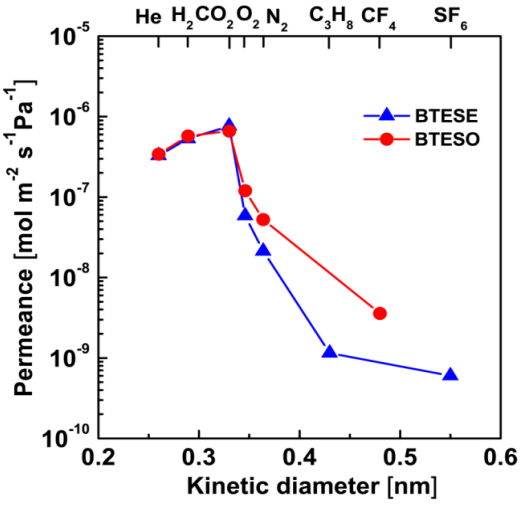

Figure 2.5 Single gas permeance for BTESE and BTESO membranes as a function of kinetic diameter at 40 ℃.

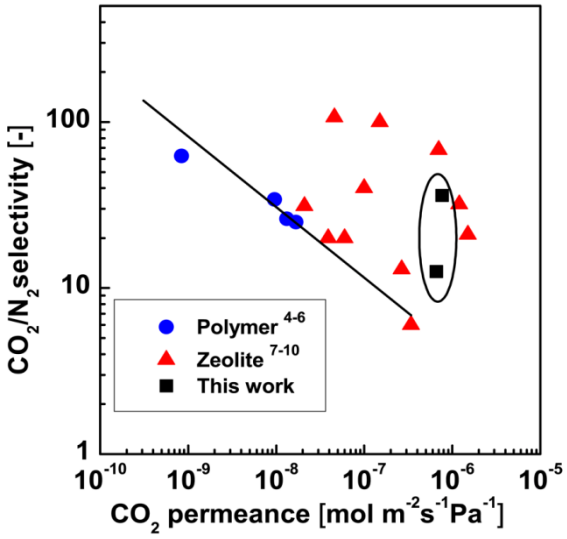

Figure 2.6 CO_2/N_2 selectivity for polymer,[4-6] zeolite[7-10] and hybrid silica (BTESE, BTESO) membranes as a function of CO_2 permeance at 20-50 ℃. The solid line shows a Robeson upper-bound trend in permeance unit. The data in the circle were drawn from this work.

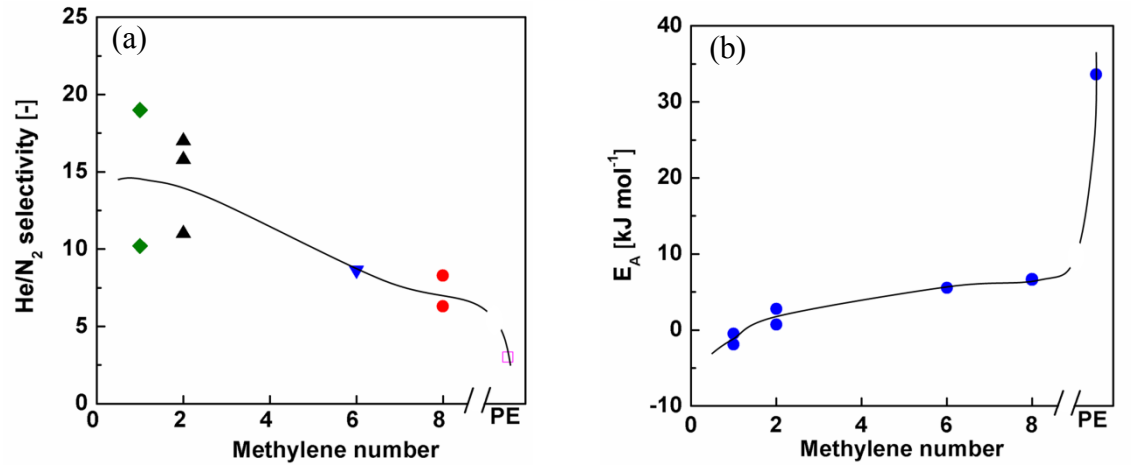

Figure 2.7 The permeation properties of organosilica membranes with different numbers of methylene and polyethylene membranes: (a) He/N_2 permeance selectivity for 1Me-8Me at 200-250 ℃ and PE at 75 ℃; (b) Apparent activation energy of N_2 as a function of methylene number. [1Me: BTESM (Si-CH_2–Si)[20, 27]; 2Me: BTESE (Si-$(CH_2)_2$–Si)[23, 36]; 6Me: BTMSH (Si-$(CH_2)_6$–Si)[this work] (Supporting Information: 1.); 8Me: BTESO (Si-$(CH_2)_8$–Si)[this work, 33]; PE: Polyethylene (-CH_2–CH_2-)$_n$[37])].

2.3.3 The effect of water vapor activity on CO_2 permeance

The effect of water vapor on CO_2 gas was tested by changing the water activity. Figure 2.8 (a) and (b) show the CO_2 and H_2O permeances for BTESE, BTESO and SR membranes in the presence of water vapor. The CO_2 permeance under humidified conditions for both BTESE and BTESO membranes were decreased largely at a low water activity compared with dry CO_2. As for the SR membrane, the CO_2 permeance was quite low, but just slightly decreased and was almost constant even at an increased water activity. To confirm the reproducibility, another set of BTESE (E2) and BTESO (O2) membranes were prepared. Figure 2.9 shows these membranes by dimensionless permeance of CO_2 (normalized by its dry permeance). In the figure, the BTESE (E2) and BTESO (O2) membranes show a trend similar to that of the BTESE (E1) and BTESO (O1) membranes over a wide range of water activities. The CO_2 permeance for BTESE membranes was decreased gradually to approximately one-hundredth at an activity of 0.83, while that was about one-tenth at water activity from 0.2 to 0.7 for BTESO membranes.

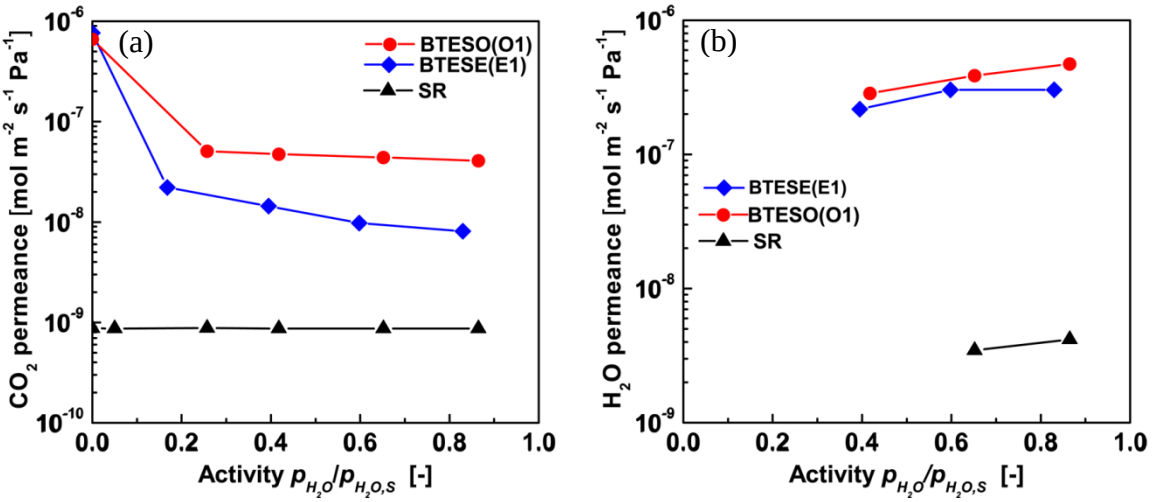

Figure 2.8 (a) CO_2 and (b) H_2O permeances for BTESE, BTESO and SR membranes as a function of water vapor activity at 40 ℃.

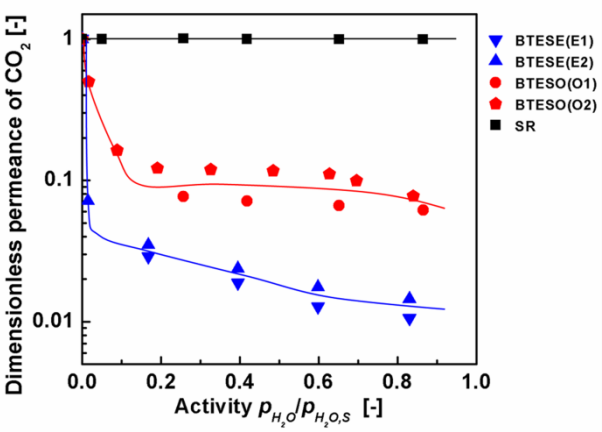

Figure 2.9 Dimensionless permeance of CO_2 as a function of water vapor activity at 40 ℃.

The different trends in decreased CO_2 permeance for the three membranes were probably due to the surface chemistry (water affinity) and structural properties. The SR membrane was homogeneous, while the two organosilica membranes were asymmetric in structure consisting of three active separation layers: particle layer, intermediate layer and top layer, as shown in Figure 2.10. The pore size of the SiO_2-ZrO_2 intermediate layer is about 1-2 nm. When the organosilica sols were coated on the intermediate layer, they formed a continuously thin layer that was indistinguishable even at 30000× image magnification. The BTESE and BTESO membranes had the same particle and intermediate layer, but with different chemical properties of organosilica top layer. As for the BTESE membrane, the top layer was more hydrophilic with microporous structure, while the BTESO was hydrophobic with less microporous structure. According to the Kelvin equation, when the material shows the properties of higher hydrophilicity and smaller pore size, the phenomenon of capillary condensation of water vapor will occur more easily. Therefore, a probable explanation to the larger decrease in CO_2 permeance for the BTESE membrane was attributed to the water adsorption in the pores and blocked CO_2 gas diffusion, while the resistance for CO_2 transport through the BTESO membrane was diminished.

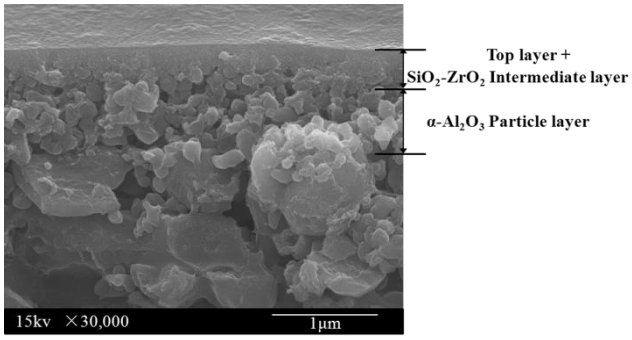

Figure 2.10 The Cross-section SEM image of the organosilica membrane.

The SR membrane was hydrophobic and had dense structures, very similar to chemical properties of BTESO. However, The BTESO membrane showed larger permeance decrease than that of the SR membrane, which was probably due to the layered structures (asymmetric). In BTESO membranes, the SiO_2-ZrO_2 intermediate and α-Al_2O_3 particle layers also showed high hydrophilic and porous properties. That means the two layers were favorable for water absorption and capillary condensation, blocking CO_2 transport through the membrane.

Water permeances are also represented as a function of water activity for the three membranes in Figure 2.8(b). It should be noted that the H_2O permeance at low water activity is not shown since the relative humidity in the permeate stream was too small (less than 2%) to be measured by the hygrometer sensor. Normally, all membranes showed higher H_2O permeances than CO_2. That is because water molecules have a high diffusivity due to a small kinetic diameter and high adsorption or solubility. The BTESO membrane showed a high water permeance similarly to the BTESE membrane, probably due to the flexible structure with ample space at 40 ^oC and high diffusivity of water in the membrane. Both of the hybrid organosilica membranes showed higher H_2O permeances than that of SR membrane, probably owing to the thinner films (less than 2 μm including three layers) than SR membrane (1 mm).

The dimensionless permeance of gas for the BTESE and BTESO hybrid organosilica membranes were compared with zeolite and polymer membranes in the presence of water vapor, as shown in Table 2.1. It should be noted that the dimensionless permeance (normalized by its dry permeance) represents the decrease degree of permeance.

Table 2.1 Dimensionless permeance of gas for zeolite, hybrid silica and polymer membranes in the presence of water vapor.

Membrane	Gas	Permeance [mol m^{-2} s^{-1} Pa^{-1}]	RH %	Dimensionless permeance [-]	Temperature [℃]	Reference
BTESE	CO_2	7.66×10^{-7}	83%	0.01	40	This
BTESO	CO_2	6.63×10^{-7}	86.5%	0.06	40	work
SAPO-34	CO_2	1×10^{-7}	60%	~ 0.008	23	39
FAU	CO_2	~ 7.8×10^{-8}	20%	~ 0.004	50	16
DDR	CO_2	2.5×10^{-7}	100%	0.44	25	10
Si- MCM-48	O_2	2×10^{-8}	90%	0.25	-	40
Al- MCM-48	O_2	~ 5×10^{-9}	90%	~ 0.1	-	40
PPO	CO_2	3.76×10^{-8}	60%	0.89	30	41
Caro-polyimide	CO_2	3×10^{-8}	60%	0.57	30	41
PDMS	CO_2	~ 6.2×10^{-9}	41%	~ 0.95	35	42
	N_2	~1.76×10^{-9}	41%	~ 0.95	35	42

In zeolite membranes, SAPO-34 as well as FAU type membranes have the properties of hydrophilic surface and a rigid microporous structure. In the presence of water vapor, these membranes showed the lowest dimensionless permeance of CO_2 [16, 39]. The decrease was explained as a reduction of zeolite pore volume by adsorption of water molecules. On the other hand, the polymers showed the highest dimensionless permeance of CO_2 compared with hybrid organosilica and zeolite membranes, probably due to the flexible “pores” or denser structures. In addition, the rubbery polymer PDMS showed less of a decrease in permeance than that of a glass polymer PPO membrane, which consisted of microvoids [41,42]. The permeance for a PDMS membrane was decreased only by 5% of the dry value, which was in agreement with the SR membrane in this work. As to the property of water affinity, the hydrophobic membranes showed less decrease of permeance in wet conditions. For example, in the case of small-pore zeolite membranes, a highly hydrophobic DDR membrane showed the gas permeance reduced to 44% of dry value, which was far less decrease than the

hydrophilic SAPO-34 membrane (0.8%) [10, 39]. In mesoporous membranes, such as hydrophobic Si-MCM-48 silica membrane, the dimensionless permeance of gas was higher than that of hydrophilic Al-MCM-48 membrane, which had the same pore structures [40]. Similar results can be found in polymer membranes. The permeance for hydrophobic PPO was just decreased by 11%, which was less than that of a hydrophilic Caro-polyimide membrane with a reduction of 43% [41]. Thus, it can be concluded that the membrane with denser structure and more hydrophobic property (dry gas permeance may be smaller), the decrease ratio of gas permeance will be smaller in the presence of water vapor.

2.3.4 CO_2 permeation properties in the presence of water vapor

The CO_2 permeation properties as a time course was shown for BTESE and SR membranes at different sweep flow rate, as shown in Figure 2.11. The feed stream was maintained at atmospheric pressure, while the N_2 as sweep gas in the permeate stream ranged from 960-200 ml/min for BTESE and 200-30 ml/min for SR membrane under atmospheric pressure. The different sweep flow rates were fed for BTESE and SR membranes to obtain CO_2 concentration within a measurement range. The CO_2 permeance based on CO_2 concentration calculated by the equation (1) did not change for BTESE membrane as well as SR membrane at a given sweep flow rate, indicating a good water stability of hybrid organosilica membranes.

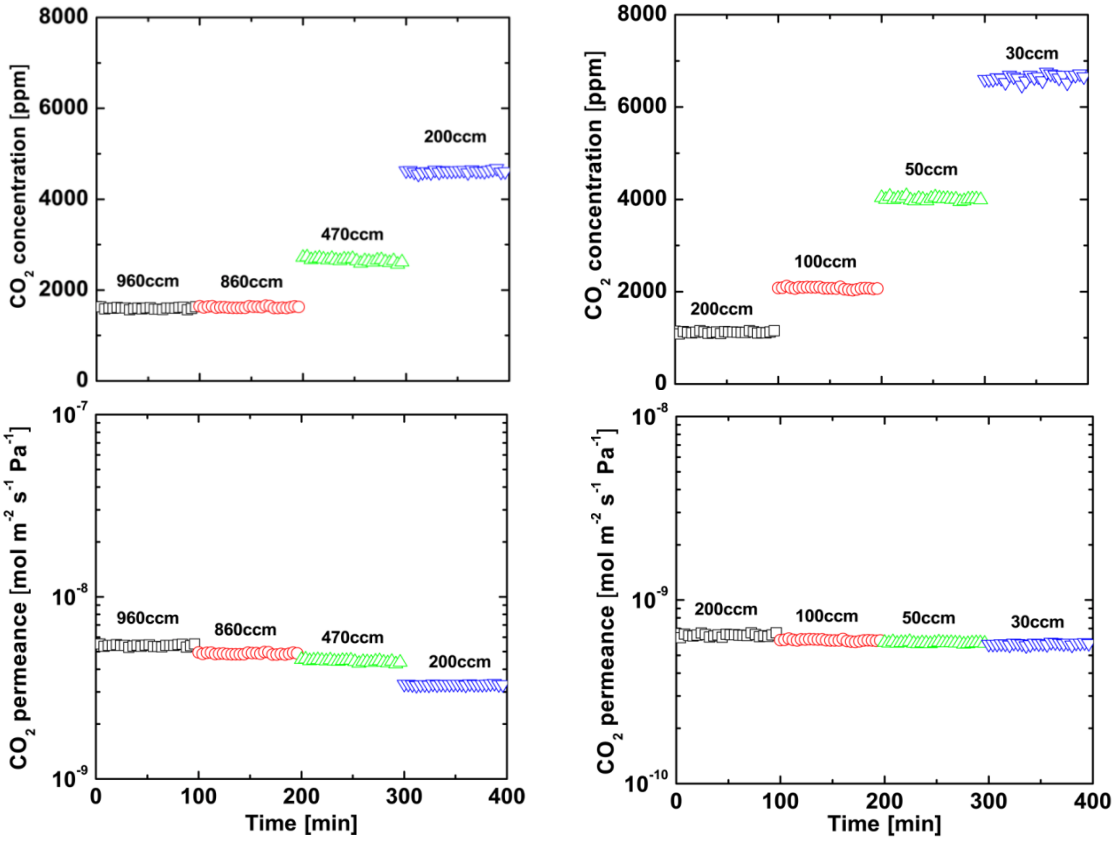

Figure 2.11 CO_2 concentration and permeance at different sweep flow rate for (a) BTESE and (b) SR membranes in the presence of water vapor (activity = 0.8) under 40 ℃.

2.4 Conclusions

The hybrid organosilica membranes of BTESE and BTESO were prepared via sol-gel method. Both membranes showed good performance for CO_2 gas separation under dry conditions. Due to the different bridging units between two silicon atoms, BTESE and BTESO membranes showed different properties on porosity in structure and water affinity. These properties resulted in different effects of water vapor on CO_2 permeation. The CO_2 permeance was decreased largely for BTESE membranes due to microporous structure and hydrophilic properties that led to water adsorption in the pores easily and decreased CO_2 gas diffusivity. The CO_2 permeance decrease ratio for BTESO membrane with a long bridging unit was smaller than BTESE membrane on account of the reduced microporocity and

hydrophobic properties. In addition, silicone rubber with a dense structure and high hydrophobic properties showed a minor effect of water vapor on CO_2 permeation.

Based on this work, we can propose a workable strategy for the choosing of membrane materials. For the application of dehydration from gas, it is better to choose a material with porous structure and hydrophilic property; for gas separation from water vapor, it is better to choose a material with dense structure and hydrophobic property.

References

[1] I.C. Omole, R.T. Adams, S.J. Miller, W.J. Koros. Effects of CO_2 on a High Performance Hollow-Fiber Membrane for Natural Gas Purification. Ind. Eng. Chem. Res. 49 (2010) 4887-4896.

[2] K. Ramasubramanian, Y.N. Zhao, W.S.W. Ho. CO_2 Capture and H_2 Purification: Prospects for CO_2-Selective Membrane Processes. AIChE J. 59 (2013) 1033-1045.

[3] R.W. Baker. Membrane Technology and Applications. Membrane Technology and Research; John Wiley & Sons Ltd: England, 2004.

[4] L.M. Robeson. The upper bound revisited. J. Membr. Sci. 320 (2008) 390-400.

[5] H. Lin, B.D. Freeman. Materials selection guidelines for membranes that remove CO_2 from gas mixtures. J. Mol. Struct. 739 (2005) 57-74.

[6] Y. Hirayama, Y. Kase, N. Tanihara, Y. Sumiyama, Y. Kusuki, K. Haraya. Permeation properties to CO_2 and N_2 of poly(ethylene oxide)-containing and crosslinked polymer films. J. Membr. Sci. 160 (1999) 87-99.

[7] K. Kusakabe, T. Kuroda, A. Murata, S. Morooka. Formation of a Y-Type Zeolite Membrane on a Porous α-Alumina Tube for gas separation. Ind. Eng. Chem. Res. 36 (1997) 649-655.

[8] V. Sebastián, I. Kumakiri, R. Bredesen, M. Menéndez. Zeolite membrane for CO_2 removal: Operating at high pressure. J. Membr. Sci. 292 (2007) 92-97.

[9] S. Li, C.Q. Fan. High-Flux SAPO-34 Membrane for CO_2/N_2 Separation. Ind. Eng. Chem. Res. 49 (2010) 4399-4404.

[10] S. Himeno, T. Tomita, K. Suzuki, K. Nakayama, K. Yajima, S. Yoshida. Synthesis and Permeation Properties of a DDR-Type Zeolite Membrane for Separation of CO_2/CH_4 Gaseous Mixtures. Ind. Eng. Chem. Res. 46 (2007) 6989-6997.

[11] Y. Yampolskii, I. Pinnau, B.D. Freeman. Materials Science of Membranes for Gas and Vapor Separation. John Wiley & Sons Ltd: England, 2006.

[12] S.R. Reijerkerk, R. Jordana, K. Nijmeijer, M. Wessling. Highly hydrophilic, rubbery membranes for CO_2 capture and dehydration of flue gas. Int. J. Greenh. Gas. Con. 5 (2011) 26-36.

[13] C.A. Scholes, S.E. Kentish, G.W. Stevens. Effects of Minor Components in Carbon Dioxide Capture Using Polymeric Gas Separation Membranes. Sep. Purif. Rev. 38 (2009) 1-44.

[14] H. Sijbesma, K. Nijmeijer, R.V. Marwijk, R. Heijboer, J. Potreck, M. Wessling. Flue gas dehydration using polymer membranes. J. Membr. Sci. 313 (2008) 263-276.

[15] G.Q. Chen, C.A. Scholes, G.G. Qiao, S.E. Kentish. Water vapor permeation in polyimide membranes. J. Membr. Sci. 379 (2011) 479-487.

[16] X. Gu, J. Dong, T.M. Nenoff. Synthesis of Defect-Free FAU-Type Zeolite Membranes and Separation for Dry and Moist CO_2/N_2 Mixtures. Ind. Eng. Chem. Res. 44 (2005) 937-944.

[17] H.H. Funke, K.R. Frender, K.M. Green, J.L. Wilwerding, B.A. Sweitzer, J.L. Falconer, R.D. Noble. Influence of adsorbed molecules on the permeation properties of silicalite membranes. J. Membr. Sci. 129 (1997) 77-82.

[18] H. L. Castricum, A. Sah, R. Kreiter, D.H.A. Blank, J.F. Vente, J.E. ten Elshof. Hydrothermally stable molecular separation membranes from organically linked silica. J. Mater. Chem.18 (2008) 2150-2158.

[19] R. Xu, J. Wang, M. Kanezashi, T. Yoshioka, T. Tsuru. Development of Robust Organosilica Membranes for Reverse Osmosis. Langmuir. 27 (2011) 13996-13999.

[20] M. Kanezashi, M. Kawano, T. Yoshioka, T. Tsuru. Organic-Inorganic Hybrid Silica Membranes with Controlled Silica Network Size for Propylene/Propane Separation. Ind. Eng. Chem. Res. 51 (2012) 944-953.

[21] G.G. Paradis, D.P. Shanahan, R. Kreiter, J.F. Vente, H.L. Castricum, A. Nijmeijer, J.E. ten Elshof. From hydrophilic to hydrophobic HybSi® membranes: A change of affinity and applicability. J. Membr. Sci. 428 (2013) 157-162.

[22] G. Li, M. Kanezashi, T. Tsuru. Preparation of organic-inorganic hybrid silica membranes using organoalkoxysilanes: The effect of pendant groups. J. Membr. Sci. 379 (2011) 287-295.

[23] M. Kanezashi, K. Yada, T. Yoshioka, T. Tsuru. Organic–inorganic hybrid silica membranes with controlled silica network size: Preparation and gas permeation characteristics. J. Membr. Sci. 348 (2010) 310-318.

[24] H.R. Lee, T. Shibata, M. Kanezashi, T. Mizumo, J. Ohshita, T. Tsuru. Pore-size-controlled silica membranes with disiloxane alkoxides for gas separation. J. Membr. Sci. 383 (2011) 152-158.

[25] M. Kanezashi, K. Yada, T. Yoshioka, T. Tsuru. Design of Silica Networks for Development of Highly Permeable Hydrogen Separation Membranes with Hydrothermal Stability. J. Am. Chem. Soc. 131 (2009) 414-415.

[26] H. Qi, J. Han, N. Xu. Effect of calcination temperature on carbon dioxide separation properties of a novel microporous hybrid silica membrane. J. Membr. Sci. 382 (2011) 231-237.

[27] R. Kreiter, M.D.A. Rietkerk, H.L. Castricum, H.M. van Veen, J.E. ten Vente, Elshof. Evaluation of hybrid silica sols for stable microporous membranes using high-throughput screening. J. Sol-Gel. Sci. Technol. 57 (2011) 245-252.

[28] N.K. Raman, C.J. Brinker. Organic "template" approach molecular sieving silica membranes. J. Membr. Sci. 105 (1995) 273-279.

[29] B. Cao, Y.G. Tang, C.Sh. Zhu. Synthesis and Hydrolysis of Hybridized Silicon Alkoxide: Si(OEt)x(OBut)4-x. Part I: Synthesis and Identificationof the Si(OEt)x(O-But)4-x. J. Sol-Gel. Sci. Technol. 10 (1997) 247-253.

[30] J. Coates. Interpretation of Infrared Spectra, A Practical Approach. Encyclopedia of Analytical Chemistry. 2000, 10815-10837.

[31] S.K. Parida, S. Dash, S. Patel, B.K. Mishra. Adsorption of organic molecules on silica surface. Adv. Colloid. Interface. Sci. 121 (2006) 77-110.

[32] K.J. Shea, D.A. Loy. Bridged Polysilsesquioxanes. Molecular-Engineered Hybrid Organic-Inorganic Materials. Chem. Mater. 13 (2001) 3306-3319.

[33] H.L. Castricum, G.G. Paradis, M.C. Mittelmeijer-Hazeleger, R. Kreiter, J.F. Vente, J.E. ten Elshof. Tailoring the Separation Behavior of Hybrid Organosilica Membranes by Adjusting the Structure of the Organic Bridging Group. Adv. Funct. Mater. 21 (2011) 2319-2329.

[34] T. Yoshioka, E. Nakanishi, T. Tsuru, M. Asaeda. Experimental study of gas permeation through microporous silica membranes. AIChE J. 47 (2001) 2052-2063.

[35] M.C. Duke, J.C. Costa, G.Q. Lu, M. Petch, P. Gray. Carbonised template molecular sieve silica membranes in fuel processing systems: permeation, hydrostability and regeneration. J. Membr. Sci. 241 (2004) 325-333.

[36] H.F. Qureshi, A. Nijmeijer, L. Winnubst. Influence of sol-gel process parameters on the micro-structure and performance of hybrid silica membranes. J. Membr. Sci. 446 (2013) 19-25.

[37] J.P.G. Villaluenga, B. Seoane. Experimental Estimation of Gas-Transport Properties of Linear Low-Density Polyethylene Membranes by an Interal Permeation Method. J. Appl. Polym. Sci. 82 (2001) 3013-3021.

[38] J.E. Lundstrom, R.J. Bearrian. Inert Gas Permeation through Homopolymer Membranes. J. Polym. Sci. Polym Physics. 12 (1974) 97-114.

[39] J.C. Poshusta, R.D. Noble, J.L. Falconer. Characterization of SAPO-34 membranes by water adsorption. J. Membr. Sci. 186 (2001) 25-40.

[40] S.K. Seshadri, Y.S. Lin. Synthesis and water vapor separation properties of pure silica and aluminosilicate MCM-48 membranes. Sep. Purif. Technol. 76 (2011) 261-267.

[41] M.P. Chenar, M. Soltanieh, T. Matsuura, A.Tabe-mohammadi, K.C. Khulbe. The effect of water vapor on the performance of commercial polyphenylene oxide and Cardo-type polyimide hollow fiber membranes in CO_2/CH_4 separation applications. J. Membr. Sci. 285 (2006) 265-271.

[42] C.A. Scholes, G.W. Stevens, S.E. Kentish. The effect of hydrogen sulfide, carbon monoxide and water on the performance of a PDMS membrane in carbon dioxide/nitrogen separation. J. Membr. Sci. 350 (2010) 189-199.

Chapter 3

Preparation of organosilica membranes on hydrophobic intermediate layers and evaluation of gas permeation in the presence of water vapor

3.1 Introduction

The separation of CO_2 was widely investigated using polymeric, inorganic and hybrid (e.g. organosilica, metal-organic frameworks) membranes in gas separation technologies [1-5]. Gas separation is generally achieved by differences in the diffusion rates and/or solution/adsorption ability of components in the membranes. Preparation of high performance membranes for CO_2 separation is very important for climate and industrial applications. Polymeric membranes are commonly used in industry due to their low cost, manufacturability and simple module design. The CO_2 permeability of polymeric membranes is usually 1-1000 barrers and the selectivity of CO_2/N_2 is lower than 100 [3,4]. Porous inorganic or hybrid membrane system, commonly consists of a macroporous support and an overlying thin, either porous or dense separation layers, offering higher permeance than polymeric membranes. The permeance of CO_2 was about 10^{-7} mol/(m^2 s Pa) and the highest selectivity of CO_2/N_2 reached 800 using modified silica membranes [5].

Most of these membranes for gas separation were measured under dry conditions. Nevertheless, in some industrial applications, such as removing CO_2 from flue gases or natural gas, membranes are used under a wet atmosphere [6-8]. When water vapor exists in the process, polymeric membranes suffer from swelling or plasticization as well as aging effects by dissolved water which exerts a strong influence on membrane performance [9-10]. Inorganic porous membranes, however, have higher thermal, chemical stability and better biofouling resistance than polymeric membranes. However, it is reported that the selectivity was unchanged but the permeance of CO_2 decreased largely for most of porous membranes under the humidified conditions [5,11-13]. These may be due to hydrophilicity of membranes

that causes the water adsorption/condensation in the rigid pores, thereby hindering CO_2 transport. For example, hydrophobic macroporous membranes are usually used in membrane distillation process, since the pores cannot be wetted by the water and only vapor not liquid can be transported [14-15]. Therefore, hydrophobic membranes with high gas separation performance as well as high resistance to water and long stability under humidified conditions are required.

For ceramic membranes, asymmetric structures usually exhibit a graded change in pore diameter from 100 nm-50 nm (α-alumina support layer) to 5-1 nm (intermediate layer), and then to 0.1-0.6 nm (＜100 nm thick, ultrathin silica top-layer), which have great potential for gas separation applications with high permeance and selectivity [5]. Microporous silica membranes which are usually prepared using tetraethoxysilane (TEOS), are unfortunately instable in the presence of water vapor [16-17]. Hybrid organosilica membranes have recently been reported using new types of alkoxides [18-26]. The hybrid materials lie in the silicon atoms connected with organic groups, including bridged and pendant polysilsesquioxanes. The success of the approach is demonstrated at this stage by depositing organosilica membranes according to well-known polymeric silica sol-gel routes [19]. These types of hybrid organosilica membranes showed good performances on gas separation and exhibited thermally and chemically stable structure in both water and water vapor [20-23]. The surface properties of hydrophilicity/hydrophobicity can be controlled by organic groups [24,25].

Till now, organosilica membranes have almost always been prepared with highly hydrophilic intermediate layers, such as γ-Al_2O_3, SiO_2-ZrO_2 or TiO_2 [5,21], as schematically shown in Figure 3.1(a). However, for gas separation under wet conditions, however, water fills the pores due to capillary condensation in the hydrophilic intermediate layers, which can be a barrier for gas transport through the membranes. In our previous work [23], BTESE and BTESO membranes coated on hydrophilic SiO_2-ZrO_2 intermediate layers showed a high CO_2 gas permeance under dry conditions but the permeance was drastically decreased in the presence of water. The decrease ratio of CO_2 permeance was approximately one-hundredth for BTESE and one-tenth for BTESO membranes.

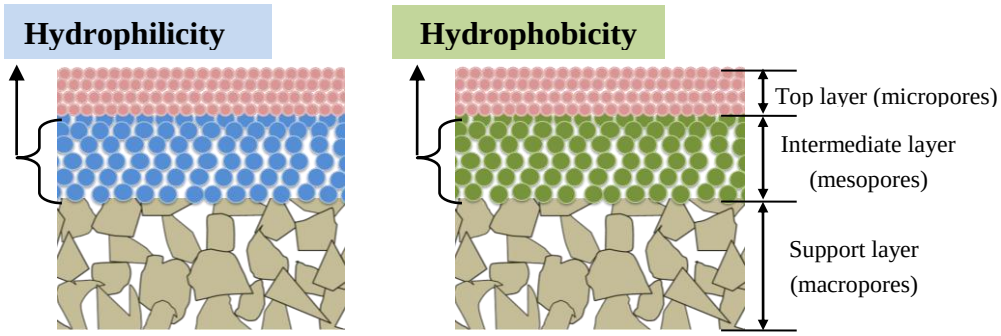

(a) Conventional structure (b) Proposed structure

Figure 3.1 Schematic structures of the porous organosilica membranes supported on intermediate layers.

In this work, to reduce the effect of water vapor on permeation properties, hydrophobic mesoporous silica layers are, for the first time, proposed as suitable intermediate layers coated on commercially available ceramic supports, as shown in Figure 3.1(b). Methyl-SiO_2 sols (Me-SiO_2) were prepared via the co-hydrolysis and condensation reaction of methyltrimethoxysilane (MTMS) and TEOS, and were used as hydrophobic intermediate layers. The conventional intermediate layer, SiO_2-ZrO_2 was used as comparison. Two types of organosilica sols prepared from bis(triethoxysilyl)ethane (BTESE) and bis(triethoxysilyl)octane (BTESO) were used for separation layer that consisted of 2 and 8 numbers of -CH_2- groups, respectively, in the linking units between the two Si atoms. The pore diameter and hydrophilicity of the intermediate and top layers of membranes were evaluated by nanopermporometry using hexane and water as condensable vapor. The gas permeation properties were examined for BTESE/Me-SiO_2, BTESO/Me-SiO_2, BTESE/SiO_2-ZrO_2 and BTESO/SiO_2-ZrO_2 membranes under dry and wet conditions. The proposed structure of organosilica coated on hydrophobic intermediate layers was found to show a high resistance to water vapor and a relatively high selectivity of CO_2/N_2.

3.2 Experimental

3.2.1 Preparation of silica sols, films and membranes

Preparation of Me-SiO_2 and SiO_2-ZrO_2 sols for the intermediate layers:

Hydrophobic Me-SiO_2 sols were prepared using TEOS and MTMS as co-precursors. Two alkoxides (molar ratio TEOS/MTMS=1) dissolved in C_2H_5OH were added to a bottle with H_2O and ammonia as the catalyst in a single step, according to a previous report [27]. Hydrophilic SiO_2-ZrO_2 sols were prepared using TEOS and ZrTB (zirconium tetra-n-butoxide) as co-precursors. The two alkoxides (molar ratio TEOS/ZrTB =1/1) were added in water with HCl as the catalyst, then boiled at 100 ^oC for 10 hours [28].

Preparation of sols for the top layer:

Two types of silica sols were prepared by hydrolysis-condensation processes using bridged alkoxide bis(triethoxysilyl)ethane (BTESE) and bis(triethoxysilyl) octane (BTESO), which consisted of 2 and 8 -CH_2- groups, repectively, in the linking units between the two Si atoms. The precursor was dissolved in ethanol, and then added with water and HCl as a catalyst under continuous stirring at 25 ℃ to develop stable and clear silica sols.

Preparation of films and membranes:

The silicon wafer as substrates was heated at 550 ^oC for one hour in an oxidation furnace to form a thin SiO_2 layer. Me-SiO_2 or SiO_2-ZrO_2 sols were spin-coated on these silicon wafers at room temperature, followed by firing at temperature 400 and 550 ^oC for 15 minutes, respectively. Then, BTESE or BTESO sols were deposited on pre-coated Me-SiO_2 or SiO_2-ZrO_2 films via spin-coating method, followed by drying and firing at 300^oC for 30 minutes. Organosilica membranes were fabricated using porous α-alumina tubes (porosity: 50%, outside diameter: 10 mm, average pore size: 1-2 μm) as supports. Before deposition of the intermediate layers, two types of α-Al_2O_3 particles (2 and 0.2 μm) were coated on the outer surface of the support followed by firing at 550 ℃ in order to cover larger pores. The subsequent procedures followed the same process as the films preparation described above.

3.2.2 Characterization of hybrid organosilica sols and membranes

The contact angles of the silica films were measured using a microscopic contact angle meter (DropMaster DM-300, KYOWA INTERFACE SCIENCE, Co., Ltd). The surfaces and cross-sections of membranes were examined by Field Emission Scanning Electron Microscopy (FE-SEM, S-4800, HITACHI).

3.2.3 Gas permeation measurement

Gas permeance was evaluated under dry and wet conditions via two types of measurements. A schematic diagram of the apparatus for the dry gas permeation tests was reported elsewhere [18]. First, the membrane was dehydrated using helium at 200 ℃ for 10 h. The pressure drop through the membranes was maintained at 1bar and the permeate stream was at atmospheric pressure. The schematic permeation equipment for gas/water vapor mixtures is shown in Figure. 2.2 The feed and permeate streams were both maintained at atmospheric pressure. N_2 was flowed in permeate streams to create a driving force as a sweep gas. The temperature was controlled at 40 ℃ in a forced-convection oven. Water activities in feed stream were controlled by the flow rate of dry and wet CO_2 stream that saturated water. A hygrometer (HygroFlex, error range: ±2%RH, Rotonic, Switzerland) was used to measure the water activity in the feed and permeate streams. CO_2 concentration in the permeate stream was measured via CO_2 sensors (GMT221 and GMT222, error range: ±0.02% and 20 ppm, Vaisala, Finland).

The CO_2 and H_2O permeance were calculated by the following equations:

$$P_i = \frac{F_i}{A} \bullet \frac{1}{\Delta p_i} \qquad (3.1)$$

where F_i is the permeated molar flow rate of component i, A is the membrane surface area, Δp_i is the logarithmic average of the partial pressure of CO_2 gas and H_2O vapor for permeation.

3.3 Results and discussion

3.3.1 Surface characterization of thin films and membranes

The contact angles and surface morphology of these films are shown in Figure 3.2 and Table 3.1, respectively. Me-SiO_2 film coated on the silicon wafer was very hydrophobic with a contact angle that could be as high as 120 °, while the contact angle of SiO_2-ZrO_2 film was 0 °, indicating a hydrophilic surface. BTESE and BTESO coated on silicon wafers showed contact angles of 58 and 86 °, respectively, which demonstrated that BTESO film is hydrophobic compared with BTESE film. When BTESE was coated on the SiO_2-ZrO_2 film, the contact angle was similar to that of coating on silicon wafer. However, as BTESE sols were coated on the hydrophobic Me-SiO_2 film, the sols were scattered on the films, forming

discontinuous and separated coated surface, which showed almost the same contact angle as that of Me-SiO_2 film, as shown in Figure 3.2c.

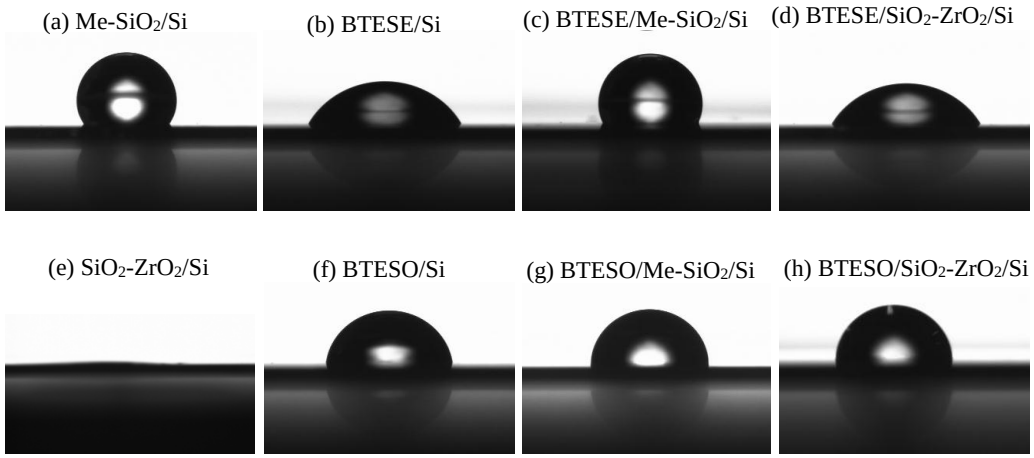

Figure 3.2 Contact angle images of Me-SiO_2, SiO_2-ZrO_2, BTESE, and BTESO films.

Table 3.1 Contact angles and surface morphology of organosilica films

Sub-layer	Coated layer	Contact angle	Surface morphology
Si*[1]	Me-SiO_2	**120 °**	Homogeneous
	SiO_2-ZrO_2	**0 °**	Homogeneous
	BTESE	**58 °**	Homogeneous
	BTESO	**86 °**	Homogeneous
Me-SiO_2*[2]	BTESE	**110 °**	Inhomogeneous
	BTESO	**91 °**	Homogeneous
SiO_2-ZrO_2*[3]	BTESE	**60 °**	Homogeneous
	BTESO	**86 °**	Homogeneous

*[1]: silicon wafer after firing at 550 °C.

*[2]: Me-SiO_2 coated on the silicon wafer and fired at 400 °C under a N_2 atmosphere.

*[3]: SiO_2-ZrO_2 coated on the silicon wafer and fired at 550 °C under an air atmosphere.

Interestingly, BTESO formed homogenous and continuous layers when coated on silicon wafer, Me-SiO_2 and SiO_2-ZrO_2 films. This is probably due to the hydrophilic and hydrophobic groups in BTESO sols. The hydrophilic portion ascribed to -OH groups resulted from the hydrolysis of ethoxide with water, and the hydrophobic portion was attributed to 8 -CH_2- chains. When the substrates show hydrophilic properties, the end of hydrophilic -OH groups of BTESO will attach to the substrates. On the contrary, the hydrophobic long -CH_2 chains will attach to the hydrophobic substrates (Me-SiO_2 surface). When BTESO was coated on Me-SiO_2, the contact angles were somewhat larger than when it was coated on SiO_2-ZrO_2 films and on silicon wafer, which can be ascribed to the rough surface of the Me-SiO_2 films.

Figure 3.3 shows the SEM images of the surface and cross-section of BTESE/SiO_2-ZrO_2, BTESO/SiO_2-ZrO_2, BTESE/Me-SiO_2, and BTESO/Me-SiO_2 membranes. All of the membranes had continuous and dense surfaces with the exception of BTESE/ Me-SiO_2. This may be because BTESE sols with polar properties were difficult to coat on the hydrophobic Me-SiO_2 film that resulted in the inhomogeneous surface. The surface chemistry was confirmed by contact angles of BTESE/Me-SiO_2/Si (Figure 3.2c). It was difficult to distinguish the top and intermediate layers in the cross-sections of SEM images, but a thin and dense separation layer can be observed, with a total thickness less than 500 nm for BTESE/SiO_2-ZrO_2 membrane. BTESO/SiO_2-ZrO_2 membrane was thicker (<1 μm) than BTESE/SiO_2-ZrO_2, which can be ascribed to BTESO penetration into the intermediate and particle layers. This is probably that the BTESO sols with 8 -CH_2- in the structures were flexible and mobile at high temperature.

(a) BTESE/SiO_2-ZrO_2 (b) BTESE/Me-SiO_2 (c) BTESO/SiO_2-ZrO_2 (d) BTESO/Me-SiO_2

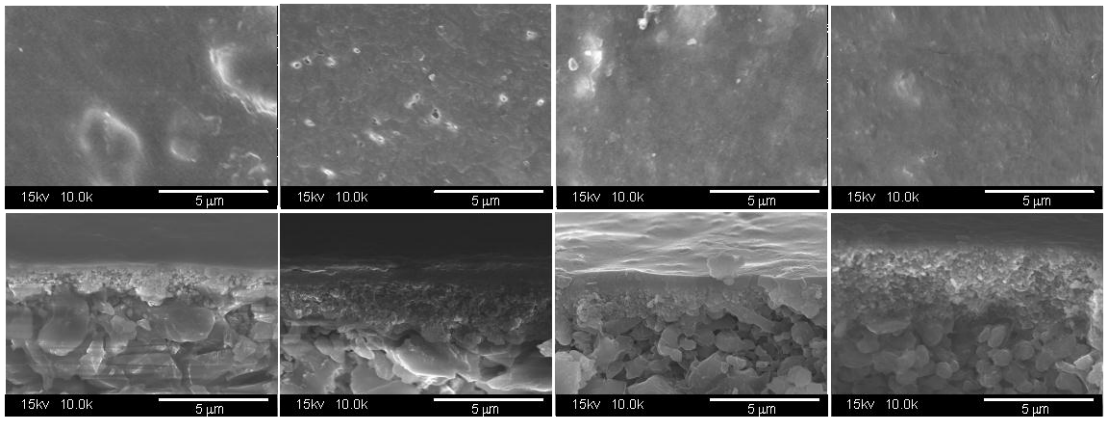

Figure 3.3 SEM images of surface and cross-section of membranes.

3.3.2. Characterization of Me-SiO_2 and SiO_2-ZrO_2 intermediate layers

Reportedly, it is possible to evaluate the pore size distribution and hydrophilicity/hydrophobicity of porous membranes via nanopermporometry using hexane and water as condensable vapors [29-31]. Nanopermporometry is based on the capillary condensation of vapor and the blocking effect of the permeation of non-condensable gases such as N_2. The pore diameter of the membranes was based on the following Kelvin equation and was successfully evaluated within a range of 0.5-30 nm [31].

Kelvin equation:

$$d_k = \frac{-4\gamma}{RT} \cdot \frac{V_m \cos\theta}{\ln(p/p_S)} \qquad (3.2)$$

where d_k is the Kelvin condensation diameter, p is the actual vapor pressure of the system, p_s is the saturated vapor pressure at the temperature T, γ is the surface tension, V_m is the molar volume of the liquid, θ is the contact angle, and R is the universal gas constant.

Figure 3.4 (a) and (b) show the nanopermporometry characterizations of SiO_2-ZrO_2 and Me-SiO_2 intermediate layers. Hexane and water was used as the condensable vapor and N_2 was used as the non-condensable gas. The dimensionless permeance (DP) of nitrogen was defined by normalized permeance at $-p/p_s$=0. The average pore size was defined as the Kelvin diameter at a DP of 50%. The secondary horizontal axis (upper) indicates the relative pressure p/p_s, for water and hexane at a certain Kelvin diameter.

For SiO_2-ZrO_2 intermediate layer, the DP of N_2 was largely decreased with Kelvin diameter (relative pressure of vapor) increased. The tendency was in a similar manner for hexane and water vapor. As the Kelvin diameter reached 3 nm for both vapors, the DP of N_2 was approached 0, which indicated that both vapors could capillary-condense in the pores and blocked the permeation of N_2. The average pore size for SiO_2-ZrO_2 layers was approximately 1 nm for both water and hexane. The large decrease in N_2 permeance measured using water vapor illustrates the hydrophilic properties of SiO_2-ZrO_2 layers where the condensation of water occurs easily in the pores. This is consistent with SiO_2-ZrO_2 films on silicon wafers, which show contact angle of 0^o.

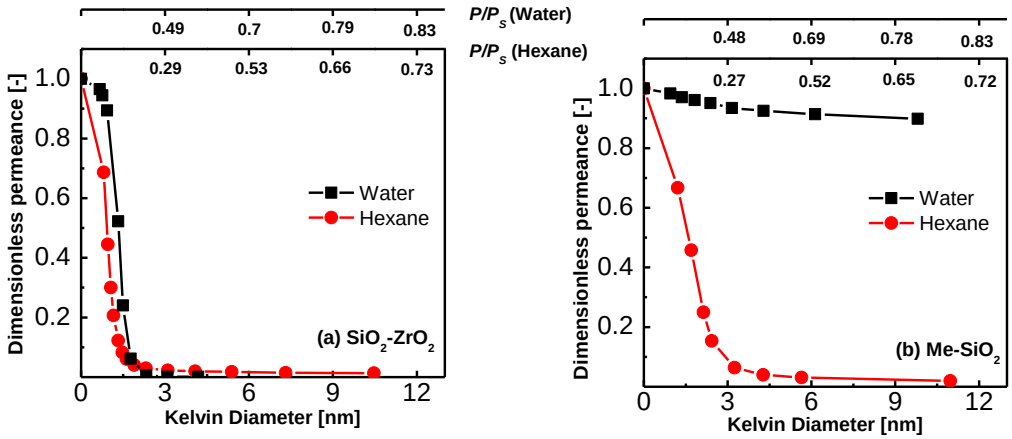

Figure 3.4 Nanopermporometry characterizations of SiO_2-ZrO_2 and Me-SiO_2intermediate layers using hexane and water as the condensable vapors.

The pore size distribution obtained using hexane vapor for Me-SiO_2 (Figure 3.4b) layers was similar to that of SiO_2-ZrO_2 (Figure 3.4a) layers. The DP of N_2 was also decreased to approximately 0, indicating total capillary-condensation of hexane occurred in the pores. The average pore size of Me-SiO_2 layers was about 1.5 nm by using the hexane vapor curve of DP at 0.5. The condensation vapor of hexane has a lower surface tension, and shows high wettability for both hydrophilic SiO_2-ZrO_2 and hydrophobic Me-SiO_2 layers. When using water as condensable vapor, however, Me-SiO_2 layers showed a much higher DP of N_2 than that of SiO_2-ZrO_2 layers. The N_2 permeance was little decreased as relative pressure of water vapor increased. The results illustrate that the water could not condense in the pores to block the permeation of N_2, which indicated that Me-SiO_2 layers were hydrophobic.

3.3.3 Gas permeation properties for hydrophilic/hydrophobic membranes.

Figure 3.5 shows the gas permeation for hydrophilic BTESE and hydrophobic BTESO coated on hydrophilic SiO_2-ZrO_2 and hydrophobic Me-SiO_2 membranes under dry conditions at 200 ℃. Both SiO_2-ZrO_2 and Me-SiO_2 membranes without top layer showed a high permeance of He and H_2 of about 10^{-5} mol/(m^2 s Ṗa), but no selectivity for CO_2/N_2. The large pore size of intermediate layers was not effective for gas separation. The transport mechanism nearly obeyed Knudsen diffusion.

After coating organosilica sols of BTESE or BTESO on Me-SiO_2 and SiO_2-ZrO_2

intermediate layers, the four membranes showed CO_2 permeance higher than 10^{-7} and H_2 permeance equal to or higher than 10^{-6} mol/(m^2 s Pa). The selectivities of these membranes are summarized in Table 3.2. Large molecules such as SF_6 are effective in evaluating the quality of microporous membranes. Good quality of membranes generally delivers high separation factors for small gases such as H_2. The selectivity of H_2/SF_6 for BTESE/Me-SiO_2 membranes was 334. Considering the fact that BTESE/SiO_2-ZrO_2 membranes showed the selectivity that was higher than 20,000, the poorer quality might be explained by the existence of defects in the BTESE/Me-SiO_2 membranes caused by inhomogeneous coatings of BTESE on hydrophobic Me-SiO_2 layers. Thus, it can be concluded that an intermediate layer plays an important role in the further continuous coating for microporous membranes.

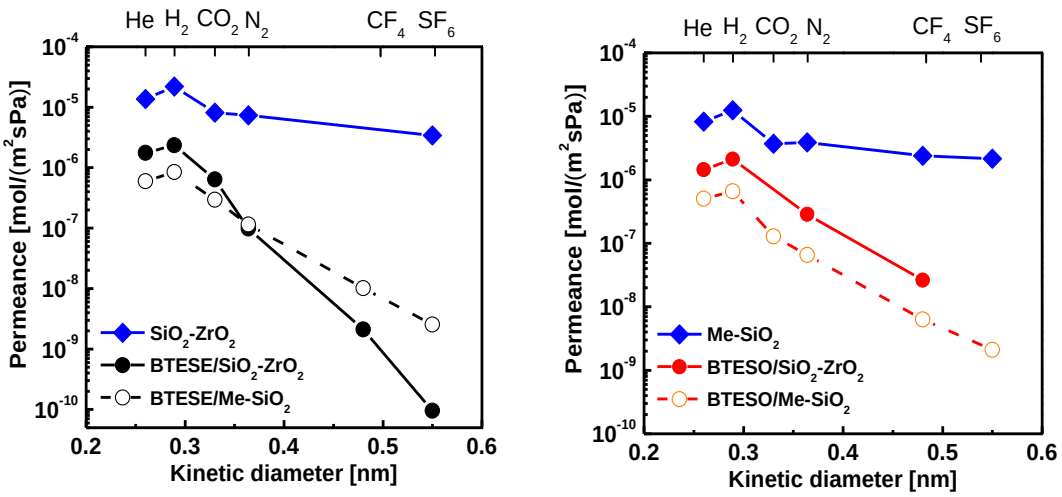

Figure 3.5 Single gas permeance for BTESE and BTESO membranes coated on Me-SiO_2 and SiO_2-ZrO_2 layers at 200°C.

On the other hand, the selectivity of H_2/CF_4 for BTESO/Me-SiO_2 and BTESO/ SiO_2-ZrO_2 membranes were similar, about 100. This may be due to both the hydrophilic (-OH) and hydrophobic (long -CH_2) portions of the BTESO-derived sols to achieve continuous coatings on both hydrophilic and hydrophobic sub-layers. BTESE/SiO_2-ZrO_2 membrane showed a larger selectivity of CO_2/N_2 compared with that of the BTESO/SiO_2-ZrO_2, because 2 methylene groups between the two Si atoms of BTESE formed a microporous structure that was suitable for CO_2 separation compared with that of the BTESO that consisted of 8

methylene groups. This is also consistent with our previous report [23].

Table 3.2 Comparison of gas selectivities for membranes at 200 ℃.

Top layer		BTESE		BTESO	
Intermediate layer		SiO_2-ZrO_2	Me-SiO_2	SiO_2-ZrO_2	Me-SiO_2
Selectivity	H_2/ N_2	24	7.4	7.3	9
	H_2/SF_6	24575	334	80.2[a]	105 [a]
	CO_2/ N_2	6.5	2.6	-	2

*[a]: H_2/CF_4

The selectivity of CO_2/N_2 for four membranes was increased as the temperature was decreased. The permeance of CO_2 was even higher than that of H_2 at low temperatures. This may be due to the surface diffusion machnism of CO_2 that resulted from high adsorption capacity at low temperature. A large selectivity obtained for BTESE/SiO_2-ZrO_2 membrane was 36 at 40 ºC, while the value is only 4 for BTESE/Me-SiO_2 membranes. The selectivity of CO_2/N_2 for BTESO/SiO_2-ZrO_2 was 12, which was similar to that of BTESO/Me-SiO_2 membranes with selectivity of 9 at 40 ºC.

3.3.4 Gas permeation for organosilica membranes in the presence of water vapor

Figure 3.6 shows the effect of relative pressure of water vapor on BTESE/Me-SiO_2 and BTESO/Me-SiO_2 membranes with the same intermediate layers. It should be noted that He instead of N_2 was used as the non-condensable gas due to a small molecular diameter that was suitable for microporous organosilica membranes. As the relative pressure of water vapor increased, the permeance for BTESE/Me-SiO_2 was decreased gradually and reached approximately 0.3 at p/p_s=1, while that for BTESO/Me-SiO_2 was decreased to 0.8. This suggests that the adsorption of water in BTESE layers was much more than that in BTESO layers that prevented the permeation of He through the membranes. The higher water adsorption of BTESE was due to the hydrophilicity, which could be confirmed by the contact angles of BTESE and BTESO.

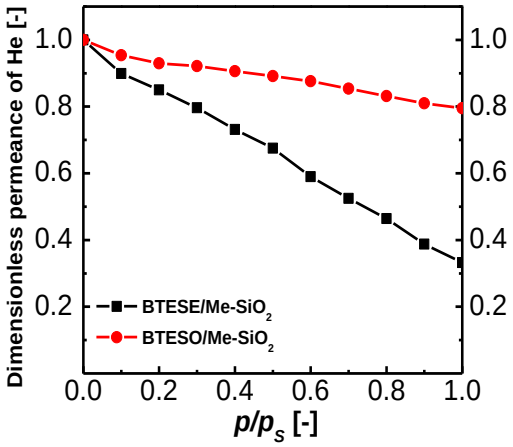

Figure 3.6 Nanopermporometry for BTESE/Me-SiO_2 and BTESO/Me-SiO_2 by using water as a condensable vapor and He as a non-condensable gas.

The permeance of CO_2 was measured for four membranes in the presence of water vapor at 40 ^oC, as shown in Figure 3.7. Homogeneous silicone rubber as polymer (supplied by Nagayanagi CO., LTD.) with 1 mm thickness was cited as comparison [23]. The CO_2 permeability is 2700 barrer with selectivity of CO_2/N_2 of 10 at 25 ^oC for this membrane. In the presence of water vapor, BTESE/Me-SiO_2 and BTESO/Me-SiO_2 with the hydrophobic intermediate layers exhibited that CO_2 permeance was decreased gradually and slightly, but the decrease was drastic at water activity p/p_s less than 0.2 for those of BTESE/SiO_2-ZrO_2 and BTESO/SiO_2-ZrO_2 membranes with hydrophilic SiO_2-ZrO_2 intermediate layers. CO_2 permeance for silicone rubber was not decreased and approximately constant as the water activity p/p_s increased, but the permeance was much lower compared with organosilica membranes.

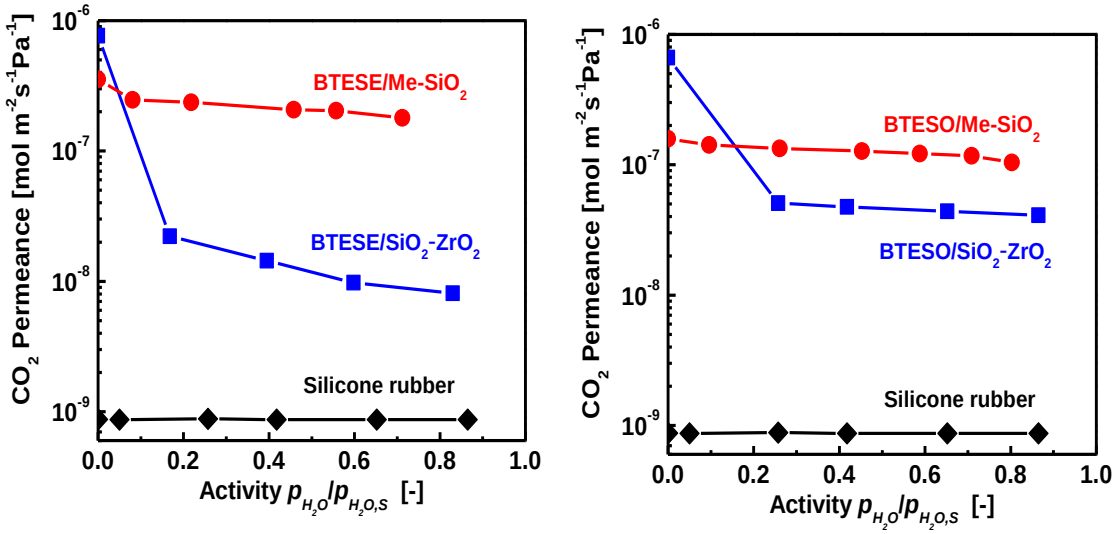

Figure 3.7 CO_2 permeance of organosilica membranes as a function of water vapor activity at 40 ^oC (Feed side: 500 ml/min, permeate side: 1000 ml/min).

The decrease ratio of permeance obtained as the dimensionless permeance (DP) of CO_2 (normalized by dry CO_2 permeance) is shown in Figure 3.8 The DP of CO_2 for all water activity p/p_s was on the order of BTESE/SiO_2-ZrO_2 < BTESO/SiO_2-ZrO_2 < BTESE/Me-SiO_2 < BTESO/Me-SiO_2 < SR. Compared the top layers of BTESE and BTESO, the CO_2 permeance of BTESE membranes was decreased more than that of BTESO membranes. For example, the DP was 0.6 (60% of dry permeance) for BTESE/Me-SiO_2 membrane, while the value was 0.8 for BTESO/Me-SiO_2 membrane at water activity of 0.45. This is due to good water affinity of BTESE layer compared with BTESO layer that prevented CO_2 permeation. The trends are consistent with the nanopermporometry in Figure 3.6. Compared the membranes with the same top layer, the permeance of membranes with hydrophilic SiO_2-ZrO layers was decreased more than that of membranes with hydrophobic Me-SiO_2 layers. When water activity was at about 0.6-0.7, BTESE/Me-SiO_2 showed 50% of dry permeance, while the permeance of BTESE/SiO_2-ZrO_2 was decreased to approximately 2%. On the other hand, for BTESO membranes with a Me-SiO_2 intermediate layer, the permeance was decreased to 74% that of the dry value and BTESO with a SiO_2-ZrO_2 intermediate layer the decrease was 7% at water activity about 0.7. The significant difference indicates that our proposed membrane structures, that is, a hydrophobic organosilica sols deposition on a hydrophobic intermediate layer, is effective in improving the gas permeance in the presence of water vapor without a

significant decrease in selectivity.

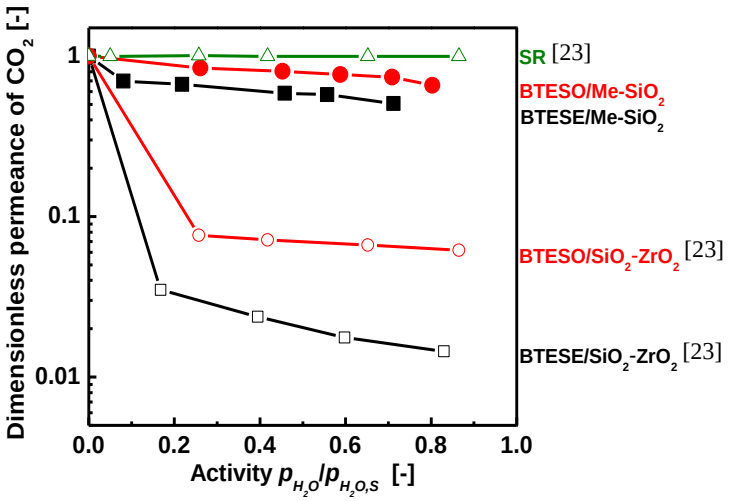

Figure 3.8 Dimensionless permeance of CO_2 as a function of water activity at 40°C.

Figure 3.8 shows H_2O permeance as a function of water activity in feed stream for BTESE/Me-SiO_2 and BTESE/Me-SiO_2 membranes, and compared with that of BTESE/SiO_2-ZrO_2 and BTESO/SiO_2-ZrO_2 membranes. Water permeance for the four organosilica membranes were greater than CO_2 and approximately constant as the water activity increased. Organosilica membranes with Me-SiO_2 intermediate layers showed water permeance were a little higher than those of BTESE and BTESO membranes with hydrophilic SiO_2-ZrO_2 intermediate layers. This may be explained as hydrophobic Me-SiO_2 layers had lower water adsorption ability and consequently a higher diffusivity of water compared with hydrophilic SiO_2-ZrO_2 layers.

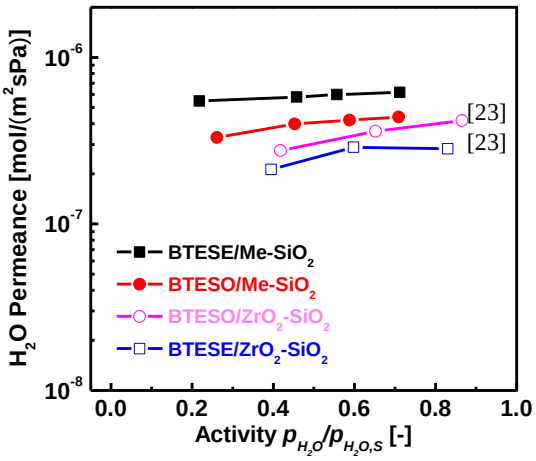

Figure 3.9 H_2O permeance for organosilica membranes as a function of water vapor activity at 40 °C

For industrial applications, long-term stability is a major factor. In feed stream, flow rate of CO_2 was kept at 500 ml/min. Hydrophobic BTESO/Me-SiO_2membrane was measured for 70 hours under an atmosphere of saturated water vapor with CO_2, as shown in Figure 3.10. The permeances of CO_2 and H_2O were maintained at a stable level. The hydrophobic organosilica membranes showed good stability in the presence of water vapor.

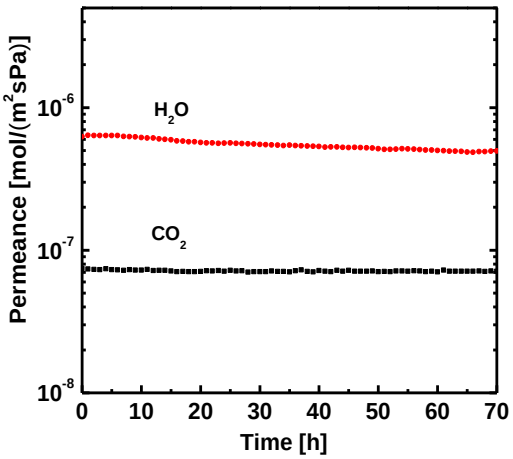

Figure 3.10 The time-course of BTESO/Me-SiO_2membrane in the presence of water vapor at 40 °C.

3.4 Conclusions

In this work, organosilica membranes were prepared using hydrophobic Me-SiO_2 as intermediate layers and applied under humidified conditions. Two types of top layers were prepared by using BTESE and BTESO sols.

(1) Hydrophobic Me-SiO_2 film was successfully prepared using the co-precursors of tetraethoxysilane (TEOS) and methyltrimethoxysilane (MTMS). The contact angle of Me-SiO_2 by spin-coating on silicon wafers was as high as 120 °, while the contact angles of conventional SiO_2-ZrO_2 film was 0 °.

(2) Based on nanopermporometry measurement, Me-SiO_2 layers showed capillary condensation of hexane, while no condensation was observed by water vapor, confirming Me-SiO_2 layers were hydrophobic compared with SiO_2-ZrO_2 layers.

(3) Under dry conditions, the selectivity of H_2/SF_6 for BTESE/ZrO_2-SiO_2 membrane was higher than 20,000, while that for BTESE/Me-SiO_2 membrane was as low as 334, indicating poorer quality that was caused by inhomogeneous coating for hydrophilic BTESE sols coated on hydrophobic Me-SiO_2 intermediate layers. On the other hand, the selectivity of H_2/CF_4 for BTESO/Me-SiO_2 membrane was similar to that of BTESO/ZrO_2-SiO_2 membrane.

(4) Under humidified conditions, CO_2 permeance was 50% that of dry permeance value for BTESE/Me-SiO_2, while it was approximately 2% for BTESE/SiO_2-ZrO_2 membrane. For BTESO membranes, the permeance decrease ratio was 74% with Me-SiO_2 as intermediate layer and 7% with SiO_2-ZrO_2 as intermediate layer. The membranes with Me-SiO_2 intermediate layers had a lower decrease in permeance than those with hydrophilic SiO_2-ZrO_2 layers. The great difference indicates the importance of the intermediate layers on the water resistance for gas permeation. In addition, the hydrophobic membranes can keep a good stability under saturated water vapor for 70 hours.

References

[1] R.W. Baker, B.T. Low. Gas Separation Membrane Materials: A Perspective. Macromol. 47 (2014) 6999-7013.

[2] A. Brunetti, F. Scura, G. Barbieri, E. Drioli. Membrane technologies for CO_2 separation. J. membr. Sci. 359 (2010) 115-125.

[3] C.E. Powell, G.G. Qiao. Polymeric CO_2 /N_2 gas separation membranes for the capture of carbon dioxide from power plant flue gases. J. membr. Sci. 279 (2006) 1-49.

[4] L.M. Robeson. The upper bound revisited. J. membr. Sci. 320 (2008) 390-400.

[5] M. Pera-Titus. Porous Inorganic Membranes for CO_2 Capture: Present and Prospects. Chem. Rev. 114 (2014) 1413-1492.

[6] Y. Yampolskii, I. Pinnau, B.D. Freeman. Materials Science of Membranes for Gas and Vapor Separation. John Wiley & Sons Ltd: England, 2006.

[7] B.T. Low, L. Zhao, T.C. Merkel, M. Weber, D. Stolten. A parametric study of the impact of membrane materials and process operating conditions on carbon capture from humidified flue gas. J. membr. Sci. 431 (2013) 139-155.

[8] S.R. Reijerkerk, R. Jordana, K. Nijmeijer, M. Wessling. Highly hydrophilic, rubbery membranes for CO_2 capture and dehydration of flue gas. Int. J. Greenh. Gas. Con. 5 (2011**)** 26-36.

[9] C.A. Scholes, S.E. Kentish, G.W. Stevens. Effects of Minor Components in Carbon Dioxide Capture Using Polymeric Gas Separation Membranes. Sep. Purif. Rev. 38 (2009) 1-44.

[10] G.Q. Chen, C.A. Scholes, G.G. Qiao, S.E. Kentish. Water vapor permeation in polyimide membranes. J. Membr. Sci. 379 (2011) 479-487.

[11] X. Gu, J. Dong, T.M. Neoff. Synthesis of Defect-Free FAU-Type Zeolite Membranes and Separation for Dry and Moist CO_2/N_2 Mixtures. Ind. Eng. Chem. Res. 44 (2005) 937-944.

[12] G. Xomeritakis, C.Y. Tsai, Y.B. Jiang, C.J. Brinker. Tubular ceramic-supported sol-gel silica-based membranes for flue gas carbon dioxide capture and sequestration. J. Membr. Sci. 341 (2009) 30–36.

[13] J.C. Poshusta, R.D. Noble, J.L. Falconer. Characterization of SAPO-34 membranes by

water adsorption. J. Membr. Sci. 186 (2008) 25-41.

[14] S. Cerneaux, I.Struzyńska, W.M. Kujawski, M. Persin, A. Larbot. Comparison of various membrane distillation methods for desalination using hydrophobic ceramic membranes. J. Membr. Sci. 337 (2009) 55-60.

[15] N.A. Ahmad, C.P. Leo, A.L. Ahmad, W.K.W. Ramli. Membranes with Great Hydrophobicity: A Review on Preparation and Characterization. Sep. Purif. Rev. 44 (2015) 109-134.

[16] M.C. Duke, J.C.D. da Costa, D.D. Do, P.G. Gray, G.Q. Lu. Hydrothermally robust molecular sieve silica for wet gas separation. Adv. Funct. Mater. 16 (2006) 1215-1220.

[17] H. Imai, H. Morimoto, A. Tominaga, H. Hiroshima. Structural Changes in Sol-Gel Derived SiO_2 and TiO_2 Films by Exposure to Water Vapor. J. Sol-Gel. Sci. Technol. 10 (1997) 45–54.

[18] M. Kanezashi, M. Kawano, T. Yoshioka, T. Tsuru. Organic-Inorganic Hybrid Silica Membranes with Controlled Silica Network Size for Propylene/Propane Separation. Ind. Eng. Chem. Res. 51 (2012) 944- 953.

[19] R. Ciriminna, A. Fidalgo, V. Pandarus, F. Béland, L. M. Ilharco, M. Pagliaro. The Sol-Gel Route to Advanced Silica-Based Materials and Recent Applications. Chem. Rev. 113 (2013) 6592-6620.

[20] H.L. Castricum, A. Sah, R. Kreiter, D.H.A. Blank, J.F. Vente, J.E. ten Elshof. Hydrothermally stable molecular separation membranes from organically linked silica. J. Mater. Chem. 18 (2008) 2150-2158.

[21] R. Kreiter, M.D.A. Rietkerk, H.L. Castricum, H.M. van Veen, J.E. ten Elshof, J.F. Vente. Evaluation of hybrid silica sols for stable microporous membranes using high-throughput screening. J. Sol-Gel. Sci. Technol. 57 (2011) 245-252.

[22] M. Elma, C. Yacou, D.K. Wang, S. Smart, J. C.D. Costa. Microporous Silica Based Membranes for Desalination. Water. 4 (2012) 629-649.

[23] X. Ren, K. Nishimoto, M. Kanezashi, H. Nagasawa, T. Yoshioka, T. Tsuru. CO_2 Permeation through Hybrid Organosilica Membranes in the Presence of Water Vapor. Ind. Eng. Chem. Res. 5 (2014) 6113-6120.

[24] G. Li, M. Kanezashi, T. Tsuru. Preparation of organic-Inorganic hybrid silica membranes usin organoalkoxysilanes: The effect of pendant groups. J. Membr. Sci. 379 (2011) 287-295.

[25] G.G. Paradis, D.P. Shanahan, R. Kreiter, H.M. Veen, H.L. Castricum, A. Sah, R. Kreiter, J.F. Vente. From hydrophilic to hydrophobic HybSi® membranes: A change of affinity and applicability. J. Membr. Sci. 428 (2013) 157-162.

[26] G. Xomeritakis, C.M. Braunbarth, B. Smarsly, N. Liu, R. Köhn, Z. Klipow-icz, C.J. Brinker. Aerosol-assisted deposition of surfactant-templated mesoporous silica membranes on porous ceramic supports. Microporous Mesoporous Mater. 66 (2003) 91-101.

[27] Y. Ma, M. Kanezashi, T. Tsuru. Preparation of organic/inorganic hybrid silica using methyltriethoxysilane and tetraethoxysilane as co-precursors. J. Sol-Gel. Sci. Technol. 53 (2010) 93-99.

[28] M. Asaeda, M. ishida, Y. Tasaka. Pervaporation Characteristics of Silica-Zirconia Membranes for Separation of Aqueous Organic Solutions. Sep. Sci. Technol. 40 (2005) 239-254.

[29] T. Tsuru, Y. Takata, H. Kondo, F. Hirano, T. Yoshioka, M. Asaeda. Characterization of sol-gel derived membranes and zeolite membranes by nanopermporometry. Sep. Purif. Technol. 32 (2003) 23-27.

[30] T. Tsuru. Nano/subnano-tuning of porous ceramic membranes for molecular separation. J. Sol-Gel. Sci. Technol. 46 (2008) 349-361.

[31] T. Tsuru, T. Hino, T. Yoshioka, M. Asaeda. Permporometry characterization of microporous ceramic membranes. J. Membr. Sci. 186 (2001) 257-265.

[32] J.E. Lundstrom, R.J. Bearrian. Inert Gas Permeation through Homopolymer Membranes. J. Polym. Sci. Polym. Physics. 12 (1974) 97-114.

[33] H.L. Castricum, G.G. Paradis, M.C. Mittelmeijer-Hazeleger, R. Kreiter, J.F. Vente, J.E. ten Elshof. Tailoring the Separation Behavior of Hybrid Organosilica Membranes by Adjusting the Structure of the Organic Bridging Group. Adv. Funct. Mater. 21 (2011) 2319-2329.

Chapter 4

Plasma-assisted multi-layered coating towards improved gas permeation properties for organosilica membranes

4.1 Introduction

Porous ceramic membranes with superior thermal and chemical stability have been widely applied in gas separation, pervaporation, membrane reactors and desalination [1-5]. High performance can be attained based on their tuneable pore sizes and adsorption ability. The surface chemistry of ceramic membranes is generally hydrophilic, which allows them to enhance water permeability in liquid separation and promote gas permeation in gas separation [3-5]. However, gas permeation typically decreases when these membranes are used under wet atmosphere such as in the practice of removing CO_2 from flue gases or natural gas [6-9]. This is because the hydrophilicity of ceramic membranes results in water capillary condensation in the pores and/or adsorption on the pore walls, which reduce the effective pores and prohibits gas transport. Therefore, ceramic membranes with hydrophobic properties are required for various applications under wet conditions [10].

Porous silica membranes are commonly fabricated with three layers: α-alumina support layer (pore size: 100-50 nm), intermediate layer (5-1 nm), and ultrathin silica top-layer (0.1-0.6 nm). The top layer mainly determines the permeability and selectivity. The thin top layer can provide a high flux of gas because the transport rate of a gas is in inverse proportion to the thickness of the membrane. The intermediate layers are coated on the support in order to prevent the penetration of silica sols into the support and form the ultrathin top layers. Until now, almost all hydrophobic silica membranes reported consisted of hydrophobic top layers prepared on hydrophilic intermediate layers such as γ-Al_2O_3, SiO_2-ZrO_2 or TiO_2 [11-15]. Although the intermediate layers make no contribution to the separation performance, water capillary condensation in the pores and/or adsorption on the pore walls could occur,

which may reduce gas permeance in the hydrophilic intermediate layers. According to calculations using the Kelvin equation, these hydrophilic layers will allow capillary condensation of water at a relative humidity of 14-68% for diameters ranging from 1-5 nm at room temperature. de Vos et al. prepared hydrophobic membranes by coating hydrophobic MeSi (400) top layers on hydrophilic γ-Al_2O_3 intermediate layers [14]. It was found some stabilization time was still needed for drying the hydrophobic membrane prior to conducting the gas permeance experiment. They concluded water adsorbed in the supported MeSi(400) membranes that was likely to be present in the hydrophilic γ-Al_2O_3 intermediate layers only using Kelvin relation. In our previous works, the hydrophobic membranes such as bis(triethoxysilyl)ethane (BTESE, Si-$(CH_2)_2$-Si) or bis(triethoxysilyl)octane (BTESO, Si-$(CH_2)_8$-Si)-derived sols were also formed on hydrophilic SiO_2-ZrO_2 intermediate layers, and the gas permeation properties were evaluated in the presence of water vapor [15]. We found that the CO_2 permeance was drastically decreased in the presence of water vapor. Thus, the introduction of hydrophobicity to an intermediate layer is necessary in real applications to avoid capillary condensation of water in humid process streams.

Silica membranes are fabricated according to well-known polymeric sol-gel routes. Alkoxides are hydrolyzed and condensed under acid or base catalysts to form sols in sizes less than 100 nm. Pore size and surface chemistry can be tuned through different precursors. To reduce defects during the formation of thin films, multi-layered coatings are commonly used via sol-gel method. Prosser et al. reported that silica films fabricated by multiple spin-coating would increase in thickness in a linear fashion as a function of the number of coatings, which reduced the tendency of the films toward cracking compared with a single-layer coating [16]. Depagne et al. reported thin silica film (<500 nm) that was built up using a multi-layered approach [17]. However, as far as the authors know, no paper has yet reported the use of multi-layered coatings in the formation of hydrophobic membranes.

Highly permeable and selective organosilica membranes were prepared on hydrophilic intermediate layers [18-21]. The condensation reactions of hydrophilic groups between coated sols and substrates were expected to enhance membrane performance. To fabricate high-performance hydrophobic membranes, the hydrophobic

surface which can be ascribed to a small number of -OH groups, should be modified to be more hydrophilic. The plasma technique has been used to activate a hydrophobic surface into a hydrophilic one in a very thin layer without changing the bulk properties [22-24]. Compared with other methods, plasma techniques show several advantages on improvement of coatings: shorter treated times, lower temperature processes, overcoming the use of potentially toxic substances or solvents, and the grafting of a wider variety of functional groups. In addition, these films are generally free of pinholes, highly resistant to corrosion and very adhesive to substrates [24,25]. Zarshenas et al. reported that the corona air plasma treatment induced polar groups on the surface of membranes [26], which led to improved gas separation properties without damaging the separation layers. Therefore, to further improve the performance of hydrophobic organosilica membranes, the use of plasma-assisted modification should be investigated, particularly for multi-layered coating. The schematic principle of plasma treatment on the surface of intermediate layers was shown in Figure 4.1.

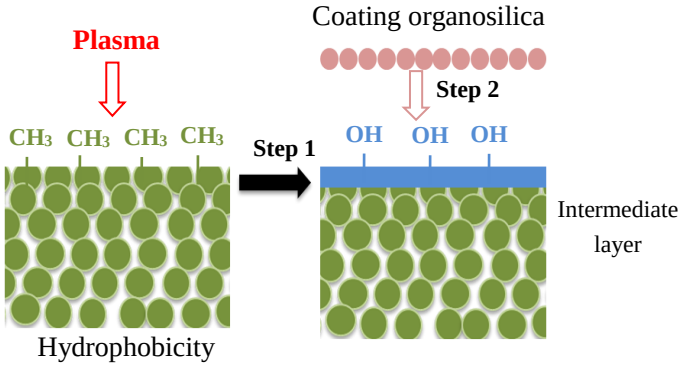

Figure 4.1 The schematic principle of plasma treatment on the surface of intermediate layers for further organosilica coatings.

In the present work, hydrophobic Me-SiO_2 sols were first prepared by co-hydrolysis and polymerization of TEOS and methyltrimethoxysilane (MTMS), and were coated on supports to fabricate Me-SiO_2 nanoporous intermediate layers. The plasma method was then used to modify the hydrophobic surface of the Me-SiO_2, thereby converting to hydrophilic surface chemistry. Finally, BTESE or BTESO-derived sols were coated on the plasma-treated surface to form separation layers. The effect of plasma on

multi-layered coating was studied and the gas permeation properties of the hydrophobic organosilica membranes under both dry and wet conditions. This work offered a new strategy to fabricate multi-layered coating of hydrophilic and hydrophobic layers for gas separation membranes.

4.2 Experimental

4.2.1 Preparation of silica sols

Hydrophobic Me-SiO_2 sols, which were used for the formation of intermediate layer, were prepared using TEOS and MTMS as co-precursors. Two alkoxides (molar ratio TEOS/MTMS=1) dissolved in C_2H_5OH were added with H_2O and ammonia as a catalyst in a bottle in a single step. The solution with the molar ratio of TEOS: MTMS: NH_3: H_2O= 1:1:1.63:67 was stirred continuously at 50 ^oC in a closed system for 8 hours and then in an open system for 2 hours to remove NH_3. The colloidal size of Me-SiO_2 sols based on the alkaline-catalyst was 10-50 nm, which was suitable for fabrication of mesoporous intermediate layers [27].

Two types of organosilica sols were prepared for the top layer, using bridged alkoxide bis(triethoxysilyl)ethane (BTESE) and bis(triethoxysilyl)octane (BTESO) via the hydrolysis-condensation process. The precursor was dissolved in ethanol, and then added with water and the acid catalyst HCl. The solutions with the molar ratio of alkoxide: H_2O: HCl= 1:120: 0.1 was continuous stirring at 25 ℃ to develop stable and clear silica sols.

4.2.2 Preparation of silica films and membranes

Prior to silica coatings, the silicon wafers as substrates were heated at 550 ℃ for 1 hour in an oxidation furnace for pre-treatment. Hydrophobic films, including Me-SiO_2, BTESE and BTESO, were all prepared via the spin-coating method. In the spin-coating process, the spin speed was increased up to 5000 rpm in 5 s and was held for 25 s.

Me-SiO_2 sols (1 wt%) were spin-coated twice on these silicon wafers at room temperature, followed by calcination at 400 ℃ under N_2 atmosphere for 30 min. One coating-cycle involved 2 rounds of spin-coating and 1 round of calcination. This

coating cycle was repeated up to 4 times. Then the surface was wiped with a cloth to investigate the adhesion of the multi-coated layers. In a similar manner, BTESE or BTESO sols (1 wt%) were spin-coated twice on silicon wafers or Me-SiO_2 films, followed by drying and calcinating at 300 ℃ under N_2 atmosphere for 30 min. As before, 1 cycle involved 2 rounds of spin-coating followed by 1 round of calcination. The cycle was repeated up to 4 times and then wiping treatment was performed with a cloth on the surface of the films.

Asymmetric organosilica membranes were fabricated using porous α-alumina tubes. The average pore size of the support was 1-2 μm with an outside diameter of 10 mm. Two types of α-Al_2O_3 suspensions (1 wt%) were prepared by using α-Al_2O_3 particles (2 and 0.2 μm) mixed with 2 wt% silica-zirconia (SiO_2-ZrO_2) solutions as a binder. First, the α-Al_2O_3 suspensions with the size of 2 μm were slip-coated with a cloth on the outer surface of the support and then were fired at 550 ℃. The step was repeated three times to cover the larger pores on the support. Second, 0.2 μm α-Al_2O_3 suspensions were further coated and then fired at 550 ℃. The coating was repeated five times to form a pore size of less than 100 nm. Third, Me-SiO_2 sols (1 wt%, 10-50 nm colloidal sols) were then coated onto the pre-heated support (200 ℃), followed by firing at 400 ℃ in N_2. The pore size of the intermediate layer was controlled to within approximately 2 nm by coating for several times. Finally, BTESE or BTESO sols that were several nanometers in size were coated on the intermediate layer to form a top layer, followed by drying and calcination at 300 ℃ for 30 min in N_2. The asymmetric structures of membranes were characterized by cross-section of Field Emission Scanning Electron Microscopy (FE-SEM, S-4800, HITACHI) images.

4.2.3 Plasma treatment on silica films and membranes

Plasma-assisted modification was conducted on the surface of films and membranes. Films or membranes were first placed into a plasma chamber (BPD-1H, SAMCO, Inc.), and were evacuated to 2 Pa via a vacuum pump. H_2O with the addition of N_2 was used at a power of 10 W at room temperature. The flow rates of H_2O vapor and N_2 were controlled at 15 ml/min and 10 ml/min, respectively, and the pressure was maintained at 20 Pa.

4.2.4 Characterization of hybrid organosilica films

The hybrid organosilica films formed on silicon wafers via spin-coating were characterized at room temperature by Fourier transform infrared (FT-IR) spectroscopy (FT-IR-4100, JASCO). The morphology of the films was characterized by atomic force microscope (AFM, nanocute, SII) in air with a non-contact mode, and the scan size was 10×10 μm. The hydrophilicity of the silica films was evaluated using a microscopic contact angle meter with FAMAS software (DropMaster DM-300, KYOWA INTERFACE SCIENCE, Co., Ltd).

4.2.5 Gas permeation measurement

Gas permeance was evaluated under dry and wet conditions. A schematic diagram of the apparatus for dry gas permeation can be found in a previous paper [20]. Prior to measurement, the membrane was dried first by helium at 200 ℃. The pressure difference across the membranes was maintained at 1 bar, and the permeate stream was maintained at atmospheric pressure. For the permeation of gas/water vapor mixtures, CO_2 gas was bubbled through water and mixed with dry CO_2 gas in the feed stream at atmospheric pressure. Water activities were controlled via the flow rate of the dry and wet streams and measured using a hygrometer (HygroFlex, error range: ±2%RH, Rotonic, Switzerland). In the permeate stream, N_2 was used as sweep gas to carry permeated CO_2 and water vapor continuously to CO_2 sensor (GMT221 and GMT222, error range: ±0.02% and 20 ppm, Vaisala, Finland) and the hygrometer. The equipment was maintained at a temperature of 40 ℃. The values for CO_2 and H_2O permeance were calculated using the following equations:

$$P_i = \frac{F_i}{A} \bullet \frac{1}{\Delta p_i} \qquad (4.1)$$

where F_i is the permeated molar flow rate of the component i, Δp_i is the logarithmic average partial pressure of component i for permeation, and A is the effective membrane area.

4.3 Results and discussion

4.3.1 Multi-coated thin films on silicon wafers

The FT-IR spectra of Me-SiO_2 films via multiple spin-coating on the silicon wafers are shown in Figure 4.2(a). The contact angles (CA) and peak area are summarized as a function of coating times, as shown in Figure 4.2(b). The peak area of intensity was calculated by integrating the absorbance from 1300-979 cm^{-1} to reveal the quantity of coated films [28]. Since silicon wafer was used as the background in the FT-IR spectra measurement, the peak area was 0 and the CA of silicon wafer was 30 ° at the coating time of 0. In Figure 4.2 (a), the peak intensity at around 1100 cm^{-1} and 1280 cm^{-1} can be ascribed to Si-O-Si and -CH_3, respectively, and these were obviously increased with increases in the coating times. The contact angles were increased from 30 ° to 120 ° after 1 time coating and remained constant even after additional coating times increased, which indicated that the surface of Me-SiO_2 films was highly hydrophobic and the substrate was fully covered by Me-SiO_2 layers. The peak area in the range of 979-1300 cm^{-1} increased in a linear trend for up to 4 times coating. The linear increase in the peak area indicates that the thickness of each coating was approximately the same, confirming excellent multi-layered coatings on hydrophobic surfaces. El-Feky et al. [29] reported preparing hydrophobic silica (Hyd-Si) from TEOS and MTES, silanol groups were mostly replaced by hydrophobic groups of -CH_3. The films showed a contact angle of 108 ° after firing at 400 ℃. The hydroxyl groups remained in the structures of $Q^3[Si(OSi)_3(OH)]$, $Q^2[Si(OSi)_2(OH)_2]$ and $T^2[RSi(OSi)_2(OH)]$ according to the characterization of powdered samples by solid-state ^{29}Si MAS NMR. The -OH groups allowed a uniform film by multi-layered coatings through condensation of silanol groups.

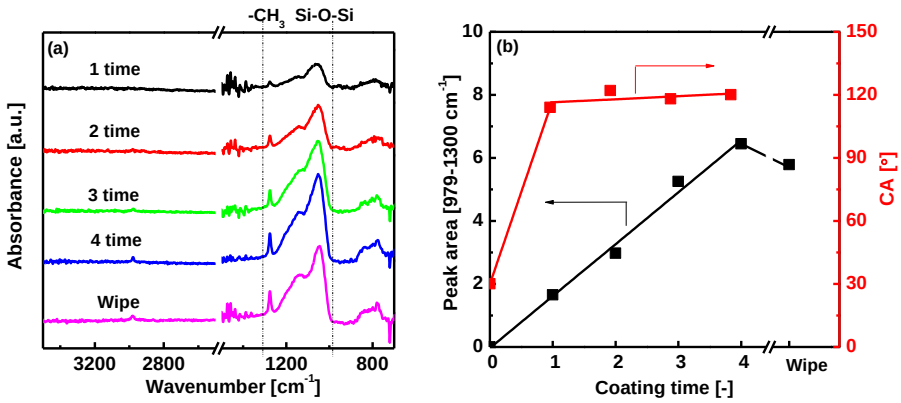

Figure 4.2 Characterization of Me-SiO_2 films coated on silicon wafers by (a) FT-IR (b) contact angles and peak areas.

Figure 4.3 (a) (b) and (c) (d) show the characterization of BTESE and BTESO films on silicon wafers, respectively. The peaks at around 1000-1100cm^{-1} that can be ascribed to Si-O-Si groups increased as the coating times increased for both BTESE and BTESO films. The peak areas ranging from 959-1180cm^{-1} for both films were approximately linear increase with coating times. The CA values for two films reached a constant above one-time coating. BTESE films showed a CA of 62 °, which was a hydrophilic surface by comparison with BTESO films, which showed a CA of 82 °.

The topographic images of the two films with one time coating were shown in Figure 4.4. The average roughness (AR) values of these films were analyzed by AFM. The BTESE film showed a highly smooth surface, with an AR of approximately 0.075 nm. The AR of Me-SiO_2 film (5.69 nm) was similar to that of BTESE films, and had the appearance of small sharp hills and valleys. The surface of BTESO film presented round protrusions with heights of several hundred nanometers and a large AR value of 79 nm. The length of the chains and compatibility of solvents and polymer played an important role in the surface morphology [30,31]. BTESE-derived sols had short chains and better solubility in ethanol, resulting in smooth and flat surfaces on silicon wafers. On the contrary, BTESO-derived sols had long chains and insufficient solubility in ethanol, and showed a high degree of roughness and protruding spheres.

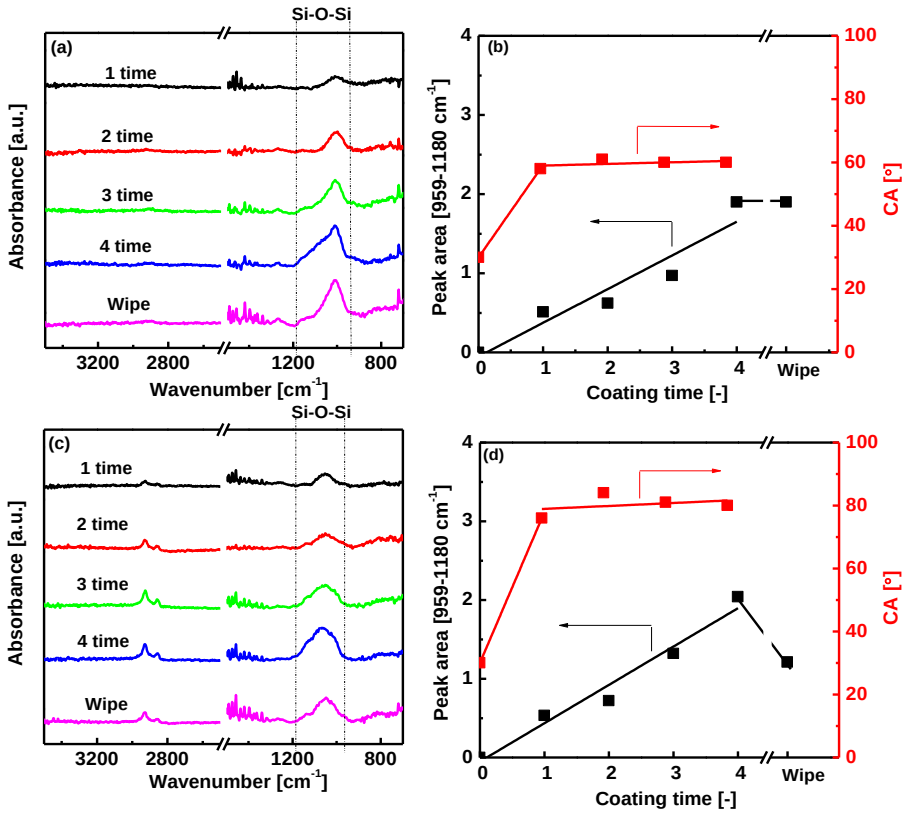

Figure 4.3 Characterization of BTESE films on silicon wafers by (a) FT-IR, (b) contact angles and peak area; and BTESO films on silicon wafers by (c) FT-IR, (d) contact angles and peak area.

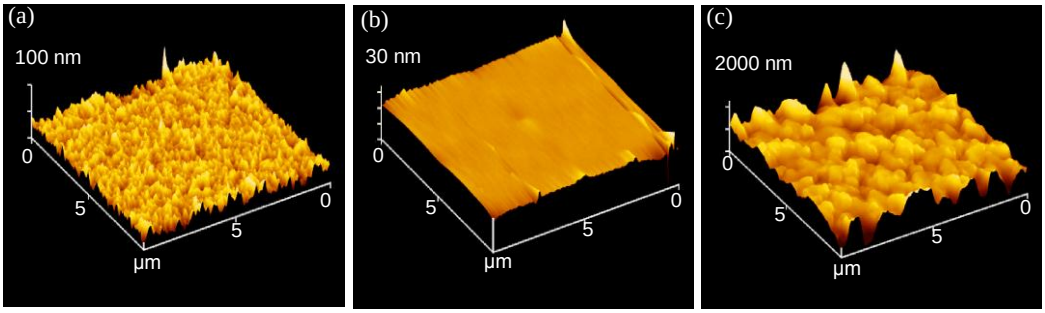

Figure 4.4 AFM images of (a) Me-SiO_2, (b) BTESE and (c) BTESO films spin-coated on silicon wafers.

Me-SiO_2, BTESE and BTESO films coated on silicon wafers showed different properties through the characterization of CA, peak area and AR. The CA was on the

order of Me-SiO_2>> BTESO >BTESE. Based on the increase in the peak area per time coating, the thickness of Me-SiO_2 was the largest of the three silica films, probably due to the larger size of the sols and higher viscosity. On the wiping treatment, the peak area was decreased for Me-SiO_2 (Figure 4.2 b) and BTESO (Figure 4.3d), which illustrated a low degree of adhesion between layers. However, the BTESE film showed no change in the absorbance area after wiping treatment, which indicated the strong adhesion. This was due to the greater number of -OH groups on the surface, confirmed by the low value of CA for BTESE. The larger degree of condensation from the silanol groups and lower roughness enhanced the adhesion of BTESE films on silicon wafers.

4.3.2 The modification of plasma conditions on the Me-SiO_2 films

The hydrophobic Me-SiO_2 films were prepared by sol-gel and spin-coating process on silicon wafers, followed by calcinations at 400 ^oC. The contact angles of films were 120^o with an average roughness of 5.69 nm. Then the deposited films were placed into a plasma chamber and evacuated to the pressure of 2 Pa using a vacuum pump. Water vapor mixed with N_2 was injected until a steady pressure of 20 Pa was reached, and RF plasma generator was activated at a power of 10W. The plasma time was investigated, as shown in Figure 4.5. As the plasma time increased, the water contact angles were gradually decreased. When the time exceeded 20 seconds, the contact angles became 0^o, indicating that the surface properties changed from hydrophobicity to hydrophilicity. In the plasma process, H_2O was converted into radical hydroxyl and other atomic and molecular fragments, which reacted with the surface of Me-SiO_2. Nakagawa et al. reported [32] that the OH and reactive sites were present on mica surface after water vapor plasma treatment, and reacted with different lengths of chains of chlorosilanes and fixed them on the surface. Thus, it is suggested that water plasma is a better method for the further silica coatings on Me-SiO_2 films.

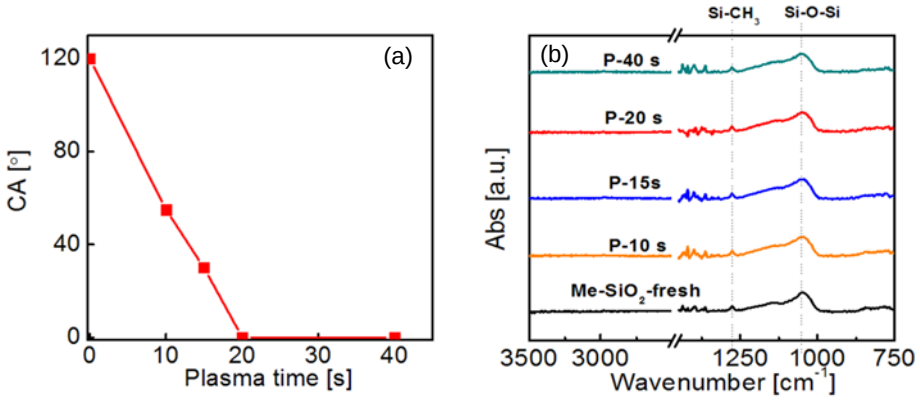

Figure 4.5 (a) Contact angles and (b) FT-IR spectra of Me-SiO_2 films at different plasma-treated times.

In the FT-IR spectra (Figure 4.5b.), the bulk structures of Si-O-Si group at about 1000-1100 cm^{-1} and Si-CH_3 vibrations at 1275 cm^{-1} were unchanged after plasma treatment. Although an outstanding enhancement in wettability was proved by the contact angles as plasma time increased from 0 to 40 s, the absorption intensity of Si-OH remained obscure in the FTIR spectra. In addition, the surface morphology with the RA 5.44 nm after plasma treatment was approximately the same as before, as shown in Figure 4.6a and 4.6b. Both surface chemical composition and surface topography determine the wettability of solid surface [33]. Given the unnoticeable variation in the surface morphology of Me-SiO_2 films, the significant wettability must have been caused by the increase in the OH groups that was induced by plasma treatment. The obscurity of the OH groups in the FT-IR spectra was due to the thinness of plasma-activated OH layer in Me-SiO_2 films at a relatively low power of 10 W and short duration of less than 40 s [22].

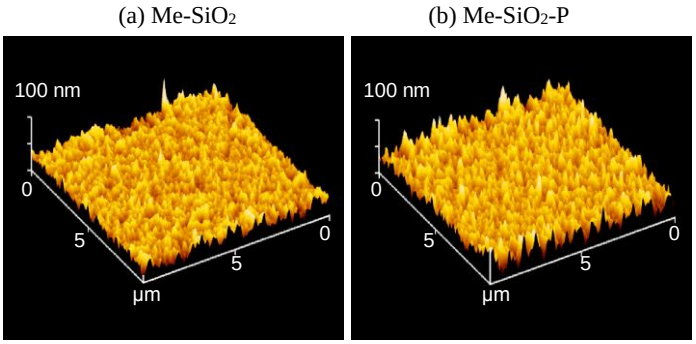

Figure 4.6 AFM images of Me-SiO_2 spin-coated on silicon wafers (a) fresh films (CA=120^o)

and (b) with plasma treatment for 20 s (CA=0º).

The relationship between the surface coverage of hydrophilic OH species and wettability (measured static contact angle θ) could be evaluated using Cassie-Baxter and related modified equations [34,35] as follows:

$$(1+\cos\theta)^2 = f_1(1+\cos\theta_1)^2 + f_2(1+\cos\theta_2)^2 \qquad (4.2)$$

$$f_1 + f_2 = 1 \qquad (4.3)$$

where θ is the static water contact angle on a chemically heterogeneous surface composed of a surface coverage f_1 of chemical groups type 1 and f_2 of groups type 2, θ_1 is the static water contact angle for a surface with f_1 =1 and θ_2 is the static water contact angle for a surface with f_2 =1. In our study, the surface was assumed to be a mixture of silanol (OH) groups of surface coverage f_1 and methylsilyl groups of surface coverage f_2. θ_1 is the contact angle of OH groups on plasma-activated surfaces, that is, 0 °. θ_2 is assumed to correspond to the maximum value that we measured for Me-SiO_2, that is, θ_2=120 °. Then we can obtain the relationship between the silanol (OH) groups f_1 with the contact angle θ:

$$f_1 = \frac{4(1+\cos\theta)^2 - 1}{15} \qquad (4.4)$$

When the contact angles θ of the surface is lower than 10º, the coverage of OH groups could be roughly calculated as: $f_1 > 0.98$. Figure 4.7 shows contact angles of Me-SiO_2 surface as a function of the coverage of OH groups.

As the surface is hydroxylated to the maximum degree, the number of OH groups per unit surface area α_{OH} is considered to be a physico-chemical constant in the Zhuravlev model [36]. The number value is $\alpha_{OH,\,AVER}$ =4.6 ~ 4.9 OH nm^{-2}. Therefore, the density of OH groups D_{OH} can be estimated as 4.59 ~ 4.8 OH nm^{-2} when the surface has a high degree of wettability (contact angles <10 °).

Therefore, in order to modify the surface properties of Me-SiO_2 films from hydrophobicity to maximum hydrophilicity without changing their bulk chemistry and morphology, plasma conditions controlled at a power of 10 W for 20 s were optimal in the present study.

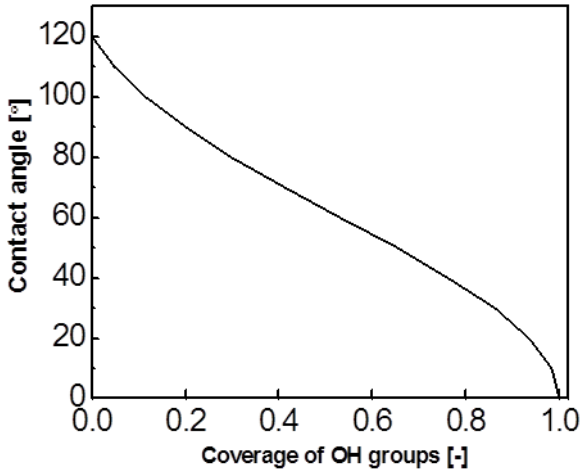

Figure 4.7 Contact angles of Me-SiO_2 surface as a function of coverage of OH groups.

4.3.3 Multi-coated thin films on Me-SiO_2 layers with plasma treatment

To prepare a hydrophobic top layer on hydrophobic substrates, BTESE sols were spin-coated on Me-SiO_2 layers which had been pre-coated 4 times of Me-SiO_2 on silicon wafers. After coating, BTESE sols were visibly scattered on the surface of Me-SiO_2 layers, and formed separated domains on the Me-SiO_2 films. The FT-IR spectra, CA and peak area are shown in Figure 4.8 (a) and (b). The CA remained at nearly 120 °, which was the value of Me-SiO_2 layers. The surface still showed the same hydrophobic properties as Me-SiO_2 films, indicating that BTESE sols could not form homogenous and continuous films on a hydrophobic Me-SiO_2 layer. It was confirmed by the photo in Figure 4.9 (a). The sols were scattered and formed separated domains on the Me-SiO_2 films. BTESE sols showed highly polar properties and good solubility in ethanol solvent with large contents of -OH groups, while Me-SiO_2 films showed a high water contact angle, indicating non-polar structures of the films. When spin-coated on the hydrophobic surface of Me-SiO_2 films with water-repellent properties, BTESE-derived sols were detached from the substrates and could not form continuous films via spin-coating, similar to water on a hydrophobic surface. Similar results were found by Petri [31] when spin-coating polymer on silicon wafers. Polystyrene (PS), poly(vinyl chloride) (PVC) and poly(vinyl butyral) (PVB), with

tetrahydrofuran (THF) as solvent were coated on silicon wafers with a polar surface. PS and PVC showed segregation on the surface, while PVB was more hydrophilic and formed continuous and homogeneous films on hydrophilic silicon wafers.

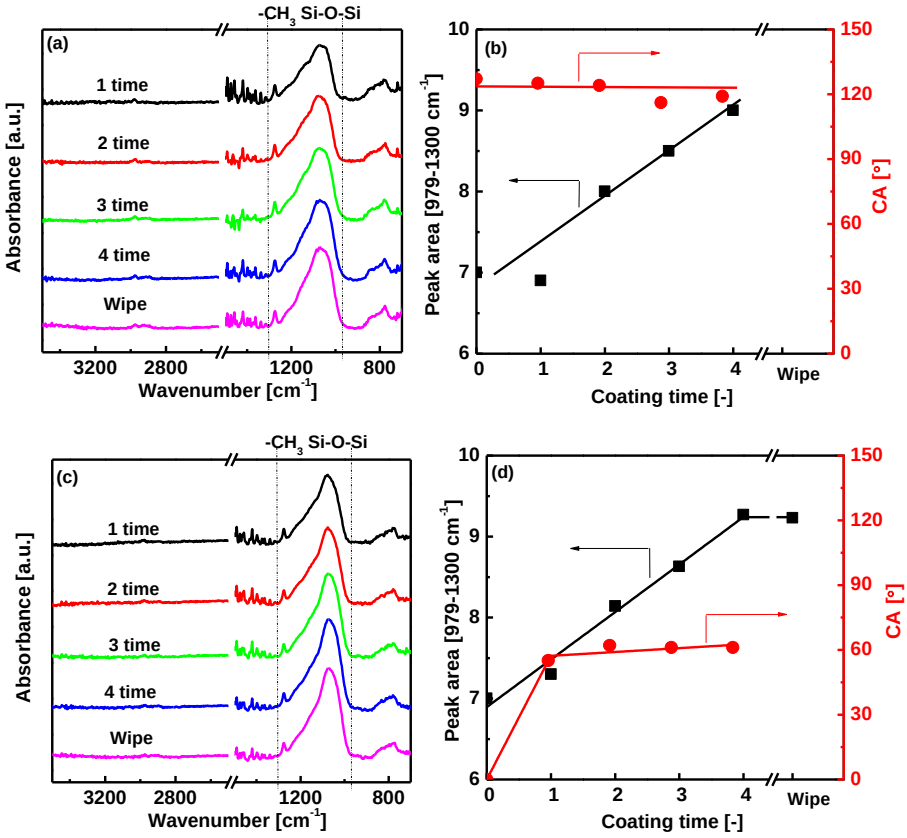

Figure 4.8 FT-TR and CA of BTESE coated on Me-SiO_2 films without (a)(b) and with plasma treatment (c)(d) as a function of coating times.

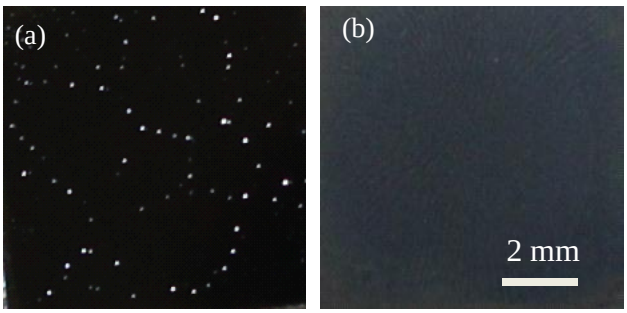

Figure 4.9 Photos of BTESE -derived sols coated on Me-SiO_2 films (a) without and (b) with plasma treatment.

Considering that BTESE sols were well coated on the hydrophilic silicon wafer (Figure 4.3), the compatibility between polar sols and the hydrophobic surface of Me-SiO_2 sub-layered films should be improved. Plasma treatments were applied to introduce hydrophilic groups on the hydrophobic surface of Me-SiO_2 layer to improve the coating properties of BTESE films. The surfaces of films were treated with H_2O-N_2 plasma at 10W at room temperature. During the plasma process, H_2O was excited to hydroxyl radical, atomic and molecular fragments, which reacted with the chemical groups on the surface of Me-SiO_2. After plasma treatment of Me-SiO_2 films for 20 s, the contact angles of the surface became 0 °. Then BTESE sols were immediately coated on the plasma-treated films.

Figure 4.8 (c) and (d) show the characterizations of BTESE films after plasma treatment. The contact angles were decreased as coating times of BTESE increased, and became constant at approximately 60 °, which was almost equivalent to that of BTESE films coated on silicon wafers (Figure 4.3b). This indicates that BTESE-derived sols fully covered on the surface of Me-SiO_2, formed homogenous and continuous films, which can be confirmed by Figure 4.9 (b). The plasma treatment was suitable for BTESE coating on hydrophobic Me-SiO_2 films.

The BTESO films coated on Me-SiO_2 layers are characterized in Figure 4.10 (a) and (b). The peak intensity was obviously increased as the coating times increased. The contact angles were decreased and became constant at 88 °as coating times increased, which was approximately the same value as BTESO films coated on silicon wafers (Figure 4.3 d). The peak area was also increased linearly with the coating time, indicating BTESO could form films with a uniform thickness. Plasma treatment was also performed on the Me-SiO_2 layer to further coat the BTESO films, as shown in Figure 4.10 (c) and (d). The FT-IR spectra and CA were the same for BTESO films coating on Me-SiO_2 surface with and without plasma treatment. The surface topography and roughness were approximately the same, as shown in Figure 4.11. Surface morphology and bulk chemical structures of BTESO coatings on Me-SiO_2 films seemed unchanged after plasma treatment.

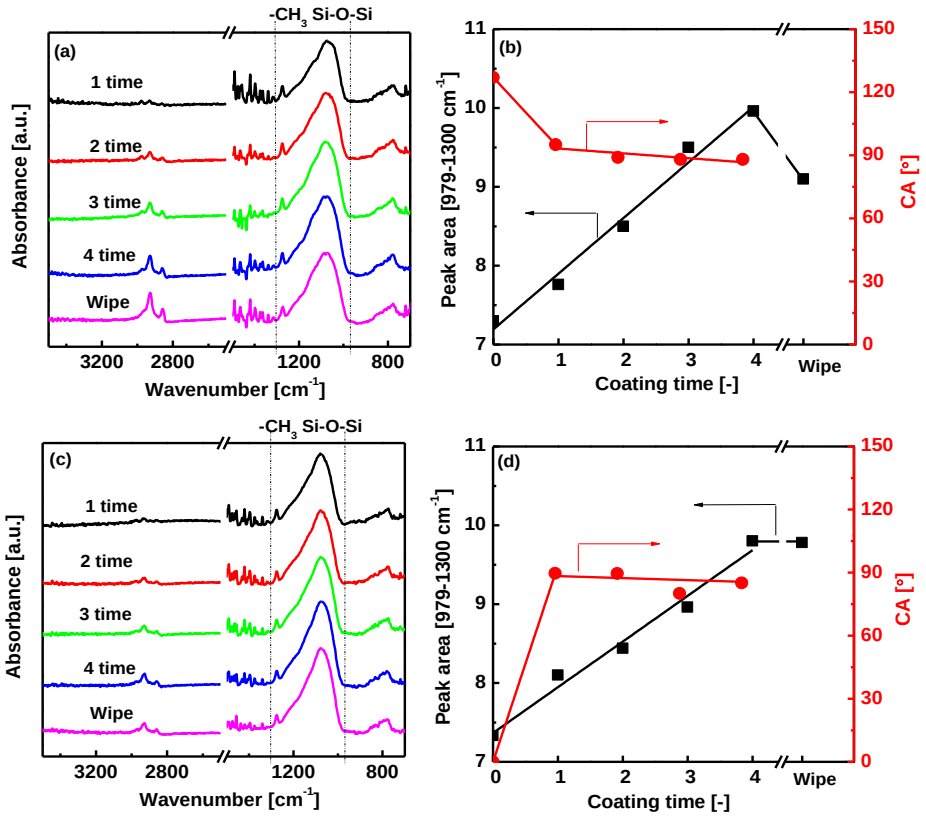

Figure 4.10 FT-TR and CA of BTESO coated on Me-SiO_2 films without (a)(b) and with plasma treatment (c)(d) as a function of coating times.

BTESO and BTESE formed films with different morphology when coated on Me-SiO_2 layers with and without plasma treatment, which may have been due to the differing chemical structures. BTESO sols consisted of the structures that contained both hydrophilic and hydrophobic portions. The hydrophilic portion of BTESO-derived sols was ascribed to -OH groups from the hydrolysis of ethoxide groups with water, and the hydrophobic portion was attributed to 8 -CH_2 chains. When the substrates show polar properties with hydrophilic properties (silicon wafer and plasma treated Me-SiO_2), the end of hydrophilic -OH groups of BTESO will attach the substrates. On the contrary, the hydrophobic long -CH_2 chains will attach the hydrophobic substrates (Me-SiO_2 surface). Kohut et al. [37] found that amphiphilic oligoester with hydrophilic and hydrophobic chains behaved as a self-adjustable interface, changing the confirmation to adapt to and enhance compatibility with

surroundings polar or non-polar media. BTESO sols could be coated on hydrophilic and hydrophobic surfaces according to its hydrophilic and hydrophobic groups.

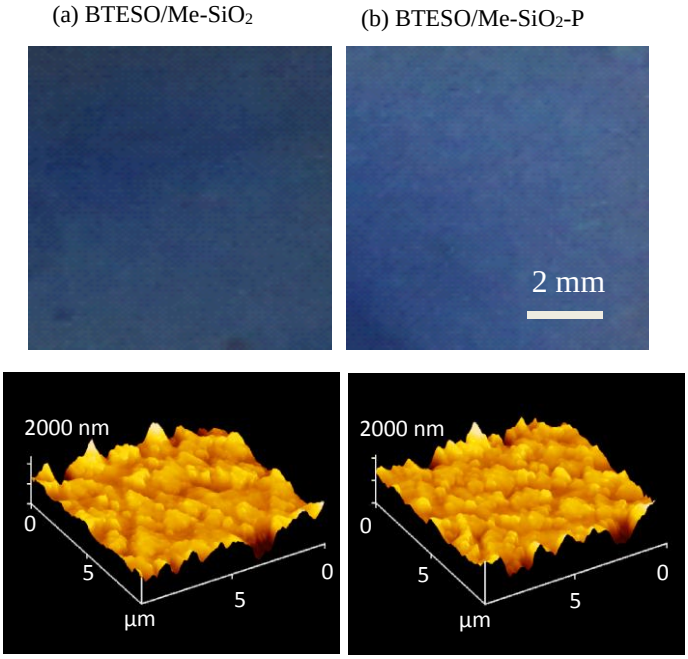

Figure 4.11 Images of BTESO films coated on Me-SiO_2 layers (a) without and (b) with plasma treatment. (Up: Photo; Down: AFM)

However, the peak area showed quite a different tendency in wiping treatment for BTESO films coated on Me-SiO_2 layers with and without plasma treatment. The peak area was largely decreased after the wiping of BTESO films without plasma treatment (Figure 5(b)), which was similar to BTESO coating on silicon wafers (Figure 3d). However, the absorbance area was not decreased for BTESO films with plasma treatment, suggesting that the adhesion force between each layer had been enhanced. This was because the species of hydroxyl radicals, the atomic and molecular fragments in H_2O-plasma process had activated the surface of Me-SiO_2, which changed the surface to reactive sites such as -OH groups [38]. The reactive sites on the Me-SiO_2 surface reacted with the silanol groups (Si-OH) of BTESO sols, and fixed BTESO on the surface [32]. Thus, it is suggested that water plasma is a better method for the multi-coating of hydrophobic sols on hydrophobic films.

4.4 Plasma treatment for multi-coated membranes

4.4.1 Characterization of Me-SiO_2 layers by plasma treatment

To prepare high-performance, thin-layered hydrophobic membranes, we proposed the use of plasma to treat the surface of hydrophobic Me-SiO_2 layers. Steen M. et al. [39] used H_2O plasma treatment on asymmetric polysulfone at a power of 25 W for 2 min that rendered membranes permanently hydrophilic and completely wettable. To avoid a thick-layer modification of hydrophobic Me-SiO_2 layers, the power and time were kept as low as 10 W and 20 s, respectively.

Me-SiO_2 intermediate layers were evaluated by nanopermporometry before and after H_2O plasma treatment, as shown in Figure 4.12. Nanopermporometry is based on the capillary condensation of vapor and the blocking effect of the permeation of non-condensable gases such as N_2 [27,40]. The dimensionless permeance of N_2 (DPN), normalized with N_2 permeance under dry conditions, is plotted as a function of the relative pressure of hexane (Figure 4.12a) and water vapor (Figure 4.12b). Kelvin diameter was calculated under an assumption of complete wetting of hexane in pores, and is shown in the top x-axis for reference.

The DPN decreased with an increase in the relative pressure of hexane, while it was not decreased in the water vapor. This was because hexane could capillary- condense in $MeSiO_2$-derived pores, whereas water vapor could not, indicating that the pores of Me-SiO_2 layers were hydrophobic. As shown in Figure 4.12 (a), the pore size distribution evaluated by hexane vapor was unchanged after plasma treatment, while the hydrophobicity of the bulk membranes obtained from water vapor (Figure 4.12b) was only slightly decreased after plasma treatment. The water plasma was confirmed to convert only the surface properties of Me-SiO_2 from hydrophobicity to hydrophilicity without damaging either the bulk hydrophobicity or the pore size.

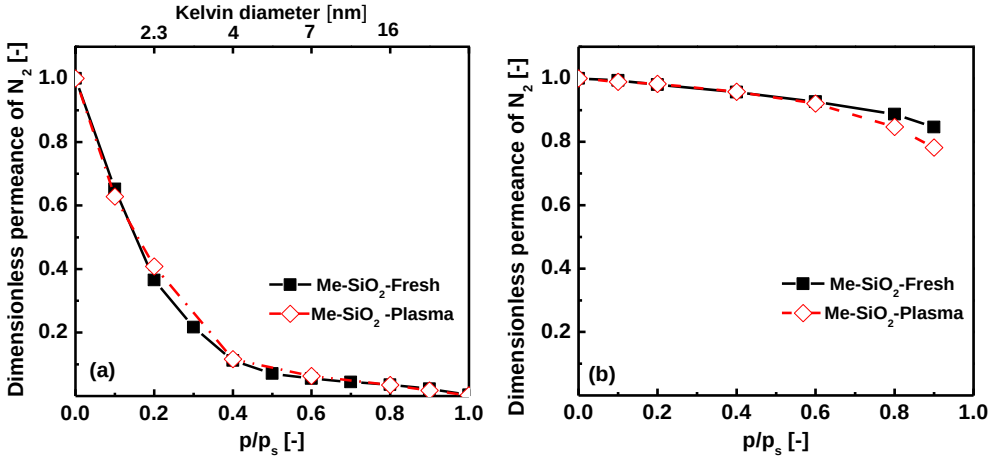

Figure 4.12 Nanopermporometry characterization of Me-SiO_2 layers with plasma treatment using (a) hexane and (b) water as condensable vapors.

4.4.2 Gas permeation properties of organosilica membranes under dry conditions

After plasma treatment, separation layers using BTESE and BTESO sols were deposited on Me-SiO_2 layers. The performance of these membranes for gas separation under dry conditions is shown in Figure 4.13. The comparisons with membranes coated on Me-SiO_2 (without plasma) and SiO_2-ZrO_2 layers are summarized in Table 4.1.

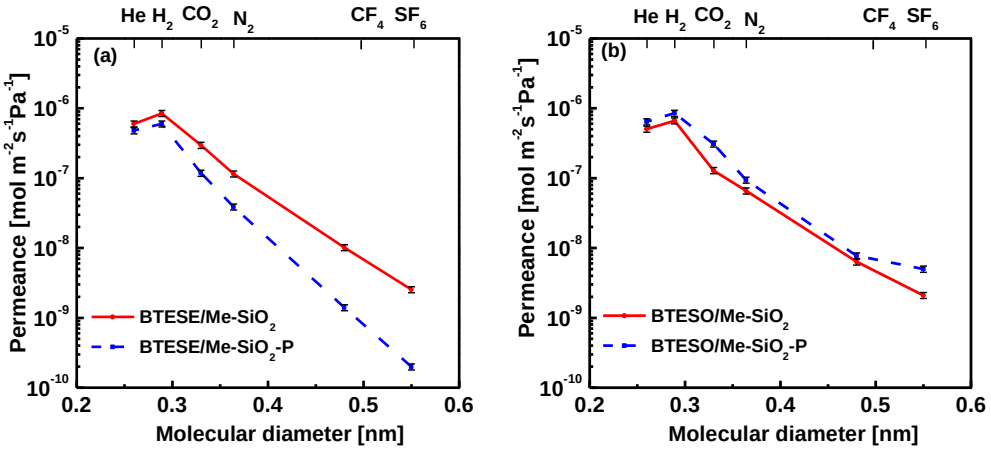

Figure 4.13 Single gas permeance at 200 ℃ for (a) BTESE and (b) BTESO membranes coated on Me-SiO_2 with and without plasma treatment.

Table 4.1 Comparison of gas selectivity of organosilica membranes top layer: BTESE, BTESO) prepared on three types of intermediate layers (Me-SiO_2-P (plasma treatment), Me-SiO_2 and SiO_2-ZrO_2) at 200 ℃.

Selectivity	BTESE (top layer)			BTESO (top layer)		
	Me-SiO_2-P	Me-SiO_2	SiO_2-ZrO_2[15]	Me-SiO_2-P	Me-SiO_2	SiO_2-ZrO_2[15]
H_2/ N_2	15	7	24	9	10	8
H_2/ CO_2	5	3	4	3	5	2
CO_2/ CF_4	84	29	-	40	20	73
H_2/SF_6	3,005	334	>10,000	170	316	446

BTESE/Me-SiO_2-P membrane (BTESE sols coated on plasma-treated Me-SiO_2 layers) showed high permeance for He and H_2, which was similar to membranes BTESE/Me-SiO_2 without plasma. As the kinetic diameters of gas increased, the differences in gas permeance for the two membranes became significant. The selectivity of H_2/N_2 was 15 and 7 for BTESE/Me-SiO_2-P and BTESE/Me-SiO_2 membranes, respectively. Moreover, the selectivity of H_2/SF_6 was 3005 for BTESE/Me-SiO_2-P membrane, which was approximately 10 times higher than for BTESE/Me-SiO_2 membrane. This indicated that defects from uncovered intermediate layers were present in BTESE/Me-SiO_2 membrane. As shown in Figure 4.14, the BTESE/Me-SiO_2 membrane showed several uncoated pinholes and a rough surface. The separation properties of gases are extensively dependent on the surface layer (separation layer). When the coatings of surface layer causes any defects, the membranes will not demonstrate good performance. BTESE/Me-SiO_2-P membrane had a smooth and homogeneous surface layer and showed high performance in gas separation. On the other hand, the selectivity of H_2/SF_6 for BTESE/Me-SiO_2-P membrane was close to that BTESE coated on hydrophilic SiO_2-ZrO_2 intermediate layers. This may have been due to the hydrophilic properties for both plasma-assisted Me-SiO_2 layers and SiO_2-ZrO_2 layers, since both layers showed contact angles of 0 °.

The hydrophilic surface of intermediate layers can make BTESE coatings form homogeneous and continuous surface layer without defects.

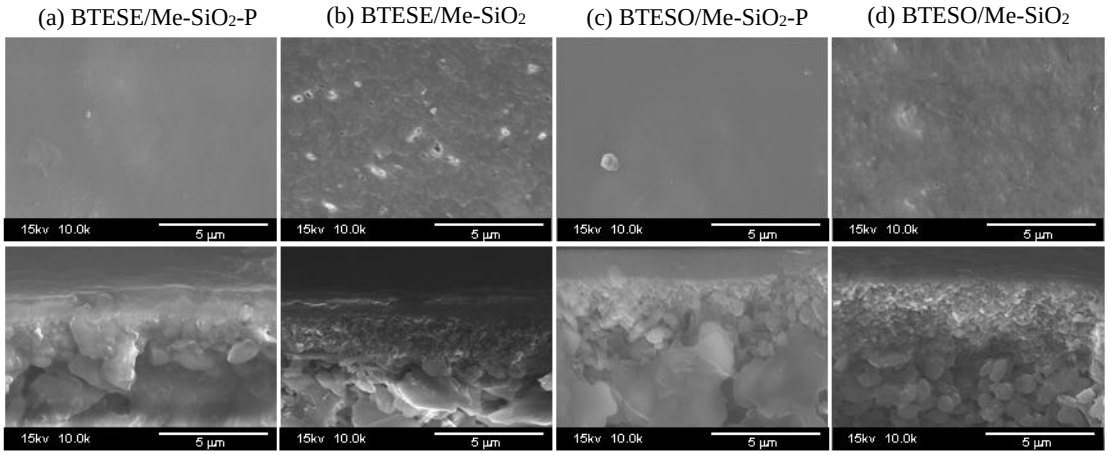

Figure 4.14 SEM images of organosilica membranes with and without plasma treatment. (Up: surface; Down: cross-section)

For BTESO membranes, the gas permeance and selectivity was nearly the same with and without plasma treatment (Figure 7 (b)). The selectivity for BTESO membranes coated on Me-SiO_2 and Me-SiO_2-P layers was also approximately the same as when BTESO was coated on SiO_2-ZrO_2 intermediate layers. This was probably due to the hydrophilic-hydrophobic portions of BTESO sols. The permeance and selectivity were not changed but the adhesion was improved after plasma treatment according to the characterizations in Figure 4.8 (d). In Figure 4.14, it can be observed that all of surfaces were smooth and defect-free with the exception of BTESE/Me-SiO_2 membranes. In the cross-sections of SEM images, the top and intermediate layers were difficult to distinguish for all the membranes, but the pore size of membranes was obviously reduced from bottom to top.

BTESE membranes showed a higher selectivity of H_2/SF_6 than BTESO membranes with either Me-SiO_2-P or SiO_2-ZrO_2 intermediate layers. This was due to the structure differences between BTESE and BTESO. BTESE with 2 methylene groups between two Si atoms formed microporous structures that were suitable for gas separation,

while BTESO with 8 methylene groups, which are more flexible, showed dense structures [15].

4.4.3 Gas permeation of organosilica membranes with plasma treatment in the presence of water vapor

BTESE/Me-SiO_2-P and BTESO/Me-SiO_2-P membranes, both of which were treated with plasma, were examined in the presence of water vapor for CO_2 permeation, as shown in Figure 4.15. The permeance for both membranes was decreased at a very low water activity, and then kept constant as the water activity increased. The silicon rubber membranes showed a constant permeance across all the range of water activity, but the permeance was approximately 100 times lower than that for the BTESE/Me-SiO_2-P and BTESO/Me-SiO_2-P membranes due to the increase in thickness (1000 μm) [15].

Figure 4.16 illustrates the dimensionless permeance of CO_2 (DP) that is normalized by dry CO_2 permeance as a function of water activity compared with the other organosilica membranes. The DP values for BTESE and BTESO membranes coated on plasma-treated Me-SiO_2 intermediate layers (BTESE/Me-SiO_2-P, BTESO/Me-SiO_2-P) were 0.23 and 0.46 at water activity around 0.75, respectively. The two membranes showed much lower decrease in permeance than BTESE and BTESO membranes prepared on ZrO_2-SiO_2 intermediate layers with DP value of 0.01 and 0.08, respectively. Compared with the BTESE/Me-SiO_2 and BTESO/Me-SiO_2 membranes without plasma treatment, the BTESE/Me-SiO_2-P and BTESO/Me-SiO_2-P membranes showed a slightly larger decrease in permeance. This was because the hydrophilic groups such as the -OH groups, which were generated by the plasma treatment on Me-SiO_2 sub-layers, may not have been totally condensed with the Si-OH groups on the surface of the top layers (BTESE or BTESO). This could have resulted in higher water adsorption at the interface of the two layers. Since the membranes with plasma treatment showed high selectivity and lower decrease in permeance, it can be concluded that plasma treatment is an effective way to improve performance for both membranes.

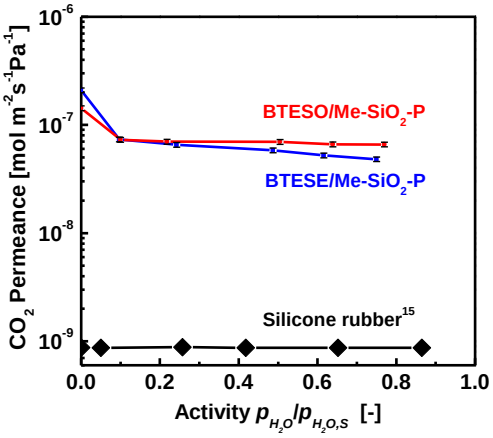

Figure 4.15 CO_2 permeance of BTESE/Me-SiO_2-P and BTESO/Me-SiO_2-P membranes as a function of water activity at 40 ℃.

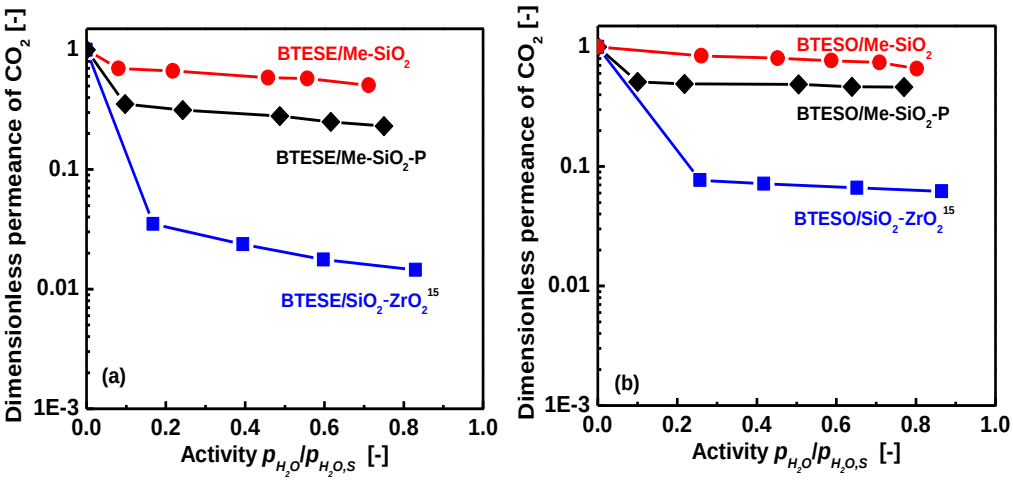

Figure 4.16 Comparison of dimensionless permeance of CO_2 for (a) BTESE and (b) BTESO membranes coated on SiO_2-ZrO_2 and Me-SiO_2 with and without plasma in the presence of water vapor at 40 ℃.

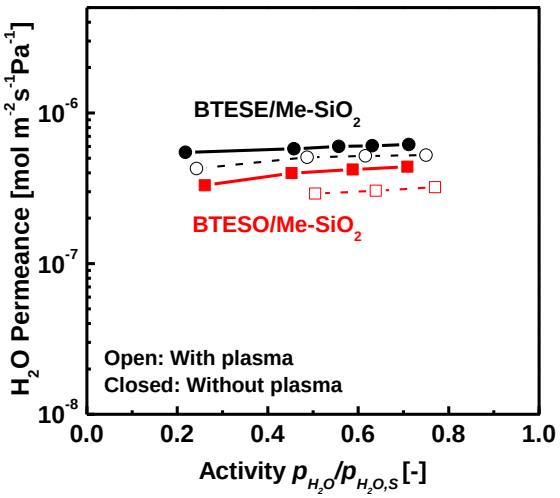

Figure 4.17 Comparison of H_2O permeance for organosilica membrane as a function of water vapor activity at 40 ℃ (Conditions: Feed side: 500 ml/min, permeate side: 1000 ml/min)

Figure 4.17 shows H_2O permeance as a function of water activity in the feed stream for BTESE/Me-SiO_2 and BTESO/Me-SiO_2 membranes with and without plasma treatment. Water permeance for the four organosilica membranes was much larger than CO_2 permeance, and it was approximately independent of the water activity. This was because water molecules had a higher diffusion due to a small diameter and high adsorption even through hydrophobic membranes. In addition, the hydrophobic organosilica membranes showed a long stability for CO_2 permeation in the presence of water vapor and liquid water.

4.5 Conclusions

Organosilica membranes were prepared to form hydrophobic top layers on hydrophobic intermediate layers via plasma-assisted multi-layered coatings. Multi-layered coating was confirmed to form hydrophobic Me-SiO_2 layers. H_2O plasma was optimized to generate hydrophilic groups on the hydrophobic surface of Me-SiO_2 layers in a thin film without changing either the bulk properties or pore size. After plasma treatment, BTESE formed homogenous and continuous films on Me-SiO_2

layers. Moreover, the plasma method improved the adhesion of BTESO films coated on Me-SiO_2 layers.

Under dry gas separation, the gas selectivity for BTESE membranes coated on plasma-treated Me-SiO_2 was improved. On the other hand, BTESO membranes showed no change after plasma treatment. In the presence of water vapor, CO_2 permeance showed a slightly larger decrease with plasma treatment than without it for both BTESE and BTESO membranes, but the decrease was much less than for the membranes with hydrophilic intermediate layers (SiO_2-ZrO_2).

References

[1] L.N. Ho, J.P. Pellitero, F. Porcheron, R. J.M. Pellenq. Enhanced CO_2 Solubility in Hybrid MCM -41: Molecular Simulations and Experiments. Langmuir. 27, (2011) 8187-8197.

[2] G. Li, T. Niimi, M. Kanezashi, T. Yoshioka, T. Tsuru. Equilibrium shift of methylcyclohexane dehydrogenation in a thermally stable organosilica membrane reactor for high-purity hydrogen production. Int. J. Hydrogen. Energ. 38 (2013) 15302-15306.

[3] P.D. Chapman, T. Oliveira, A.G. Livingston, K. Li. Membranes for the dehydration of solvents by pervaporation. J. Membr. Sci. 318 (2008) 5-37.

[4] M. Elma, C. Yacou, D. K. Wang, S. Smart, J. C. D. Costa. Microporous Silica Based Membranes for Desalination. Water. 4 (2012) 629-649.

[5] M. Pera-Titus. Porous Inorganic Membranes for CO_2 Capture: Present and Prospects. Chem. Rev. 114 (2014) 1413-1492.

[6] J.C. Poshusta, R.D. Noble, J.L. Falconer. Characterization of SAPO-34 membranes by water adsorption. J. Membr. Sci. 186 (2008) 25-41.

[7] G. Xomeritakis, C.Y. Tsai, C.J. Brinker. Microporous sol-gel derived aminosilicate membrane for enhanced carbon dioxide separation. Sep. Purif. Technol. 42 (2005) 249-257.

[8] C.A. Scholes, S.E. Kentish, G.W. Stevens. Effects of Minor Components in Carbon Dioxide Capture Using Polymeric Gas Separation Membranes. Sep. Purif. Rev. 38 (2009) 1-44.

[9] B.T. Low, L. Zhao, T.C. Merkel, M. Weber, D. Stolten. A parametric study of the impact of membrane materials and process operating conditions on carbon capture from humidified flue gas. J. membr. Sci. 431 (2013) 139-155.

[10] Q. Wei, F. Wang, Z.R. Nie, C.L. Song, Y.L. Wang, Q.Y. Li. Highly Hydrothermally Stable Microporous Silica Membranes for Hydrogen Separation. J. Phys. Chem. B 112 (2008) 9354-9359.

[11] N.A. Ahmad, C.P. Leo, A.L. Ahmad, W.K.W. Ramli. Membranes with Great Hydrophobicity: A Review on Preparation and Characterization. Sep. Purif. Rev. 44

(2015) 109-134.

[12] S. Cerneaux, I.Struzyńska, W.M. Kujawski, M. Persin, A. Larbot. Comparison of various membrane distillation methods for desalination using hydrophobic ceramic membranes. J. Membr. Sci. 337 (2009) 55-60.

[13] C.C. Wei, K. Li. Preparation and Characterization of a Robust and Hydrophobic Ceramic Membrane via an Improved Surface Grafting Technique. Ind. Eng. Chem. Res. 48, (2009) 3446–3452.

[14] R.M. de Vos, W.F. Maier, H.Verweij. Hydrophobic silica membranes for gas separation. J. Membr. Sci. 158 (1999) 277-288.

[15] X. Ren, K. Nishimoto, M. Kanezashi, H. Nagasawa, T. Yoshioka, T. Tsuru. CO_2 Permeation through Hybrid Organosilica Membranes in the Presence of Water Vapor. Ind. Eng. Chem. Res. 5 (2014) 6113-6120.

[16] J.H. Prosser, T. Brugarolas, S. Lee, A. J. Nolte, D. Lee. Avoiding Cracks in Nanoparticle Films. Nano. Lett. 12 (2012) 5287-5291.

[17] C. Depagne, S. Masse, T. Link, T. Coradin. Bacteria survival and growth in multi-layered silica thin films. J. Mater. Chem. 22 (2012) 12457-12460.

[18] Kanezashi, M.; Yada, K.; Yoshioka, T.; Tsuru, T. Design of Silica Networks for Development of Highly Permeable Hydrogen Separation Membranes with Hydrothermal Stability. J. Am. Chem. Soc. 131 (2009) 414-415.

[19] M.C. Duke, J.C.D. Costa, D.D. Do, P.G. Gray, G.Q. Lu. Hydrothermally Robust Molecular Sieve Silica for Wet Gas Separation. Adv. Funct. Mater. 16 (2006) 1215-1220.

[20] S.M. Ibrahim, R. Xu, H. Nagasawa, A. Naka, J. Ohshita, T. Yoshioka, M. Kanezashi, T. Tsuru. Insight into the pore tuning of triazine-based nitrogen-rich organoalkoxysilane membranes for use in water desalination. RSC Adv. 4 (2014) 23759-23769.

[21] R. Xu, J.H. Wand, M. Kanezashi, T. Yoshioka, T. Tsuru. Tailoring the A ffinity of Organosilica Membranes by Introducing Polarizable Ethenylene Bridges and Aqueous Ozone Modification. ACS Appl. Mater. Interfaces. 5 (2013) 6147-6154.

[22] L.L. Pranevicius, D. Milcius, S. Tuckute, K. Gedvilas. Preparation of hydrogenated-TiO_2/Ti double layered thin films by water vapor plasma treatment. Appl. Sur. Sci. 258 (2012) 8619-8622.

[23] A. Pakdel, Y. Bando, D. Golberg. Plasma-Assisted Interface Engineering of Boron Nitride Nanostructure Films. Nano. 8 (2014) 10631-10639.

[24] K. Lionti, B. Toury, C. Boissière, S. Benayoun, P. Miele, Hybrid silica coatings on polycarbonate: enhanced properties, J. Sol-Gel. Sci. Technol. 65 (2013)52-60.

[25] J.Y. Kim, D-M. Lee, J-K. Kim, S-H. Yang, J-M. Lee, Effects of H_2/O_2 mixed gas plasma treatment on electrical and optical property of indium tin oxide. Appl. Sur. Sci. 265 (2013) 145-148.

[26] K. Zarshenas, A. Raisi, A. Aroujalian. Surface modification of polyamide composite membranes by corona air plasma for gas separation applications. RSC Adv. 5 (2015) 1 9760-19772.

[27] T. Tsuru, T. Nakasuji, M. Oka, M. Kanezashi, T. Yoshiok. Preparation of hydrophobic nanoporous methylated SiO_2 membranes and application to nanofiltration of hexane solutions. J. Membr. Sci. 384 (2011) 149-156.

[28] Z. Olejniczak, M. Łeczka, K. C-Kowalska, K. Wojtach, M. Rokita, W. Mozgawa. ^{29}Si MAS NMR and FTIR study of inorganic-organic hybrid gels. J. Mol. Struct. 744-747 (2005) 465-471.

[29] H.H. El-Feky, K. B Briceño, E.O. Jardim, J.S. Albero. T. Gumí Novel silica membrane material for molecular sieve applications. Microporous and Mesoporous Materials. 179 (2013) 22-29.

[30] V. Purcar, I. Stamatin, O. Cinteza, C. Petcu, V. Raditoiu, M. Ghiurea, T. Miclaus, A. Andronie. Fabrication of hydrophobic and antireflective coatings based on hybrid silica films by sol-gel process. Surf. Coat. Technol. 206 (2012) 4449-4454.

[31] D.F.S. Petri. Characterization of Spin-coated Polymer Films, J. Braz. Chem. Soc. 13 (2002) 695-899.

[32] T. Nakagawa, M. Soga. Contact Angle and Atomic Force Microscopy Study of Reactions of n-Alkyltricholosilanes with Muscovite Micas Exposed to Water Vapor Plasmas with Various Power Densities. Jpn. J. Appl. Phys. 36 (1997) 6915-6921.

[33] A.V. Rao, S.S. Latthe, S.L. Dhere, S.S. Pawar, H. Imai, V. Ganesan, S.C. Gupta, P.B. Wagh. Control on wetting properties of spin-deposited silica films by surface silylation method. Appl. Sur. Sci. 256 (2010) 2115-2121.

[34] J.N. Israelachvili, M.L. Gee. Contact Angles on Chemically Heterogeneous Surfaces. Langmuir. 5 (1989) 288-289.

[35] B. Liberelle, S. Giasson. Chemical End-Grafting of Homogeneous Polystyrene

Monolayers on Mica and Silica Surfaces. Langmuir. 23 (2007) 9263-9270.

[36] L.T. Zhuravlev. The surface chemistry of amorphous silica. Zhuravlev model. Colloids Surf. A. 173 (2000) 1-38.

[37] A. Kohut, S. Ranjan, A. Voronov, W. Peukert, V. Tokarev, O. Bednarska, O. Gevus, S. Voronov. Design of a New Invertible Polymer Coating on a Solid Surface and Its Effect on Dispersion Colloidal Stability. Langmuir. 22 (2006) 6498-6506.

[38] L. Meagher, R. M. Pashley. The Interaction Forces between Silica and Plasma-Treated Polypropylene surfaces in Aqueous Solutions. J. Coll. Int. Sci. 185 (1997) 291-296.

[39] M.L. Steen, L. Hymas, E.D. Havey, N.E. Capps, D.G. Castner, E.R. Fisher. Low temperature plasma treatment of asymmetric polysulfone membranes for permanent hydrophilic surface modification. J. Membr. Sci. 188 (2001) 97-114.

[40] T. Tsuru, T. Hino, T. Yoshioka, M. Asaeda. Permporometry characterization of microporous ceramic membranes. J. Membr. Sci. 186 (2001) 257-265.

Chapter 5

Conclusions

5.1 Summary of this study

Organosilica membranes prepared from intermediate layers to separation layers with hydrophobic property were proposed to achieve high gas performance under wet conditions in this dissertation. Separation layers derived from bridged organosilanes, BTESE and BTESO were examined for CO_2 separation. SiO_2-ZrO_2 with hydrophilicity and Me-SiO_2 with hydrophobicity as intermediate layers were researched under wet conditions for gas performance. The modification of plasma treatment on the surface of Me-SiO_2 films was optimized, and the effect of plasma treatment on the morphology and separation performance for the membranes was studied. The main conclusions in the thesis were summarized as follows.

1. Two types of organoalkoxysilanes, bis(triethoxysilyl)ethane (BTESE) and bis(triethoxysilyl)octane (BTESO) were used as precursors to prepare membranes via sol-gel method. The two membranes showed distinct properties of porosity and water affinity because of the differences in the bridging methylene numbers between the two Si atoms. Under dry conditions, the BTESE and BTESO membranes showed CO_2 permeances as high as 7.66×10^{-7} and 6.63×10^{-7} mol m^{-2} s^{-1} Pa^{-1} with CO_2/N_2 selectivities of 36.1 and 12.6 at 40 ℃, respectively. In the presence of water vapor, CO_2 permeance was decreased for both membranes, but the effect of water vapor on CO_2 permeation was slighter for BTESO membranes than it was for BTESE membranes due to more hydrophobicity and denser structures with a longer linking-bridge group. In addition, silicone rubber with a dense structure and high hydrophobic properties showed a minor effect of water vapor on CO_2 permeation. The hybrid organosilica membranes both showed good reproducibility and stability in water vapor.

2. In this work, organosilica membranes were prepared using hydrophobic Me-SiO_2 as

intermediate layers and applied under humidified conditions. Hydrophobic Me-SiO_2 film was successfully prepared using the co-precursors of tetraethoxysilane (TEOS) and methyltrimethoxysilane (MTMS). The contact angle of Me-SiO_2 by spin-coating on silicon wafers was as high as 120 °, while the contact angles of conventional SiO_2-ZrO_2 film was 0 °. Based on nanopermporometry measurement, Me-SiO_2 layers showed capillary condensation of hexane, while no condensation was observed by water vapor, confirming Me-SiO_2 layers were hydrophobic compared with SiO_2-ZrO_2 layers. Under dry conditions, the selectivity of H_2/SF_6 for BTESE/ZrO_2-SiO_2 membrane was higher than that for BTESE/Me-SiO_2 membrane, indicating poorer quality that was caused by inhomogeneous coating for hydrophilic BTESE sols coated on hydrophobic Me-SiO_2 intermediate layers. Under humidified conditions, The membranes with Me-SiO_2 intermediate layers had a lower decrease in permeance than those with hydrophilic SiO_2-ZrO_2 layers. The great difference indicates the importance of the intermediate layers on the water resistance for gas permeation. In addition, the hydrophobic membranes can keep a good stability under saturated water vapor for 70 hours.

3. Organosilica membranes were prepared to form hydrophobic top layers on hydrophobic intermediate layers via plasma-assisted multi-layered coatings. Multi-layered coating was confirmed to form hydrophobic Me-SiO_2 layers. BTESE-derived sols were directly spin-coated on the Me-SiO_2 films, resulting in separated and scattered coatings. H_2O plasma was optimized to generate hydrophilic groups on the hydrophobic surface of Me-SiO_2 layers in a thin film without changing either the bulk properties or pore size. After plasma treatment, BTESE formed homogenous and continuous films on Me-SiO_2 layers. The plasma on Me-SiO_2 films had no effect on either the chemical structure or the morphology of BTESO coating. This probably was due to the polar (-OH) and non-polar (long -CH_2) portions of the BTESO structures. However, the plasma method improved the adhesion of BTESO films coated on Me-SiO_2 layers.

For gas separation applications, the corresponding BTESE membranes showed great improvement in gas selectivity after the plasma treatment of hydrophobic Me-SiO_2 layers. On the other hand, BTESO membranes showed no change after plasma treatment. In the presence of water vapor, CO_2 permeance showed a slightly larger decrease with plasma treatment than without it for both BTESE and BTESO membranes, but the decrease was much less than for

the membranes with hydrophilic intermediate layers (SiO_2-ZrO_2).

5.2 Prospective

Membranes gas separation is a potential process in industry application. Hydrophobic organosilica membranes provide high water resistance and good hydrothermal stability in the presence of water vapor. The CO_2 permeance was nearly constant in the presence of water for hydrophobic membranes in this work. Plasma treatment was used to modify the intermediate layers, improved the selectivity of CO_2/N_2 for BTESE membranes. However, the gas performance was not good enough for hydrophobic membranes as that for hydrophilic membranes. Membranes prepared with uniform and continuous layers without defects that include cracks, segregation, or scattered points on the substrates will demonstrate good performance. Therefore, future works should mainly concentrate on how to improve the hydrophobic intermediate layers and the hydrophobic top layers to prepare defect-free membranes.

List of Publications

Papers:

(1) **Xiuxiu Ren,** Kanji Nishimoto, Masakoto Kanezashi, Hiroki Nagasawa, Tomohisa Yoshioka, Toshinori Tsuru*, CO_2 Permeation through Hybrid Organosilica Membranes in the Presence of Water Vapor, *Ind. Eng. Chem. Res.* 2014, 53(14) 6113-6120.

(2) **Xiuxiu Ren,** Masakoto Kanezashi, Hiroki Nagasawa, Toshinori Tsuru*, Plasma treatment of hydrophobic sub-layers to prepare uniform multi-layered films and high-performance gas separation membranes, *Appl. Surf. Sci.* 2015, 349, 415-419.

(3) **Xiuxiu Ren,** Masakoto Kanezashi, Hiroki Nagasawa, Toshinori Tsuru*, Plasma-assisted multi-layered coating towards improved gas permeation properties for organosilica membranes, *RSC Adv.* 2015, 5, 59837-59844.

(4) **Xiuxiu Ren,** Masakoto Kanezashi, Hiroki Nagasawa, Toshinori Tsuru*, Preparation of organosilica membranes on hydrophobic intermediate layers and evaluation of gas permeation in the presence of water vapor, *J. Membr. Sci.* 2015, 496, 156-164.

Proceedings:

(1) **Xiuxiu Ren,** Masakoto Kanezashi, Hiroki Nagasawa, Tomohisa Yoshioka, Toshinori Tsuru*. HIGH PERFOMANCE OF ORGANOSILICA MEMBRANES FOR CO_2 SEPARATION UNDER HUMIDIFIED CONDITIONS.*ICSST14, Nara, Japan, 2014.10.*

(2) **Xiuxiu Ren,** Kaniji Nishimoto, Masakoto Kanezashi, Hiroki Nagasawa, Tomohisa Yoshioka, Toshinori Tsuru*. Hydrophobic Organosilica Membranes for CO_2 Permeation in Presence of Water Vapor. *ICOM 2014, Suzhou, China, 2014, 7.*

(3) **Xiuxiu Ren,** Masakoto Kanezashi, Hiroki Nagasawa, Tomohisa Yoshioka, Toshinori Tsuru*. Transport of dissolved CO_2 through organic-inorganic hybrid silica membranes. *AMS 8, Xi'an, China, 2013, 7.*

Acknowledgements

First and foremost, I gratefully acknowledge the help of my supervisor, Professor Toshinori Tsuru, for his constant encouragement and expert guidance. He has offered me valuable suggestions in the academic studies, and spent much time reading drafts and provided me with inspiring advice. Moreover, he always praised and encouraged me when I have a little progress in the experiment. His encouragement and unwavering support has sustained me through frustration and depression. I benefit a lot from his guidance and his spirit in the pursuit of education and research work.

I would like to express my heartfelt gratitude to Prof. Tomohisa Yoshioka, Prof. Hiroki Nagasawa, especially Prof. Masakoto Kanezashi, who have instructed me in many insightful criticisms and guidance in either experiment or writings. They helped me a lot in the lab and gave constant concern about my life.

I am grateful to my tutor, Mr. Kazuki Mtsunari, who helped me a lot in my study and daily life after I came to Japan. I would like to thank all other group membranes in Separation Technology Lab. They helped me a lot in the past three years. Someday, I may meet someone of you in one corner on some street in the future, or I will never meet you guys again in my life. But you guys left me a wonderful and happy memory in my youth age.

Last, my thanks would go to my beloved family for their loving considerations and great confidence in me all through these years. I also gratitude to my friends and my fellow classmates who gave me their help and time in listening to me and helping me work out my problems during the difficult.